UNIVERSITÀ
DEGLI STUDI
DI TRIESTE

UNIVERSITÀ DEGLI STUDI DI TRIESTE

XXXVII CICLO DEL DOTTORATO DI RICERCA IN

Nanotecnologie

Borsa cofinanziata 50% MUR 50% ELETTRA Sincrotrone Trieste

Lipid bilayers as model systems for plasma membranes: experimental synergy to tackle growing complexity

Settore scientifico-disciplinare: **FIS/03**

DOTTORANDO / A
ELENA FERRAGUZZI

COORDINATORE
PROF. ALBERTO MORGANTE

SUPERVISORE DI TESI
PROF. CASALIS LOREDANA

CO-SUPERVISORE DI TESI
DR. PIETRO PARISSE

ANNO ACCADEMICO 2023/2024

UNIVERSITÀ DEGLI STUDI DI TRIESTE

XXXVII CICLO DEL DOTTORATO DI RICERCA IN

Nanotecnologie

Borsa cofinanziata 50% MUR 50% ELETTRA Sincrotrone Trieste

Lipid bilayers as model systems for plasma membranes: experimental synergy to tackle growing complexity

Settore scientifico-disciplinare: **FIS/03**

DOTTORANDO / A
ELENA FERRAGUZZI

COORDINATORE
PROF. ALBERTO MORGANTE

SUPERVISORE DI TESI
PROF. CASALIS LOREDANA

CO-SUPERVISORE DI TESI
DR. PIETRO PARISSE

ANNO ACCADEMICO 2023/2024

Table of contents

Abstract

Plasma membranes are dynamic and complex structures that play a central role in regulating various cellular processes, including communication, signalling, and transport. Composed primarily of a lipid bilayer made by 500-1000 diverse lipid species, the membrane exhibits a highly heterogeneous organization, with cholesterol acting as a key component that modulates membrane structure and function. In particular, cholesterol plays a fundamental role in regulating specific protein localization and dynamics within the lipid bilayer, promoting the formation of lipid rafts (LRs), nano-sized membrane domains (10-200 nm) that facilitate the regulation of cellular functions such as receptor signalling and membrane trafficking. Given the small size of the LRs and their rapid dynamics, LRs localization (and correlation with cholesterol content) in native physiological systems remains a significant challenge.

In this study the influence of cholesterol on lipid rafts formation and in the modulation of membrane stiffness and fluidity has been investigated, through a bottom-up approach, i.e. by building multi-component membrane mimics, which represent the outer leaflet of eukaryotic cell membranes, in terms of ratios between the different lipid families. This novel 4-element membrane mimic allowed for adjustments of cholesterol concentration, up to physiologically relevant values, provided a controlled environment to investigate how cholesterol concentration modulates lipid organization and facilitates LRs assembly, affecting membrane biophysical properties, as stiffness and fluidity, and how these properties modify in different physiological conditions. By means of atomic force microscopy (AFM) nanoscale topographic imaging, AFM nanoindentation spectroscopy, confocal laser scanning fluorescence microscopy (CLSM) and fluorescence recovery after photobleaching (FRAP), we have collected quantitative information on membrane properties such as lipid rafts coverage and height, domains stiffness and molecular diffusion within the domains, as a function of cholesterol content, namely 7 and 33 mol%. For that, we used as a model supported lipid bilayers (SLBs) obtained from monodispersed 100 nm diameter liposomes, made of the desired lipid composition. AFM high-resolution imaging allowed distinguish between liquid ordered (Lo) and liquid disordered (Ld) phases, as a function of cholesterol content. Also, it allowed to optimize physiological conditions, as type of buffer, humidity and temperature, to follow the evolution of Lo and Ld as a function of cholesterol content. In agreement with the literature, CLSM showed that the Lo phase resulted enriched with cholesterol and saturated lipids, and that is more ordered (Lo- Ld AFM relative height higher) and tightly packed (as from diffusion data obtained by FRAP) then the Ld phase. Conversely, the Ld phase is fluid and loosely packed, enriched by unsaturated lipids, hosting a lower amount of cholesterol, with respect to the Lo phase, presenting overall an increased lipid mobility. Cholesterol therefore, facilitates the formation of the Lo phase by organizing some lipids into ordered domains while maintaining some degree of membrane fluidity. Through AFM force spectroscopy, we directly quantified the stiffness of the different membrane phases (Lo and Ld) at the two cholesterol concentrations. We found that at high cholesterol the stiffness of the Lo phase was about 2-fold higher with the respect to low

cholesterol content, while surprising the stiffnesses of the relative Ld phases were very similar. These results obtained in label-free conditions, corroborated FRAP lipid diffusion experiments results, proving the high value of the synergic, experimental platform, utilized in this thesis work. Domain evolution versus temperature was also studied via high-speed AFM imaging (40 frames/sec), showing that cholesterol contributed to decrease the transition temperature of the Lo phase, as expected from the melting temperatures of individual lipid components. These data were in agreement with differential scanning calorimetry results we obtained on the same systems. After the characterization of the biomimetic SLBs models, we studied their interaction with small extracellular vesicles (EVs), nanosized vesicles produces by cells, delimited by a lipid membrane and containing a molecular cargo rich in RNA, DNA, proteins and metabolites, and used for cell-cell communication. By means of high-res AFM topography, we observed the role of membrane stiffness and fluidity in the mechanisms of EVs uptake, fusion and cargo delivery. This analysis has relevant implications for the understanding of cellular communication and for eventually testing drugs to regulate EVs uptake. In the final phase of the PhD research, we optimized the production of giant unilamellar vesicles (GUVs), which are large (μm -sized), spherical structures consisting of a single lipid bilayer, that can mimic the properties of cellular membranes, to match the lipid composition of the SLBs. GUVs provide a platform for developing pore-spanning membranes (PSMs), which offer a more native-like environment for studying membrane-confined processes, such as receptor-ligand interactions. PSMs combine the structural stability of supported membranes with the functional flexibility of free-standing bilayers, making them ideal for integrating membrane proteins and investigating complex dynamics.

Overall, this PhD work provides comprehensive insights into the mechanisms by which cholesterol regulates lipid raft formation, and crucial membrane properties such as fluidity and stiffness, with critical implications for understanding membrane dynamics in physiological context. Our biomimetic membrane platforms serve as valuable tools for investigating cholesterol's impact on membrane behaviour, highlighting the essential role of cholesterol in maintaining membrane integrity and functionality, presenting new opportunities for future research in drug delivery, cancer biology, and cellular signalling.

Aim of the thesis

The aim of this thesis was to develop multi-component eukaryotic model membrane systems with a lipid composition designed to closely mimic the outer leaflet of the cell membrane, while ensuring high stability and reproducibility. We dedicated substantial time and effort to reconstitute these models with physiological cholesterol concentrations, enabling an in-depth study of cholesterol's impact on membrane properties. Our research illuminates how cholesterol affects lipid organization, regulates membrane fluidity, and it's involved in the formation of lipid rafts—specialized membrane domains involved in the regulation of multiple cellular processes. We achieved precise control over membrane reconstitution, allowing for adjustments in cholesterol ratios, physiological conditions, and overall membrane production. The study provides quantitative data on key biophysical properties such as stiffness and fluidity. We investigated the formation and dynamic evolution of lipid rafts in response to varying cholesterol levels, leading to the development of multidisciplinary platforms that closely mimic the architecture and functionality of the plasma membrane. By systematically varying cholesterol concentrations, we were able to observe how lipid rafts not only assemble but also reorganize over time, revealing their critical role in membrane integrity and cellular signalling. This research highlights the significant potential of model membranes as versatile tools for analysing EVs uptake mechanism within biomimetic membrane systems. Our findings demonstrate that these platforms can simulate the complex interactions between EVs and membrane components, providing valuable insights into the mechanisms of vesicle uptake, fusion, and cargo delivery. Furthermore, by enabling the precise manipulation of lipid composition and membrane dynamics, our model systems pave the way for future studies on the impact of membrane organization on various cellular processes. To achieve these objectives, have been mainly used two techniques: AFM and Quantitative fluorescence microscopy. AFM was utilized due to its label-free, non-invasive nature, making it ideal for imaging biological samples with high molecular resolution. This technique provides detailed topographic images of the sample under physiological conditions, allowing for precise visualization of surface features and structural details at the nanoscale without the need for additional labelling or sample preparation. AFM was also employed in force spectroscopy mode to obtain detailed information on the nanomechanical properties of the membranes, in particular the stiffness. This mode was particularly useful for highlighting contrasts between different lipid phases, providing insights into variations in membrane stiffness and mechanical behaviour across distinct lipid domains. We employed CLSM as our fluorescence technique, with a specific focus on FRAP. FRAP experiments were instrumental in providing quantitative data on the diffusion coefficients of different membrane phases, offering dynamic insights into the mobility and behaviour of lipids within the membrane. By measuring the rate at which fluorescence recovers after photobleaching, FRAP allowed us to assess how different lipid phases interact and how cholesterol influences their diffusion characteristics.

The investigation of parameters such as fluidity and stiffness, was driven by their significance as potential biomarkers in pathological contexts, including cancer. Understanding these parameters is crucial because changes in membrane fluidity and stiffness can reflect alterations in cellular processes and disease states. For instance, variations in membrane fluidity and stiffness are often associated with cancer progression, where altered lipid organization and mechanical properties may impact tumour cell behaviour, drug resistance, and metastasis. By characterizing these biophysical properties, we aim to identify markers that could provide insights into disease mechanisms and potentially inform diagnostic and therapeutic strategies. We utilized SLBs, - that are artificial membrane systems composed of amphiphilic lipid molecules, where the hydrophilic head groups face the aqueous environment, and the hydrophobic tails interact to form a bilayer, - as platforms to study interactions with small extracellular vesicles isolated from umbilical cord mesenchymal stem cells (UC MSCs), sourced from GMP production provided by Mario Gimona's lab at Paracelsus Medical University Salzburg. These experiments were designed to elucidate how variations in membrane stiffness and fluidity influence vesicle uptake and the different interaction pathways they may follow. By analysing these interactions, we aimed to gain deeper insights into the impact of membrane biophysical properties on vesicle behaviour, which is crucial for understanding processes such as cellular communication and material delivery.

In the final part of our work, we optimized the conditions to reconstitute GUVs, that are large, spherical structures consisting of a single lipid bilayer surrounding an aqueous interior. Typically measuring tens of μm in diameter, GUVs are large enough to be easily observed under a light microscope. We developed GUVs at the equivalent lipid composition of the SLBs previously investigated. The rationale behind this is that GUVs are crucial for PSMs, which serve as versatile tools for investigating membrane-confined processes using a bottom-up approach. PSMs offer a unique advantage by combining the structural stability of a substrate with the benefits of membrane suspension, allowing for the integration of membrane receptors. This integration helps create a more native-like system for studying complex interactions and dynamics. The production of PSMs is still undergoing optimization, and we will provide a brief overview of this process in future plans. The ability to suspend bilayers with PSMs not only supports structural integrity but also enhances the system's functionality by facilitating the incorporation of membrane receptors and other integral proteins, thus offering a more accurate model for exploring membrane behaviour and receptor interactions.

Thesis Outline

The outline of this thesis is described as follows:

Chapter 1 introduces the context of the research, focusing on the nanoscale tools and techniques that are essential for investigating plasma membrane (PM) biophysics. This chapter emphasizes the structural complexity and dynamic behaviour of the PM, providing a foundational understanding for the study.

Chapter 2 explores the dynamics and complex nature of the plasma membrane, beginning with an overview of lipids as core structural components. This chapter examines cholesterol's critical role in defining membrane fluidity, permeability, and structural organization. Additionally, lipid rafts are introduced as contributors to the functional organization within the membrane. Following this, biomimetic systems used for studying PM structure and function—such as liposomes and supported lipid bilayers—are presented, alongside with the relevant applications of extracellular vesicles, which are integral to this research.

Chapter 3 provides an in-depth description of the materials and methods employed in the study. It includes detailed procedures for preparing liposomes, supported lipid bilayers and giant unilamellar vesicles, as well as protocols for synthesizing and characterizing gold nanoparticles. Optimization procedures for pore-spanning membranes are outlined, followed by an overview of the characterization techniques used in membrane analysis. These techniques include Atomic Force Microscopy (AFM), AFM nanomechanics, Confocal Fluorescence Microscopy, Fluorescence Recovery After Photobleaching (FRAP), and Differential Scanning Calorimetry (DSC).

Chapter 4 presents a detailed analysis of the experimental data. This includes the optimization and characterization of four-component SLBs in physiological buffer solutions, measurement of membrane thickness across different biomimetic models, and investigation of SLB morphology and lipid raft organization using AFM. Additionally, the influence of buffer composition on lipid raft structure is examined. This chapter also includes a qualitative assessment of the mechanical properties of nanoscale liposomes, a quantitative evaluation of membrane stiffness across various biomimetic systems, and an analysis of fluidity and mobility parameters in different membrane models.

Chapter 5 presents SLBs as a model to investigate the mechanisms of EV uptake. This includes a comparative study on EV uptake mechanisms in different buffer conditions, enhancing the understanding of vesicle-membrane interactions.

Chapter 6 summarizes the key findings of this research, discussing the implications of these results for the field of PM biophysics and EV interactions. It also suggests potential directions for future research in this area.

Appendix A summarizes preliminary results on GUVs and PSMs reconstitution to replicate key characteristics of eukaryotic membranes, enabling the study of complex cellular processes such as lipid phase separation and protein interaction.

List of the figures

which is an intermediate state between the gel phase and the disordered phase. Preferential interaction of Cholesterol with sphingolipids. Adapted from Barba-Bon et al., 2020 [81].

Pag 35: Table 2.1 Different research approaches in membrane biology. The table emphasise key areas of focus, including controlled experimental environments, the replication of natural systems, the study of lipid behavior, the modeling of complex interactions, technological advancements, and the investigation of disease-related mechanisms. It outlines how different strategies are employed to recreate membrane conditions, investigate lipid phase transitions, model protein-lipid interactions, develop drug delivery systems, and understand disease-related changes in membrane properties. Each approach contributes to a deeper understanding of membrane dynamics, stability, and functionality, both in natural and experimental contexts.

Pag 36: Figure 2.6 A typical phase diagram for ternary lipid bilayers, consisting of a low-melting-temperature (unsaturated) lipid, a high-melting-temperature (saturated) lipid, and cholesterol, shows the coexistence of various membrane domains. These include Ld and Lo, gel (So), and pure cholesterol crystal phases. The diagram also features a critical point, marked by a star, where lateral mixing becomes pronounced. Figure from [89]

Pag 41: Figure 2.7 Origin and composition of extracellular vesicles. Figure from [107].

Pag 46: Figure 3.1 Schematic illustration of the thin film hydration method protocol that was employed to produce liposomes. Liposomes have been used both to reconstitute SLBs and to probe the mechanical properties through the interactions with gold nanoparticles monitored with Uv-Vis spectroscopy. (Created with Biorender.com).

Pag 47: Figure 3.2 Vertical chamber setup used for GUVs preparation. A lid containing two platinum (Pt) wires, coated with a lipid mixture, is placed on top. When an alternating current (AC) electric field is applied, GUVs form as the lipids swell and detach from the wires. After vesicle formation, the lid can be replaced with an elongated chamber. If sucrose is used as the swelling solution, glucose can be added to the observation buffer, causing the GUVs to sink to the bottom for easy observation and harvesting. Readapted from [119].

Pag 49: Figure 3.3 Potential Lennard-Jones [126]

Pag 51: Figure 3.4 Schematic presentation of atomic force microscope. Adapted from [130]

Pag 53: Figure 3.5 Formation of supported lipid bilayers (SLBs) via the vesicles fusion method (a), along with the SLB indentation process using AFM-FS (b). The force–separation curve demonstrates a typical discontinuity in the approach curve, which occurs when the bilayer is punctured. The various stages in the indentation process and the corresponding features of the force curve are linked by arrows. Figure adapted from [136].

Pag 56: Figure 3.6 Hertz Model Theory for Force-Distance Curve Fitting. (Courtesy of L.Puricelli).

Pag 56: Figure 3.7 Ray path in a confocal LSM. Adapted from [143]

Pag 57: Figure 3.8 A region of interest (ROI) is selected, bleached using a high-intensity laser, and the fluorescence recovery within the ROI is monitored over time. Below is an example from an actual experiment in a myoblast cell line (myo3) homogeneously expressing GFP-Myosin III before bleaching. (2) Initially, the fluorescence intensity starts at a pre-bleach level (Ii), then sharply decreases to a low value (I0) when the intense laser bleaches the fluorophores in the ROI. Over time, the fluorescence signal recovers from I0 to a maximal plateau value (IN). From this recovery curve, along with equations (a) and (b), key parameters such as the mobile fraction (Mf), immobile fraction (IMf), and the half-time of recovery (I1/2) can be determined. A reference photobleaching curve (light blue line) is included to correct for fluorescence loss during data acquisition. The recovery curve (I0 to IN) provides critical information to calculate the diffusion constant and assess the binding dynamics of fluorescently labeled proteins. A more precise method for obtaining the half-life and immobile/mobile fractions, suitable for automation, involves nonlinear curve fitting of the experimental data using the simple exponential model described by equation (c). Readapted from [146].

Pag 63: Figure 4.1 Molecular structures of three phospholipids used in this work: 18:1 (Δ9-Cis) PC (DOPC), 18:0 PC (DSPC), and SM (Sphingomyelin, Brain, Porcine). DOPC is an unsaturated phosphatidylcholine with one double bond, while DSPC and SM are saturated lipids with 18:0 fatty acid chains. These lipids are critical components of membrane models due to their distinct interactions with cholesterol and their roles in modulating membrane fluidity and raft formation. Image source: Avanti polar lipids website.

Pag 63: Table 4.1 Percentage of lipids (m/m) used to reconstitute SLBs at two different cholesterol concentrations (7 mol % and 33 mol%). The molar ratio of DOPC:DSPC: SM is kept constant to evaluate the effect of cholesterol in determining LRs behaviour.

Pag 64: Figure 4.2 AFM topography images (1) of SLBs reconstituted with constant ratio of DOPC:DSPC:SM at two different cholesterol concentrations [7% mol% (low) and 33% mol % (high)] in HEPES/NaCl (10mM, 150mM) buffer. Panel 2 displays the relative height profiles highlighting the mismatch between the lipid rafts and the liquid-disordered phase (Ld) of the membrane.

Pag 65: Figure 4.3 Statistical analysis of LRs relative height variation with cholesterol concentration is presented in the panel 1. Panel 2 displays the statistical analysis of the surface area (%) at the two different cholesterol concentrations.

Pag 66: Figure 4.4 Visualization of the solid-ordered phase (So) formation in SLB Composed of DOPC, DSPC, and SM. This figure illustrates the distinct separation between Ld and So phase with measurable differences in fluorescence intensity. Panel a) display the CLSM images showing the phase separation between Ld-So. Panel b) display the AFM topography image in which the bright islands

represent the thicker So phase, while the brown matrix is the Ld phase. The relative height profile taken along the white line in the AFM image, showing a clear height difference between the Ld and So phases, with the So phase protrude from Ld phase approximately 2 nm. Magenta: Ld phase, green: Lo phase.

Pag 69: Figure 4.5 CLSM images of SLBs in which has been fluorescently labeld the entire Lo phase with 18:0 NDB-DSPE 1) and cholesterol with Bodipy-Chol dye 2) (green). The Ld phase (magenta) has been fluorescently labeld with ATTO-655-DOPE in both cases. The scale bar is 5 μm.

Pag 69: Figure 4.6 AFM images and thickness analysis of SLBs with 7 mol % and 33 mol % cholesterol concentrations. The AFM images on the left show the surface of SLBs at the two cholesterol levels, with circled regions indicating defects used to measure the thickness of the lipid bilayers. The graph on the right displays the relative thickness of the Ld and Lo phases at 7 mol % and 33% cholesterol. The table below summarizes the measured thickness values for each phase.

Pag 71: Figure 4.7 AFM topography images of the SLB composed of DOPC: DSPC:SM (48.6:27.8:16.6) and 7 mol % Cholesterol, fused on mica, illustrating the effect of temperature on lipid raft formation dynamics. Lipid rafts are protruded from the liquid- disordered phase, composed primarily of DOPC, and their morphology is highly temperature-dependent. The images represent different temperatures: (a) 24°C (b) 25°C, (c) 26°C, (d) 27°C, (e) 28°C, (f) 29°C, (g) 30°C, (h) 31°C, (i) 32°C, (j) 33°C, (k) 31°C. Each frame has been acquired after 5 min. Image size = 5x5 μm, with a scale bar of 2μm

Pag 72: Table 4.2 Statistical height values of LRs at various temperatures for the supported lipid bilayer with the 7 mol % cholesterol concentration. The data reveal a distinct trend: as the cholesterol concentration increases, the height of the lipid rafts decreases. However, it is important to note that some data points deviate from this general trend. These anomalies may be attributed to the dynamic nature of lipid rafts, which can experience fluctuations and rearrangements due to changes in temperature. Such variations can affect the raft height and lead to outliers in the data.

Pag 72: Table 4.3 Statistical percentage of membrane area occupied by the two distinct lipid phases, liquid-disordered and liquid-ordered, at various temperatures for the SLB at the lowest cholesterol level. As temperature increases, the proportion of membrane area covered by lipid rafts, decreases. At 34°C, specific values for the areas of the Ld and Lo phases are not provided due to the observation of complete phase mixing, which results in a uniform distribution of lipid molecules and the absence of distinct phase separation.

Pag 73: Figure 4.8 AFM topography images of the SLB composed of DOPC:DSPC:SM (35:20:12) and 33 mol % Cholesterol, fused on mica, illustrating the effect of temperature on lipid raft formation dynamics. LRs protruded from the liquid-disordered phase, composed primarily of DOPC, and their morphology is highly temperature-dependent. The images represent different temperatures: (a) 24°C,

(b) 25°C, (c) 26°C, (d) 27°C, (e) 28°C, (f) 29°C, (g) 30°. Each frame has been acquired after 5 min. Image size = 5x5 μm, with a scale bar of 2 μm

Pag 73: Table 4.4 Height values of LRs at various temperatures for the SLB with 33 mol % cholesterol concentration. As cholesterol concentration increases, the height of the LRs decreases. This trend suggests that higher cholesterol levels lead to a reduction in the height of the lipid rafts, likely due to increased packing density and altered membrane fluidity.

Pag 74: Table 4.5 Percentage of membrane area occupied by the two distinct lipid phases, liquid-disordered and liquid-ordered, at various temperatures for the SLB at the 33 mol% cholesterol level. As temperature increases, the proportion of membrane area covered by LRs, or the Lo phase, decreases. At 30°C, specific values for the areas of the Ld and Lo phases are not provided due to the observation of complete phase mixing at this temperature, which results in a uniform distribution of lipid molecules and the absence of distinct phase separation.

Pag 74: Figure 4.9 Scatter plots depicting the variation in surface area of the two phases as a function of temperature under the two cholesterol conditions investigated. In the case of SLBs with 7 mol % cholesterol, complete mixing between the two phases occurs at 34°C. However, as cholesterol content increases (33 mol %), the mixing between the two phases takes place at a lower temperature (30°C). This suggests a different degree of membrane fluidity, which, as expected, is closely dependent on temperature. 2) Scatter plots illustrating how the relative height of the LRs at the two different cholesterol concentrations changes with temperature. The trend in both cases point to a decrease in the relative height as the temperature increases.

Pag 75: Figure 4.10 Differential Scanning Calorimetry (DSC) thermogram showing the heat capacity change (ΔCp) as a function of temperature (T) for lipid bilayers at two different cholesterol concentrations (7 mol % and 33 mol %) during both heating and cooling cycles. The red and black curves represent the heating and cooling processes for the sample with 7% cholesterol, respectively, while the blue and green curves represent the cooling and heating processes for the sample with 33% cholesterol. The presence of a pronounced peak around 40°C in the 7% cholesterol sample indicates a phase transition, while the 33% cholesterol sample shows a much more subdued transition, reflecting the impact of cholesterol concentration on the thermotropic behaviour of the membrane.

Pag 77: Figure 4.11 AFM images of SLBs composed of 7 mol % cholesterol at various temperatures. Images (a-f) show the formation and evolution of the LRs domains as the temperature is increased from 16°C to 24°C, with no significant changes in domain size and density. Panels (a) and (f) represent the system at 24°C before and after thermal cycling, showing reversible domain formation. Images (g-h) display the expected behaviour of the bilayer at higher temperatures (29°C, 32°C, and 34°C), where the lipid domains are dissolved, resulting in a smooth bilayer surface with no visible domains.

Pag 77: Figure 4.12 AFM images showing the temperature-dependent behaviour of SLBs with 33 mol % cholesterol. (a) SLB morphology at 24°C, showing well-defined lipid rafts. (b-f) Sequential heating from 16°C to 24°C with temperature increments of 2°C. The images demonstrate minimal changes in lipid raft morphology and area coverage as the temperature increases, indicating stability of the membrane phases up to 24°C. (g) Upon heating to 28°C, complete mixing of membrane phases is observed, with no distinct raft structures present. (h) After reheating to 16°C, the lipid rafts reorganize but exhibit different morphology compared to the initial state at 24°C, indicating a reversible but altered membrane phase organization. (i) The SLB shows raft formation at 16°C after the cooling process, demonstrating the temperature sensitivity and cholesterol's role in membrane phase behaviour. Scale bars: 2 μm.

Pag 80: Figure 4.13 AFM topography images (1) of SLBs reconstituted with DOPC: DSPC:SM (35:20:12) in HEPES buffer (10mM) at two different cholesterol concentrations (7 mol% and 33 mol%) are presented. Panel 2 displays the height profiles highlighting the mismatch between the lipid rafts and the liquid-disordered phase of the membrane.

Pag 80: Figure 4.14 Statistical analysis (Panel 1) of the surface area percentage as cholesterol levels increase. Statistical analysis of lipid raft height variation with cholesterol concentration is presented in panel 2. Comparison with the SLBs reconstituted in HEPES/NaCl indicates that there is no significant decrease in height as cholesterol concentration increases. This suggests that the effect is enhanced in the presence of NaCl.

Pag 81: Figure 4.15 Comparison of LR heights under the two different buffer conditions clearly demonstrates the effect of NaCl on modulating lipid organization within the rafts.

Pag 83: Figure 4.16 Panel a) shows the spectrum of citrate-capped gold nanoparticles (red) and, in blue, the spectrum of gold nanoparticles interacting with pure DOPC liposomes. Panel c) illustrates the interaction mechanism between AuNPs and vesicles with varying membrane stiffness. When AuNPs adhere to a soft membrane, they undergo significant wrapping by the membrane, leading to the aggregation of AuNPs on the vesicle surface. In contrast, when AuNPs dock on a stiffer membrane, the wrapping is less pronounced, preventing the clustering of AuNPs. Caselli et.all [186].

Pag 84: Figure 4.17 UV-VIS spectra of HCit@AuNPs (Green) and liposomes matching the concentrations of SLBs synthesized in HEPES 10mM/NaCl 150mM (1:10) buffer and HEPES 10mM, composed of 7% cholesterol (red) and 33% cholesterol (green), incubated with HCit@AuNPs. There is a SPR modulation effect induced by cholesterol and this effect is highlighted in presence of NaCl.

Pag 86: Figure 4.18 Representative experimental force curves acquired by AFM on the Lo phase of SLBs with 7% (yellow curve) and 33% (brown curve) mol cholesterol concentration, highlighting the breakthrough points, characterized by a sudden change in the curve slope, where the force applied by

the tip overcome the mechanical resistance of the bilayer and break it, reaching the underlying rigid and undeformable substrate.

Pag 87: Figure 4.19 3x3 μm2 AFM topographic maps obtained on a SLB sample with 7% mol cholesterol concentration, acquired before (a) and after (b) performing single force curves on the selected spots, numbered and marked by red crosses. Yellow continuous circles and blue dashed circles highlight the spots selected on the Lo and Ld phases, respectively.

Pag 87: Figure 4.20 Overall statistics of the breakthrough force values for both phases and cholesterol concentrations, along with the corresponding median +/- median absolute deviation values. A total number of force curves comprised between one and two hundreds have been analysed for each case.

Pag 90: Figure 4.21 FRAP data for supported lipid bilayers (SLBs) are shown. The liquid-ordered (Lo) phase is fluorescently labelled with NBD-DSPE (green), and the liquid- disordered (Ld) phase is labelled with ATTO 655-DOPE (magenta). The scale bar represents 10 μm. At low cholesterol levels, the diffusion coefficient of the Lo phase is 0.215 $\mu m^2/s$, with a diffusion time (τ) of 4.68 seconds. As cholesterol levels increase, the diffusion time decreases to τ=1.08 seconds, and the diffusion coefficient rises. This trend indicates that the dynamics of fluorescence recovery accelerate with higher cholesterol levels, reflecting increased lipid mobility and enhanced fluidity in the Lo phase.

Pag 93: Figure 5.1 AFM Topography Images of SLBs Composed of 7 mol % Cholesterol interacting with Serum-free EVs. The images depict the temporal evolution of the SLB surface morphology during a 1-hour interaction with EVs. The time points highlight key stages in the interaction process, capturing the dynamic changes occurring at the nanometer scale. a) t_0 = after 5 min of incubation min b) t_2: Further evolution in the surface morphology is observed, indicating progressing interaction. c) t_3: A continued shift in topography d) t_4 e) t_5, f) t_6: Intermediate phase of interaction, illustrating significant morphological adaptations. g) t_7 h) t_8 = After 1 hour. A final time point showing the rapid response of the SLB, capturing smaller, rapid shifts. Each time point provides a snapshot of the lipid bilayer's response to EV exposure, contributing to an overall understanding of the interaction kinetics and potential mechanisms involved in SLB-EV binding or fusion processes.

Pag 94: Figure 5.2 a) graph depicting changes in surface area (%) over time for EVs the liquid-disordered phase (Ld), and the liquid-ordered phase (Lo) of SLBs containing 7% cholesterol, and b) a table providing the corresponding numerical surface area data for each component at different time points.

Pag 96: Figure 5.3 AFM Topography Images of SLBs Composed of 33% Cholesterol Interacting with EVs in Serum-Free Conditions across two distinct regions (Region 1 and Region 2). These images capture the evolution of SLB surface morphology during a 1-hour interaction with EVs. a) and e) t_1 = 5 min: Initial interaction stage, showing early surface modifications and the onset of lipid

reorganization or EV-SLB binding. b) and f) t_2 = 10 min: Continued surface development indicates progression in the interaction, with potential differences in responses between the two regions. c) and g) t_3 = 12 min: More pronounced topographical changes reflect deeper interactions and ongoing binding or fusion processes. d) and h) t_4 = 19 min: Significant structural alterations indicate deeper integration of EVs into the SLB, with variations in modifications observed between the regions.

Pag 97: Figure 5.4 Interaction of EVs serum free with SLBs composed of 33% cholesterol in two regions, labelled Region 1 and Region 2. Panel a) shows graphs depicting the temporal changes in surface area (%) occupied by EVs, the liquid-disordered phase (Ld), and the liquid-ordered phase (Lo) in each region. Panel b) includes tables with numerical values for the surface area (%) occupied by EVs, Ld, and Lo phases at each time point (t_1 to t_4). In both regions, the Ld phase steadily increases in surface area, while the Lo phase gradually decreases, indicating lipid raft disruption. EVs also show a consistent increase in surface area, reflecting ongoing interaction with the SLBs.

Pag 98: Figure 5.5 AFM Topography Images of SLBs composed of 7 mol% Cholesterol Interacting with EVs in Ringer buffer, highlighting two distinct regions (Region 1 and Region 2). The images capture the evolution of the SLB surface morphology during a 1-hour interaction with EVs. a) and e) t_1 = 5 min: Initial stage of interaction, showing early surface modifications in both regions, marking the onset of lipid reorganization or EV-SLB binding. b) and f) t_2 = 10 min: Further surface development, indicating the progression of interactions with potential differences in the response between the two regions. c) and g) t_3 = 15 min: More pronounced topographical shifts, reflecting deeper interactions and ongoing binding or fusion processes. d) and h) t_4 = 25 min: Significant structural changes, with clear alterations in surface morphology, suggesting strong EV-SLB interactions.

Pag 100: Figure 5.6 The figure presents two panels: a) a graph depicting changes in surface area (%) over time for the EVs, the liquid-disordered phase (Ld), and the liquid- ordered phase (Lo) of supported lipid bilayers (SLBs) containing 7% cholesterol, and b) a table providing the corresponding numerical surface area data for each component at different time points.

Pag 100: Figure 5.7 AFM Topography Images of SLBs Composed of 33% Cholesterol Interacting with EVs ringer buffer s across two distinct regions (Region 1 and Region 2). These images capture the evolution of SLB surface morphology during a 1-hour interaction with EVs. a) and e) t_1 = 5 min: Initial interaction stage, showing early surface modifications and the onset of lipid reorganization or EV-SLB binding. b) and f) t_2 = 10 min: Continued surface development indicates progression in the interaction, with potential differences in responses between the two regions. c) and g) t_3 = 15 min: More pronounced topographical changes reflect deeper interactions and ongoing binding or fusion processes. d) and h) t_4 = 23 min: Significant structural alterations indicate deeper integration of EVs into the SLB, with variations in modifications observed between the regions.

Pag 102: Figure 5.8 a) graph depicting changes in surface area (%) over time for Ringer-EVs, the liquid-disordered phase (Ld), and the liquid-ordered phase (Lo) of SLBs containing 33mol% cholesterol. b) Table providing the corresponding numerical surface area data for each component at different time points.

Pag 102: Figure 5.9 AFM topographic images illustrate the interactions between EVs and SLBs composed of DOPC, DSPC, and SM at two different cholesterol concentrations: a) and c) with 7 mol % cholesterol and b) and d) with 33 mol % cholesterol. Panels a) and b) display the topography images of the SLB with 7 mol % and 33 mol % cholesterol, respectively, interacting with serum-free EVs, along with the corresponding height profiles shown below. Panels c) and d) present the topography images of the SLB at the same cholesterol concentrations (7 mol % and 33 mol %) interacting with Ringer EVs, also accompanied by the respective height profiles below.

Pag 103: Figure 5.10 AFM topographic image of sEVs adsorbed on mica substrate with the height profiles. Vesicles have a size ranging from 13 nm to 20 nm.

Pag 108: Figure A 1.1 GUVs (2D sections) have been reported, where the entire Lo phase has been fluorescently labeled in green with NBD-DSPE and the Ld phase in magenta with ATTO655-DOPE, for the two investigated cholesterol concentrations (Panel 1). Consistent with AFM results, the area covered by the ordered domains increases with cholesterol concentration, leading to an enlargement of the ordered domains. Panel 2) shows the intensity profiles. The scale bar is 10 μm.

Pag 111: Figure A 2.1 AFM topography images and corresponding height profiles of pore-spanning membranes functionalized with a Self-Assembled Monolayer (SAM) of 6- mercaptohexanol (6MH). After functionalization, Sample 1 (top) was washed, and GUVs were incubated at 55°C for 2 hours. Top image: The AFM topography shows the surface morphology after SAM functionalization. Profiles 1 and 2 depict the cross-sectional height measurements over the designated areas, confirming uniform pore coverage with some depth variability, indicated by the differences in height in the plotted profiles. Middle (a) and bottom (b) images: These images represent the system after incubation. Profiles 1 and 2 measure the depth of the structures, revealing significant changes after incubation, potentially indicating partial pore coverage or vesicle deformation. The height profiles highlight the structural evolution post-incubation, with noticeable differences in depth and membrane coverage compared to the initial state. a) 3.5x3.5 μm b) 4x4 μm of the PSM after the spread of the GUVs. (pore diameter = 500nm).

Pag 111: Figure A.2.2 AFM topography image of pore-spanning membranes after functionalization with a self- assembled monolayer (SAM) of 6MH. The pore diameter is 500 nm, and the image size is 8x8 μm, with a 2-hour incubation time of the GUVs. The height profiles corresponding to the blue, red, and black lines are plotted on the right, illustrating variations in surface topography.

Chapter 1: The context

1.1 Plasma membrane (PM) biophysics through nanoscale tools and techniques

In the word Nanotechnology, the prefix ‘nano’ originates from the Greek word meaning ‘dwarf’ or something very small and denotes one billionth of a meter (10^{-9} m) [1]. This multidisciplinary field involves the engineering and the manipulation of materials at the nanoscale level, ranging from 1 to 100 nm [2]. At this scale, materials exhibit unique properties due to surface and quantum effects, which differ from those at bulk scales, enabling the development of novel materials, devices, and systems [3]. R. Feynman is considered the father of nanotechnology, as he first introduced the concept of manipulating matter at an atomic level [4]. This discipline, which combines science and technology, has resulted in some of the most astonishing scientific breakthroughs and led to the greatest increase in knowledge in the life sciences over the last few decades [5-7].

In the field of biophysics, nanotechnology plays a pivotal role in advancing biological engineering by enabling the design and synthesis of complex systems that are either biologically based or biologically inspired. Through the manipulation of materials at the nanoscale, scientists can create nano systems that mimic natural biological processes or enhance existing biological functions. This includes the development of nanomaterials for drug delivery, where nanoparticles can target specific cells or tissues with high precision, and the engineering of biosensors that can detect and monitor biological molecules at extremely low concentrations. Nanotechnology also facilitates the creation of biomimetic structures, such as artificial cells or nanostructured scaffolds for tissue regeneration, pushing the boundaries of what is possible in synthetic biology and medicine. In addition, the possibility to build nanoscale devices has implications that will influence diverse fields, such as nanomedicine, and anticancer therapies and diagnostics [8]. This approach is expected to facilitate the rational and systematic design of systems applicable across all scales of biological structures, from individual molecules to entire cells [9]. The most important functional part of the cells is the cell membrane, widely acknowledged as complex systems [10]. However, there is no universally accepted definition of a "complex system." In biology, every form of life is considered complex, even if it is unicellular [11]. Within the realm of complexity, terms like "self-organization" and "coexistence" are commonly recognized as features that characterize complexity. [12] The term "Complex" originates from the Latin verb "cum-plectere," which translates to "to intertwine together.” (P.L. Gentili). It holds a distinct etymology from the word "complicated," despite often being considered synonymous in everyday language. "Complicated" stems from the Latin verb "cum-plicare," meaning "to fold together." What is deemed "complicated" is intricately folded and therefore capable of being unfolded. Conversely, what is labelled "complex" is interwoven and cannot simply be unfolded; instead, it requires untangling (P.L.Gentili, 2018). Over the past decades, research has been focused on

understanding the mechanisms governing the organization of cell membranes and the interactions that regulate cellular life. The plasma membrane is fluid, meaning that its component proteins and lipids can move laterally within the membrane's plane, allowing for a flexible and dynamic structure [13-15]. This fluidity enables the membrane to rapidly adapt to various environmental and cellular stimuli, such as changes in temperature, mechanical stress, or interactions with other cells. The lateral mobility of proteins and lipids is crucial for many cellular processes, including signal transduction, membrane trafficking, and the formation of specialized domains like lipid rafts. These dynamic changes in membrane composition and structure are essential for the cell's ability to respond to external signals, maintain homeostasis, and regulate interactions with its surroundings. The identification of the molecular origins of many interactions that dictate the dynamic lateral organization and mobility of membrane lipids and proteins remains challenging as well as membrane protein biogenesis and multi-subunit protein complex assembly [16]. This deficit in molecular detail stands in contrast to other areas of cell biology where significant progress has been achieved in pinpointing the molecules involved in various phenomena. For example, there is extensive literature on membrane transport and ion channels, as well as studies on the electrical properties of cell membranes. These studies have shed light on the mechanisms of nutrient uptake, ion balance, and signal transmission across membranes [17-18]. However, when focusing on the potential role of specific lipids or classes of proteins in driving reactions at the membrane interface or modulating the membrane itself, there remains a lack of precise data associating a particular species with a specific role [19]. This challenge arises from the difficulty in studying the isolated behaviour of a single species within the membrane, especially in in vivo experiments. Despite advances in understanding membrane transport, ion channels, and the electrical properties of cell membranes, pinpointing the exact contributions of individual lipids or proteins is still challenging due to the complex and dynamic nature of membrane environments [20]. To understand the driving forces behind the structural and dynamic organization of cellular membranes, computer simulations have become indispensable [21,22]. However, the scientific community is also questing for experimental platforms. In response to this, to follow such complexity biomimetic lipid membranes have been recognized as powerful tool to elucidate crucial processes that regulates cellular life [23-27]. The fundamental structure of the cell membrane is the phospholipid bilayer, which forms a stable barrier between two aqueous compartments. Proteins embedded within the phospholipid bilayer perform specific functions, such as selective transport of molecules and cell-cell recognition. Experimental models have been developed with the aim of preserving this structure, whether in a planar supported form (such as SLBs and suspended lipid bilayers) or in a spherical shape (like liposomes and GUVs). Biomimetic membranes offer a groundbreaking method for selectively investigating the roles of lipids and proteins in modulating plasma membrane activity. These advanced artificial systems can be meticulously engineered to replicate the composition and functionality of biological membranes, enabling researchers to explore the intricate mechanisms governing membrane-related processes in a controlled environment. By closely mimicking essential properties such as lipid bilayer fluidity,

asymmetry, and protein distribution, biomimetic membranes facilitate the study of critical phenomena, including membrane fusion, protein-lipid interactions, and signalling dynamics. These platforms not only deepen our understanding of fundamental biological processes but also allow for real-time hypothesis testing, paving the way for innovative therapeutic strategies and targeted drug delivery systems. Moreover, the capacity to systematically manipulate lipid compositions and protein expressions within these models empowers researchers to dissect the contributions of specific membrane components across various physiological and pathological contexts. This precise control is invaluable for elucidating the complex interplay between membrane structure and function, ultimately advancing our understanding of cellular processes and disease mechanisms. One of the most distinctive features of biomimetic membranes is the ability to precisely regulate environmental factors such as species concentration at different temperature, and humidity level. This control allows for the detailed examination of how external conditions influence membrane fluidity, protein-lipid interactions, and the organization of membrane sub-domains. Furthermore, biomimetic membranes can be tailored with specific physiological buffers, making them ideal for studying cellular processes under near-native conditions. The field of membrane biophysics is diverse and can be broadly divided into two distinct and competing themes, as illustrated in Figure 1.1. The top-down approach designs systems based on a natural organism, which serves as a host for engineering new functions (GPMVs). In contrast, the bottom-up methodologies focused on assembling artificial biomimetic systems from fundamental biological or synthetic compounds, with the goal of creating functional synthetic cell machinery. This approach starts with individual components such as lipids, proteins, nucleic acids, and other biomolecules, which are then organized into more complex structures. By precisely controlling the assembly of these basic building blocks, researchers can recreate the behaviour of living cells key cellular functions, such as membrane formation and signalling pathways.

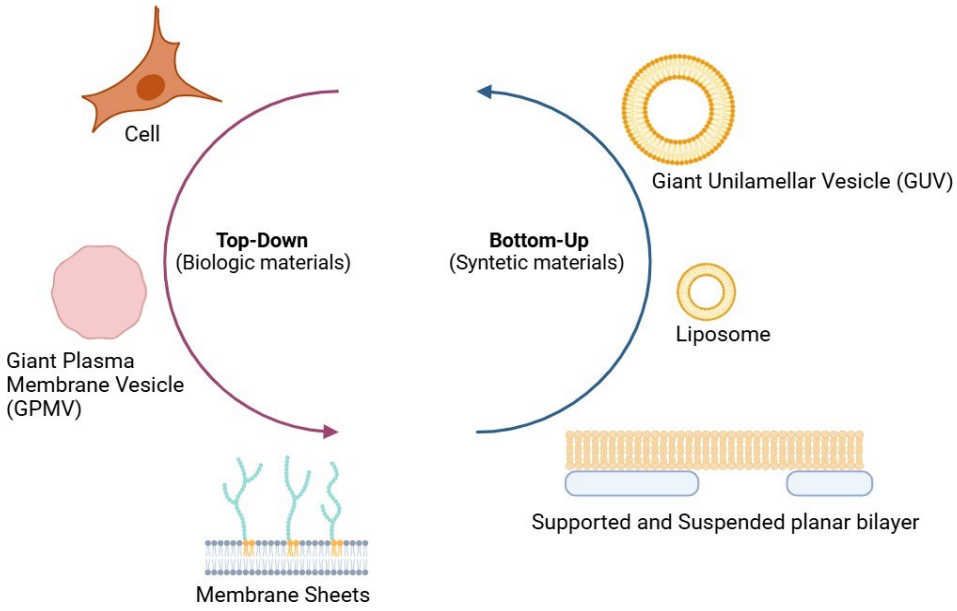

Figure 1.1 Model systems for studying cellular membranes can be categorized into two main approaches: top-down approach simplifying the complexity of cellular structures by isolating specific membrane components from the cell. It focuses on examining these individual parts to understand their roles and interactions within the broader membrane context. In contrast, bottom-up approach builds increasingly complex membrane systems using synthetic materials. It aims to recreate or model membrane properties by assembling components from the molecular level up to more intricate structures. Reproduced from [27].

In this work, we have employed a bottom-up approach to reconstitute complex model systems of eukaryotic cell membranes, specifically focusing on understanding lipid organization. By systematically incorporating a diverse array of lipids, including phospholipids, cholesterol, and sphingolipids, we investigated how their interactions influence membrane fluidity, phase separation, and the formation of lipid rafts. These insights are crucial for elucidating the biophysical principles underlying membrane dynamics and their impact on cellular functions, such as signal transduction, membrane trafficking, and protein sorting. Furthermore, this approach not only enhances our understanding of lipid organization but also provides a versatile platform for studying the effects of various physiological conditions, including changes in temperature, pH, and ionic strength, on membrane behaviour. These model systems were meticulously characterized using a combination of advanced techniques, including atomic force microscopy imaging and force spectroscopy, dynamic fluorescence microscopy, and differential scanning calorimetry. This comprehensive approach provided detailed insights into lipid organization and interactions within the membrane, revealing key aspects of membrane structure and dynamics. This research not only deepens our understanding of lipid organization at the molecular level but also contributes to broader efforts in developing synthetic systems that mimic natural membrane environments, providing valuable insights for applications in the field of membrane biophysics.

Chapter 2: Introduction

2.1 PM: Highly complex and dynamic systems

The eukaryotic PM is an intricate and dynamic structure essential for maintaining cellular integrity and supporting a range of vital cellular functions. Composed of a diverse array of lipids, proteins, and carbohydrates, this membrane not only serves as a selective barrier that regulates the exchange of substances between the cell and its environment but also plays a key role in cellular communication, signal transduction, and membrane trafficking. Its fluid and adaptable nature allows the membrane to respond to environmental changes and cellular needs, thereby facilitating processes such as endocytosis, exocytosis, and cellular adhesion [28-29]. The composition of the PM is highly heterogeneous. The lipid bilayer, which forms the fundamental structural framework, is primarily composed of phospholipids, cholesterol, and sphingolipids [30-32]. This diverse lipid composition contributes to the membrane's complexity and functionality, supporting its role in maintaining cellular integrity and facilitating various cellular processes. Proteins embedded within this bilayer, including integral and peripheral proteins, serve various functions such as transport, signalling, and maintaining the membrane's structural integrity [33,34]. In addition to these major components, the plasma membrane also contains glycoproteins and lipoproteins, which contribute to cell recognition and signalling. Water and ions, although present in smaller amounts, are essential for maintaining osmotic balance and facilitating biochemical processes within the cell [35]. These components create a highly complex and dynamic environment, which presents significant challenges for exploration and study. Historically, the initial model proposed by Singer and Nicolson in 1972 [36] characterized the PM as a fluid mosaic, where lipids are arranged in a fluid state and membrane proteins diffuse within this fluid matrix. This model did not account for any lateral organization within the membrane. Nowadays, the description of the PM has changed drastically, starting with the studies of Klausner and Wolf in 1980. In fact, the lipid bilayer has a lateral organization and in lipids self-organize. In this scenario the heterogeneous lateral distribution is due to the preferential interaction of cholesterol and sphingolipids into a nanometer domains called lipid rafts. The functional diversity of the membrane arises from the varied local organization of lipids and proteins, the presence of the LRs and the differences in structural profiles and composition across different regions of the membrane. PM is an asymmetric system, meaning the outer and inner leaflets have different lipid compositions, which is important for membrane curvature and signalling [37]. The asymmetry of the PM is not only due to the differing lipid compositions of the two leaflets but also to variations in the degree of saturation of the acyl chains and the polarity of the head groups. These features contribute to the distinct biophysical properties of each leaflet. For instance, the outer leaflet is typically enriched with phosphatidylcholine and sphingomyelin, which often have saturated acyl chains, while the inner leaflet contains more phosphatidylethanolamine and phosphatidylserine, which generally have unsaturated acyl chains [38]. Studies have shown that this lipid asymmetry is crucial for the proper

functioning of cellular membranes. It is well accepted that the plasma membrane of eukaryotic cells is composed of approximately 65% phospholipids, 10% sphingolipids, and 25% sterols. Specifically, the outer leaflet is predominantly composed of phosphatidylcholine (PC) lipids, as well as sphingolipids like sphingomyelin and glycosphingolipids. In contrast, the inner leaflet mainly consists of phosphatidylethanolamine (PE) lipids, and negatively charged phosphatidylserine (PS) lipids [39]. PS lipids are known to be predominantly located in the inner leaflet of the plasma membrane, contributing to the membrane's asymmetry and playing a critical role in cellular signalling and membrane structure. Figure 2.1 summarizes the PM asymmetry.

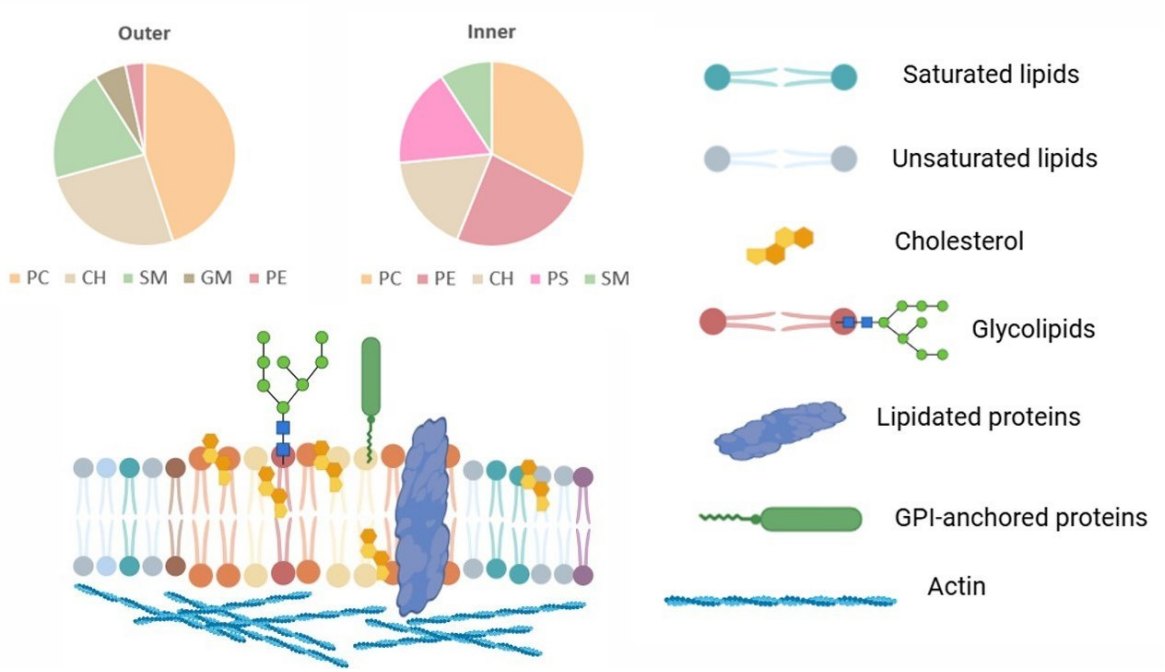

Figure 2.1 In the PM of normal eukaryotic cells, phosphatidylcholine (PC) and sphingomyelin (SM) are predominantly present in the outer leaflet. Phosphatidylethanolamine (PE) and phosphatidylinositol (PI) primarily reside in the inner leaflet, while phosphatidylserine (PS) is almost exclusively located in the inner leaflet of the plasma membrane. Readapted from [38].

2.2 Lipids: The building blocks of the PM

Lipids are the most abundant species in the PM, that self-assemble to form the lipid bilayer. Lipid bilayer plays crucial roles as energy reserves, signalling molecule sources, and scaffolds for protein binding [41-43]. Lipid bilayer consist of a diverse group of lipids characterized by their solubility in non-polar organic solvents, such as chloroform, and their insolubility in water [44]. Lipids can be either hydrophobic or amphiphilic. Amphiphilic lipids, with their hydrophilic head and hydrophobic tail, are crucial for forming cellular membranes, where they self-assemble into bilayers, creating a stable barrier between the aqueous environments inside and outside the cell. This dual nature allows them to align into a monolayer, with the hydrophilic heads facing the water and the hydrophobic tails facing each other. PM encases the cell, distinguishing it from the extracellular environment, while internal membranes compartmentalize various metabolic processes within organelles. Lipids exhibit

a remarkable diversity, which can be classified from a chemical perspective due to their varied chemical structures. Each lipid possesses a unique structure, allowing for the existence of stereoisomers that exhibit distinct chemical properties. Additionally, lipids differ in their composition, particularly in the ratios in which they are present within cellular membranes. This diversity is exemplified by the varying lipid compositions found in different organelles and membrane subdomains. The compositional diversity between the lipids is relevant because affects the collective behaviour of the lipids in membrane. As reported in the figure 3 lipids (glycerophospholipids, sphingolipids and sterols), can be classified according to their origin into 3 main classes: Glycerophospholipids are the principal constituents of the lipid mass in eukaryotic plasma membranes, with phosphatidylcholine being the most abundant class. They originate from a glycerol backbone and are composed of a hydrophilic head group (usually containing a phosphate) and two hydrophobic fatty acid tails. Sphingolipids are characterized by a backbone composed of sphingosine, a long-chain amino alcohol, instead of glycerol, which is typical of other types of lipids like glycerophospholipids [45]. This class of lipids is characterized by the presence of a hydroxyl and an amide group between the polar head group and the non-polar hydrocarbon chain. The hydroxyl group of sphingosine acts as a hydrogen bond donor, while the amide group serves as a hydrogen bond acceptor. In this chemical configuration, the primary interactions between sphingolipid molecules occur within the plane of the membrane [46]. Sphingomyelin is the most prominent component of this category and is primarily found in the external leaflet of the membrane, similar to other lipids in this group, as ceramides. Unlike glycerophospholipids and sphingolipids, which share a similar structure, sterols consist of a steroid motif with a hydroxyl group at carbon 3 and a side chain at carbon 17. [47] This class of lipids is crucial for maintaining membrane properties, such as rigidity and fluidity. The most abundant sterol in PM is cholesterol and unlike glycerophospholipids and sphingolipids, have similar structures, cholesterol features a 5-ring backbone structure attached to a hydroxyl group. This hydroxyl group interacts with water and the polar head groups of adjacent lipids. Cholesterol is a crucial component of cellular membranes, where it modulates membrane fluidity, stability, and permeability.

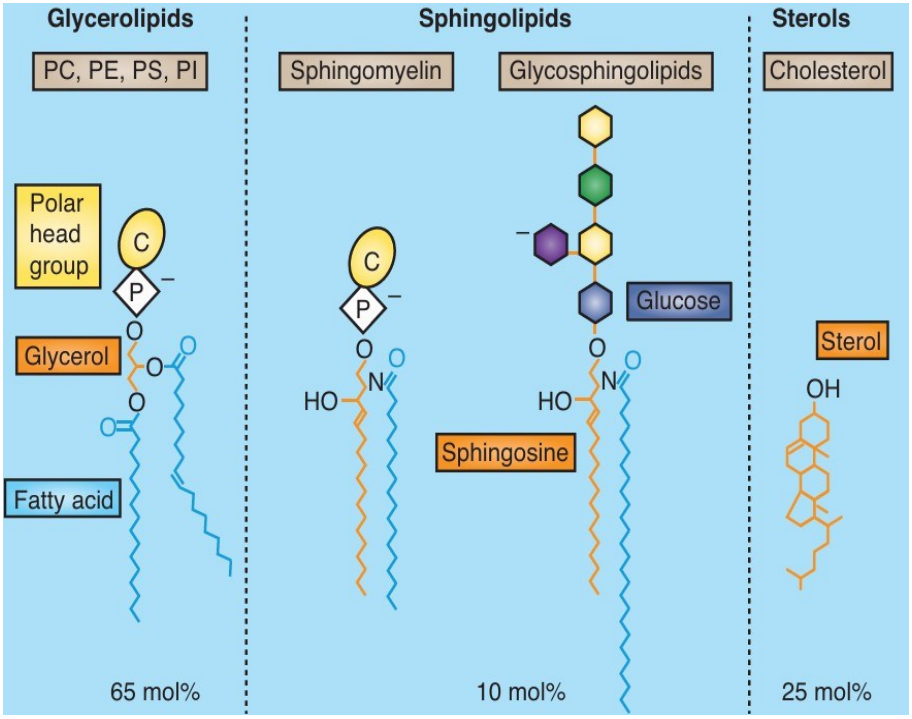

Figure 2.2 Lipids in mammals exhibit a wide structural and functional diversity. Phospholipids, including phosphatidylcholine (PC), phosphatidylethanolamine (PE), phosphatidylserine (PS), and phosphatidylinositol (PI), are characterized by a glycerol backbone. Sphingolipids, such as sphingomyelin, are defined by the presence of a sphingosine backbone. Sterols, exemplified by cholesterol, possess a distinctive four-ring core structure. Glycolipids, including glycosphingolipids, are distinguished by the incorporation of carbohydrate residues into their molecular framework [48].

As mentioned previously, the lipid bilayer is a fluid system, and its overall fluidity is influenced by the length and degree of unsaturation of the acyl chains, as well as by the temperature [48]. The Tm of lipids is a critical parameter that determines the physical state of lipids within a membrane, and it is influenced by factors such as the length and saturation of their fatty acid chains. At the Tm, the lipid bilayer transitions from a gel-like solid state, where lipids are tightly packed with limited mobility, to a more fluid state with increased lipid mobility. Below the Tm, lipids exist in a solid or gel phase, characterized by ordered fatty acid chains and low membrane fluidity. Above the Tm, they enter the liquid-crystalline phase, becoming more disordered and enhancing membrane fluidity. The fluidity enables molecules to diffuse within the plane of the lipid bilayer, allowing them to interact with each other. Such interactions are essential for regulating crucial cellular processes, including cell division, movement, and growth. Changes in fluidity can significantly impact cellular processes by altering the behaviour and interactions of membrane components [49]. This membrane property is closely related to another important characteristic: viscosity. When the acyl chains are more tightly packed together, membrane fluidity decreases. More generally, fluidity refers to the movement of lipids within the membrane. As reported in several studies, lipids can diffuse transversely across the membrane plane, migrating between the two membrane leaflets in a process known as flip-flop [50-51] This movement is slow because it requires the relocation of the hydrophilic lipid headgroup into the hydrophobic

region of the plasma membrane. This process is energetically unfavourable, which is why flip-flop typically occurs on a time scale ranging from seconds to minutes for lipids such as ceramide and cholesterol, while it can extend to hours or days for phosphatidylcholine (PC) and sphingomyelin. The rate of this movement depends on the lipid composition and the presence of specific proteins, such as flippases, which facilitate this translocation [52]. In addition to flip-flop, lipids also move laterally within the leaflets via lateral diffusion [53]. This type of movement can lead to membrane heterogeneities, where specific lipids, such as SM and cholesterol, cluster into distinct membrane domains [54]. From the other hand, lateral diffusion is the movement of lipids within the same leaflet of the bilayer. This process is relatively fast, with lipids moving laterally at a rate on the order of μs to second, enabling the lipid bilayer to remain fluid and dynamic. Phosphatidylcholine molecules with saturated and longer acyl chains tend to pack closely together, whereas those with unsaturated and shorter chains are less tightly packed due to the presence of C-C double bonds in the acyl chains. Temperature also affects membrane fluidity: at lower temperatures, membranes with saturated acyl chains become more rigid, while higher temperatures increase membrane fluidity by reducing packing density [55]. Apart of the lipids the most abundant species of the PM are the proteins that have a different functionality within the PM. Membrane proteins, though fewer in number than lipids, account for about 50% of the membrane's mass due to their large molecular size [56]. Transmembrane and peripheral proteins are the most abundant in the PM and they play crucial roles in the structure and function. Transmembrane proteins (30% of the lipidome) penetrate and span the entire lipid bilayer, often with segments embedded within the hydrophobic core of the membrane. These proteins have hydrophilic regions that protrude into the extracellular and cytoplasmic environments. One of the primary roles of transmembrane proteins is transport. They form channels and pores, allowing specific ions and molecules to cross the membrane. Additionally, transmembrane proteins are key players in signal transduction. Acting as receptors, they bind to signalling molecules. This binding trigger intracellular signalling pathways that regulate various cellular responses [57]. Peripheral proteins, on the other hand, are attached to the membrane's surface, either on the cytoplasmic or extracellular side. They interact with transmembrane proteins or lipid polar head groups and do not penetrate the hydrophobic core. Peripheral proteins are deeply involved in signal transduction [58]. They relay signals received by transmembrane receptors to intracellular targets, amplifying and regulating these signals. Furthermore, peripheral proteins link the plasma membrane to the cytoskeleton, aiding in maintaining cell shape, facilitating movement, and supporting intracellular transport [59]. Additionally, peripheral proteins help organize and stabilize membrane microdomains, contributing to the formation and maintenance of lipid rafts and other specialized regions. Another class of protein in the PM are the lipoproteins, chemically attached to membrane lipids and can be found on both sides of the membrane. Water, the solvent for all molecules in living matter, is incorporated in cell membranes either as bound water to the polar groups exposed on the membrane molecules or as unbound (bulk) water within pores and ionic channels. Ions are associated with membranes through adsorption to the membrane surfaces or by transiting through ionic

channels or ion pumps. Overall, membrane proteins, both integral and peripheral, are vital for the proper functioning of the eukaryotic plasma membrane. Another class of membrane components is the Glycolipids, that are combinations of simple sugars and lipids, where glucose is covalently attached to the lipid sphingosine. Cell membranes contain 2–10% glycolipids, which are involved in various cellular processes. The interaction between membrane proteins and sugars generates glycoproteins that are exposed exclusively on the extracellular side of the membrane, forming the glycocalyx. [60] Common ions associated with membrane structure and functions include H^+, Na^+, K^+, Cl^-, Ca^{++}, and HCO_3^-. The presence and interaction of these components ensure the structural integrity and functionality of the plasma membrane, enabling it to perform a wide range of biological activities. Eukaryotic cells continuously change their lipid composition throughout their life, adapting in response to various stimuli. According to the literature, it is well accepted that the plasma membrane of healthy cells is composed of approximately 50% lipids and 50% proteins, with sugars and other components present in smaller amounts. Another important characteristic of the plasma membrane is that the lipid bilayers exhibit different lipid compositions between the two leaflets, making the investigation of lipid activity even more challenging. This complexity and variability in lipid composition are crucial for cellular function, affecting membrane fluidity, signalling pathways, and interactions with the cellular environment. Several papers in literature reported that the lipid deregulation is involved in several disease, for instance cancer and metabolic disease. Advanced techniques such as fluorescence microscopy, mass spectrometry, and nuclear magnetic resonance (NMR) spectroscopy are often employed to study these dynamic changes in membrane composition and function in real-time. Understanding these dynamics is essential for comprehending various cellular processes, including cell signalling, membrane trafficking, and cellular responses to external stimuli. Figure 2.3 [61] illustrate the various types of lipid movements within a membrane, along with their corresponding time and length scales. Depending on the process to be studied, it is necessary to use a specific technique capable of probing a specific time range. For example, imaging methods (Fluorescence microscopy and atomic force microscopy) are ideal for studying rapid lipid dynamics and molecular interactions occurring on the scale of seconds to minutes.

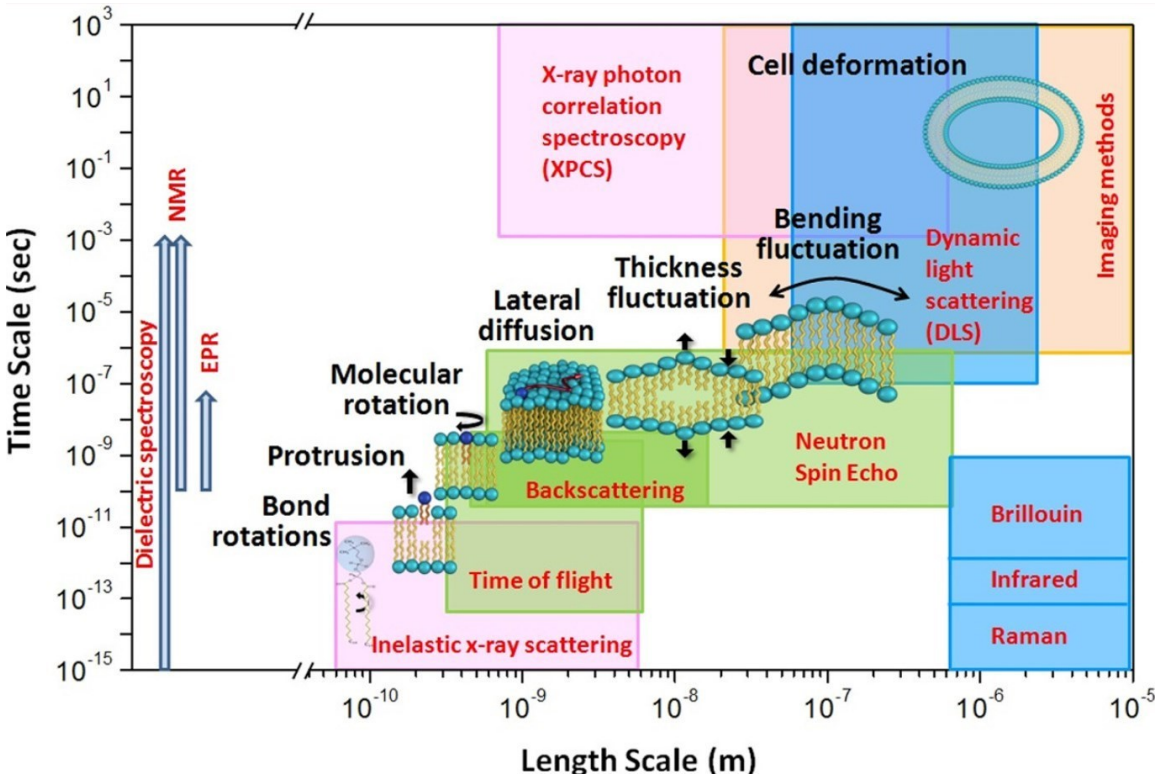

Figure 2.3 The types of lipid movements within a membrane, along with their corresponding time and length scales. [61]

2.3 Cholesterol: The Architect of Membrane Structure and Function

Cholesterol is an essential structural component of the plasma membrane, playing a crucial role in defining its integrity, functional and dynamic behaviour [63]. Chemically, cholesterol interacts with the fatty acid chains of phospholipids, inserting itself between them to prevent tight packing [64]. This action modulates the membrane's fluidity, making it less permeable to small molecules and ions while enhancing its mechanical stability. The hydroxyl group (-OH) located at the 3-position on the A-ring is the only hydrophilic part of the cholesterol molecule. When cholesterol is embedded in the membrane, this polar group extends toward the aqueous environment, allowing it to interact with the polar head groups of phospholipids. At the 17- position on the D-ring, cholesterol has a branched hydrocarbon chain. This nonpolar, hydrophobic tail interacts with the fatty acid chains of phospholipids within the membrane, contributing to cholesterol's role in stabilizing the lipid bilayer. By maintaining an optimal level of fluidity, cholesterol ensures that the membrane remains sufficiently flexible to accommodate various physiological processes without compromising its barrier function [65,66]. From a biophysical perspective, cholesterol is a key regulator of membrane organization, particularly in the formation of lipid rafts. These are specialized, cholesterol- enriched domains that provide a more ordered and tightly packed environment compared to the surrounding membrane [67]. Lipid rafts play a crucial role in the lateral segregation of proteins and lipids, enabling the clustering of signalling molecules and receptors essential for efficient signal transduction and membrane trafficking processes [68]. The formation and modulation of these membrane domains by

cholesterol are particularly relevant in the pathogenesis of various diseases, including breast cancer [69]. Cholesterol-rich lipid rafts for instance, play a crucial role in enhancing the clustering and activation of growth factor receptors like HER2/neu, resulting in stronger signalling that promotes cell division and tumour growth. HER2/neu, part of the epidermal growth factor receptor (EGFR) family, is key to regulating cell growth and survival. Elevated cholesterol stabilizes HER2/neu within lipid rafts, increasing its concentration and activity, which amplifies signal transduction, leading to enhanced cell proliferation and resistance to apoptosis. In HER2-positive breast cancer, hypercholesterolemia can worsen outcomes by intensifying growth signalling through these lipid rafts. This suggests that targeting cholesterol metabolism or disrupting lipid raft formation could be potential therapeutic strategies for inhibiting HER2-driven cancers [70- 71]. Research shows that in estrogenic receptor-positive (ER+) breast cancer, elevated cholesterol levels are linked to more aggressive tumor characteristics and a poorer prognosis.

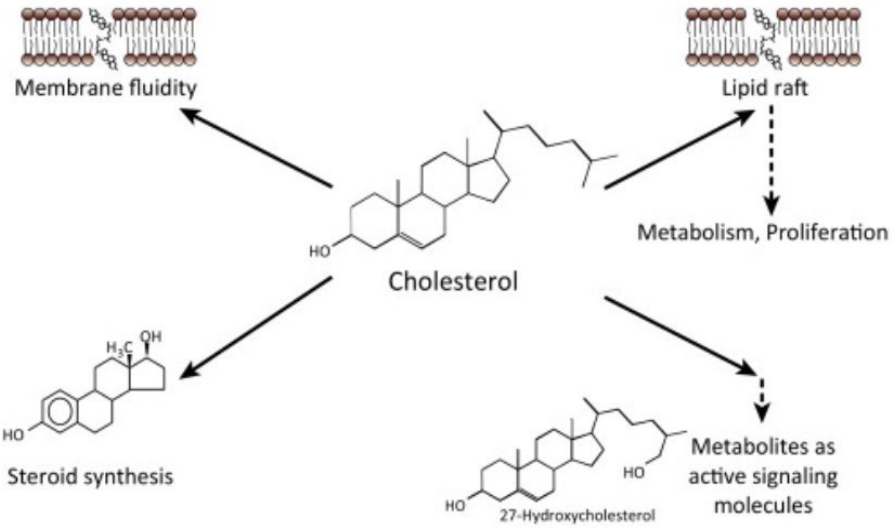

Figure 2.4 Cholesterol plays a vital role in various cellular functions, particularly in cancer cell biology. It is crucial for membrane synthesis and may become a limiting factor in rapidly proliferating cancer cells. Cholesterol also facilitates the formation of lipid rafts, which are essential for signalling pathways like AKT (polyglutamine-containing protein that participates in transcriptional regulation and neuronal health.) It regulates gene expression and interacts with other proteins to influence cellular signalling pathways that drive cell survival and growth. Moreover, cholesterol serves as a precursor for steroid hormone synthesis. Recent studies reveal that cholesterol metabolites, such as 27-hydroxycholesterol (27HC), can activate signalling through estrogenic receptors (ER) or liver X receptors (LXR), contributing to breast cancer progression. Figure from [71].

Cholesterol's role in the formation of lipid rafts is particularly important in this subtype, as it can enhance the signalling pathways that drive cancer cell growth and survival [72]. Cholesterol's rigid ring structure and its ability to induce order in adjacent lipid molecules are fundamental to the stability and function of these rafts. Cholesterol also influences the membrane's mechanical properties [73,74] such as elasticity, thickness, and curvature, which are vital for cellular processes like vesicle

formation, membrane fusion, and endocytosis. By increasing bilayer thickness and reducing membrane compressibility, cholesterol enhances the membrane's resistance to deformation, thereby playing a critical role in the mechanics of vesicle budding and fusion. These properties are particularly important in the context of extracellular vesicles, small, membrane-bound particles released by cells into the extracellular environment The presence of cholesterol in both the EV membrane and the target cell membrane can significantly impact the efficiency of vesicle docking, fusion, and cargo delivery, thereby influencing intercellular communication and various physiological and pathological processes, including those relevant to therapeutic applications. Cholesterol's impact on the structural and functional aspects of the plasma membrane underlines its importance in maintaining cellular homeostasis and its potential as a target for modulating membrane- associated processes in various diseases [75].

2.4 Membrane phases and lipid rafts

The relative dimensions of the lipid head group and hydrophobic tails critically influence the lipid's shape and the membrane's intrinsic curvature. Consequently, lipid composition can be regulated to facilitate membrane deformation via spontaneous curvature [76]. Lipids with elongated and saturated fatty acid chains, such as sphingolipids, contribute to membrane thickening and reduced fluidity due to the dense packing of their hydrophobic tails and enhanced lipid–lipid interactions [77]. This tight packing results in a more rigid membrane structure. In contrast, lipids containing unsaturated fatty acids exhibit kinks in their acyl chains, hindering close packing, and thereby increasing membrane fluidity. One way that lipids execute their functions is through modulating membrane physicochemical properties. Depending on the composition and temperature, the lipid bilayer can exhibit different levels of order and fluidity [78,79]. Each lipid has a specific parameter known as the Tm (transition temperature), which defines the density of lipid packing within the membrane. The Tm is the temperature at which a lipid transitions from a more ordered, gel-like state to a more fluid, liquid-crystalline state [80]. This transition impacts the overall fluidity and functionality of the membrane, influencing processes such as membrane protein activity, diffusion of molecules, and membrane fusion. At a given temperature, the lipid bilayer can exist in either a Ld phase or a gel phase (So), (in absence of cholesterol). These phases can transform into each other through different kinds of phase transitions that are reversible. In the gel phase, lipids have fully extended and closely packed acyl chains, whereas in the liquid disordered phase, the acyl chains are randomly oriented and fluid. As the length of the hydrocarbon chains increases, van der Waals interactions become stronger, requiring more energy to disrupt the ordered packing. Consequently, the phase transition temperature increases. The presence of a cis double bond into the acyl group introduces a kink in the chain, which requires much lower temperatures to induce an ordered packing arrangement. Lipids like sphingomyelin or DSPC usually have higher transition temperatures compared to unsaturated ones like DOPC.

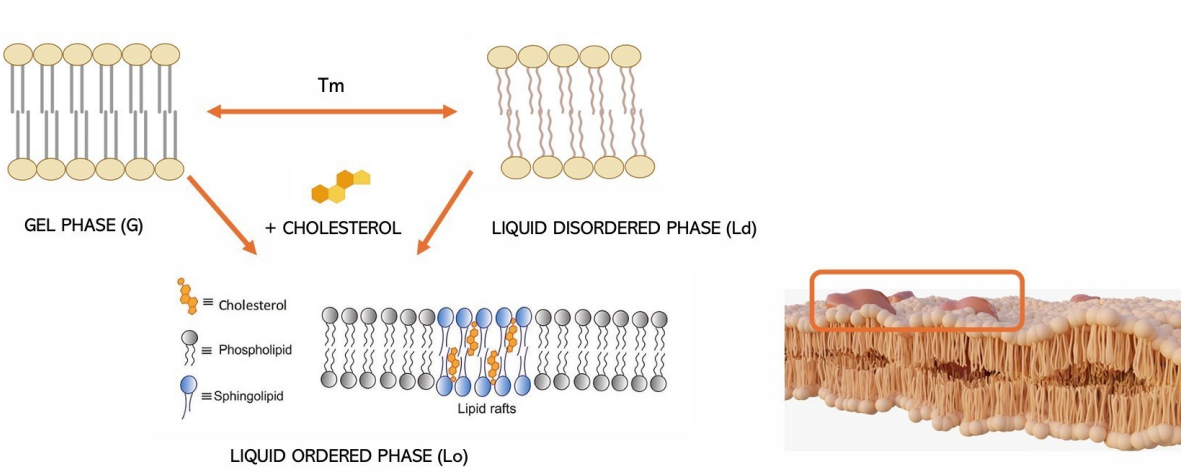

Figure 2.5 Schematic representation of lipids phase transition. Above a certain melting temperature and in the absence of cholesterol, lipid membranes undergo reversible phase transitions from a gel phase (So) to a Ld phase. In the presence of cholesterol, membranes can adopt a Lo phase, which is an intermediate state between the gel phase and the disordered phase. Preferential interaction of Cholesterol with sphingolipids. Adapted from Barba-Bon et al., 2020 [81].

The presence of cholesterol significantly increases the complexity of the membrane since it is involved in the formation of an important phase known as the Lo phase. Cholesterol interacts with both saturated and unsaturated lipids, modulating the membrane's fluidity and stability [82]. Despite its ability to interact with both lipid phases, cholesterol has been shown to prefer interacting with ordered unsaturated lipids like sphingomyelin, although the exact reasons for this preference are not entirely clear. By doing so, it helps create regions within the membrane that exhibit a higher degree of order compared to the more fluid, disordered regions, thereby contributing to the functional compartmentalization of the membrane. Cholesterol can induce stiffening in liquid-disordered membranes while simultaneously increasing fluidity in gel- phase membranes. Since cholesterol molecules preferentially interact with saturated lipids, regions of the membrane rich in saturated lipids become enriched with cholesterol, forming Lo domains. These domains are commonly known as lipid rafts [83]. This local phase separation suggests that the plasma membrane contains lateral heterogeneities characterized by the ability to recruit membrane proteins. Membrane rafts are defined as small (10-200 nm), heterogeneous, and highly dynamic domains enriched in sterols and sphingolipids, which compartmentalize cellular processes [84,85]. These small rafts can sometimes be stabilized into larger platforms through protein-protein and protein-lipid interactions. For instance, cholesterol and sphingolipids stabilize these nanodomains through hydrogen bonding and interactions between their saturated hydrophobic chains. This demonstrates that sterols and sphingolipids function synergistically due to their specific interactions. Additionally, lipids interact across the bilayer, not just within it. These lipid-lipid interactions are crucial for the formation of nanodomains and influence other membrane-associated processes by collectively affecting membrane properties. This underscores the multifaceted roles of lipids in maintaining the structural and functional integrity of cellular membranes. The membrane functions as more than just a simple

barrier; it acts as a two-dimensional reaction platform for a multitude of biochemical processes. To facilitate these reactions efficiently and rapidly, it has been proposed that the membrane is compartmentalized. This compartmentalization optimizes local environments for the activity of specific membrane proteins. Although many biological functions depend on local environments with specific compositions, the physical nature and driving forces behind their formation remain subjects of ongoing discussion. Various types of microdomains have been identified. The "lipid raft" model posits that lipid composition is the primary driving force for membrane heterogeneity. Artificial membranes composed of (unsaturated) phospholipids, (fully saturated) sphingolipids, and cholesterol spontaneously phase separate into a (liquid-ordered) "raft" phase and a liquid-disordered phase. Phases, which differ in their lipid tail organization, can differentially segregate proteins in vitro [86]. The simplistic binary model of the cell membrane, divided into raft and non-raft regions, fails to capture its complexity. The membrane consists of more than just three types of lipids, which could lead to the formation of multiple liquid phases with distinct properties. Even in membranes with only three components, asymmetry between the two leaflets can result in the presence of three distinct phases. Moreover, the concept of lipid rafts as stable structures has been called into question. Recent experiments suggest that live cell membranes, at physiological temperatures, are near a miscibility critical point, causing substantial fluctuations in composition. A key question is whether these fluctuations last long enough to drive significant protein segregation. These fluctuations may also be linked to and stabilized by membrane shape changes. Interestingly, even heterogeneous model systems that show no visible phase separation above the miscibility critical temperature have demonstrated inhomogeneities on the scale of tens of nanometers. This implies that membrane organization can occur on a nanometric scale, even in the absence of clear phase separation [87]. One of the major challenges that continues to spark controversy when discussing lipid rafts is the fact that they are extremely difficult to visualize and study in real cell membranes. Various studies provide evidence for the presence of lipid rafts, but due to their nanometric size and their fast dynamics, they are very challenging to study in real systems as they require super- resolution techniques. However, model membrane systems come into play here, as they have allowed researchers to demonstrate and, more importantly, study lipid rafts.

2.5 The context: Biomimetic PM

Biomimetic membranes, which mimic the structure and function of natural biological membranes, have proven to be invaluable in deepening our understanding of lipid behaviour and phase transitions. These artificial systems leverage principles drawn from the complex and highly evolved design of biological membranes, providing insights that are often difficult to obtain through traditional methods [88]. Biomimetic membranes incorporate key elements and principles inspired by nature, such as the lipid bilayer's composition and organization, allowing researchers to replicate and study the dynamic characteristics of biological membranes under controlled conditions. This approach allows for the investigation of key aspects of lipid behaviour, including how lipids interact, organize, and respond to

environmental changes. Biomimetic membranes offer valuable insights into the complex nature of phase transitions in lipid systems. In natural membranes, lipids are not evenly distributed; rather, they form distinct domains with varying levels of order and fluidity. Biomimetic membranes are exceptionally powerful tools in biophysics research due to their ability to closely replicate the structure and functionality of natural biological membranes. Table 2.1 outlines the advantages of developing model bio membranes.

Controlled Environment	Mimicking Natural Systems	Studying Lipid Behavior and Phase Transitions	Modeling Complex Interactions	Advancing Technology Development	Exploring Disease Mechanisms
Recreate and manipulate specific membrane conditions in a controlled laboratory setting	Biological membranes function in their native context	Observation of how lipids arrange themselves into ordered and disordered phases	Including proteins, lipids, and extracellular vesicles	Drug delivery systems	Study of alterations in membrane properties
Vary lipid compositions	Phase transitions	Revealing insights into membrane fluidity, stability	Integration of various components	Biosensors	Understanding membrane dynamics
Control environmental factors such as temperature and pH	Lipid organization and Protein interactions	Formation of specialized domains such as lipid rafts	Membrane-bound proteins function and interact within their native-like environment	Resembles the biological environment	Development of diagnostic and therapeutic strategies

Table 2.1 Different research approaches in membrane biology. The table emphasise key areas of focus, including controlled experimental environments, the replication of natural systems, the study of lipid behaviour, the modelling of complex interactions, technological advancements, and the investigation of disease-related mechanisms. It outlines how different strategies are employed to recreate membrane conditions, investigate lipid phase transitions, model protein-lipid interactions, develop drug delivery systems, and understand disease-related changes in membrane properties. Each approach contributes to a deeper understanding of membrane dynamics, stability, and functionality, both in natural and experimental contexts.

For example, a ternary lipid mixture membrane model consisting of three components—a high-Tm lipid, a low-Tm lipid, and cholesterol—demonstrates fundamental aspects of complex membrane phase behaviour. Depending on the melting temperature of the lipids and their relative molar concentrations, the system exhibits a specific phase diagram that outlines the various phases and any coexisting phases, as illustrated in Figure 2.6. In this phase diagram, the black phase boundaries are experimentally determined and reflect macroscopically observable phase separations. These boundaries mark regions where nanoscopic lipid domains coexist within the membrane. The phase diagram of the bio membrane not only highlights the coexistence of membrane domains but also enhances our understanding of the role of cholesterol concentration in the system. It illustrates how cholesterol influences the boundaries between coexisting phases, such as liquid-ordered Lo and Ld phases, or liquid- solid coexistence.

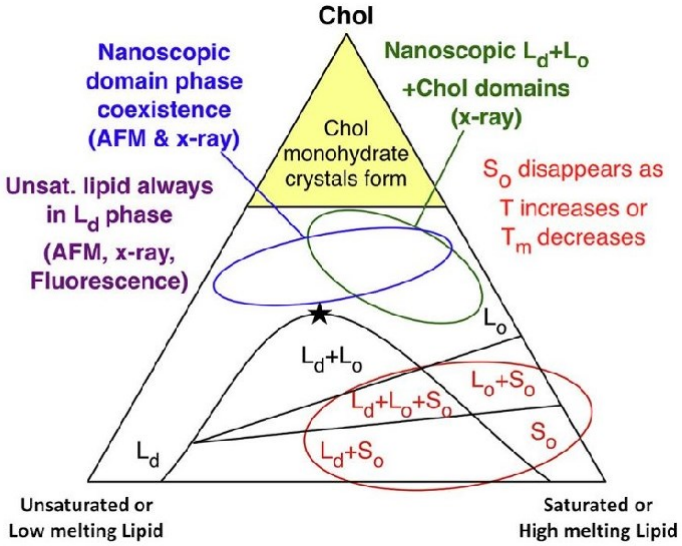

Figure 2.6 A typical phase diagram for ternary lipid bilayers, consisting of a low-melting-temperature (unsaturated) lipid, a high-melting-temperature (saturated) lipid, and cholesterol, shows the coexistence of various membrane domains. These include Ld and Lo, gel (So), and pure cholesterol crystal phases. The diagram also features a critical point, marked by a star, where lateral mixing becomes pronounced. Adapted from [89]

The most used model systems include liposomes, SLBs and GUVs. These models have been extensively utilized to investigate a broad spectrum of phenomena, such as protein-lipid interactions, lipid phase separation, membrane fusion, and molecular trafficking. Liposomes, which are spherical vesicles composed of lipid bilayers, are particularly useful for studying drug delivery and membrane dynamics. Supported lipid bilayers, which are adhered to a solid surface, offer insights into membrane properties and interactions with external factors. GUVs, being large, single-layered vesicles, provide a more macroscopic view of membrane behaviour and phase transitions. The primary advantages of these model systems lie in their ability to be tailored with various parameters and their compatibility with a wide range of analytical techniques. This versatility enables researchers to scrutinize the roles of individual components in regulating the biological processes of cell membranes with high precision.

2.6 Liposomes

Liposomes are spherical vesicles formed through the self-assembly of lipid molecules. These systems can be classified in different categories depending on the size and number of lamellae: Multi Lamellar Vesicles (MLVs) are characterized by three or more, lipid bilayers and have a size range from 500 nm to 5 μm, Small Unilamellar vesicles (SUVs) display one lipid bilayer and have a size that between 20 nm to 200 nm, Large Unilamellar Vesicles (LUVs) have a size ranging from 200 nm to 1 μm [90]. Several methods have been proposed to reconstitute liposomes, as the sonication followed by fusion onto flat substrate or thin-film hydration method followed by extrusion. The thin-film hydration method is among the most widely used techniques for obtaining a monodisperse size distribution of liposomes. This method generally begins with the creation of a thin lipid film in a round-bottom flask

through the evaporation of an organic solvent [91]. When the dispersion medium is added and agitated, heterogeneous liposomes form. Finally, by extruding them through polycarbonate membranes, uniform small liposomes are produced. The bio-mimetic models are used in several applications, for instance as a drug carrier due to their amphipathic nature, which allows for the loading of various therapeutic molecules based on their solubility. Studying liposomes involves a variety of techniques to analyse their properties, stability, and interactions. For instance, DSC measures the heat flow associated with phase transitions in materials as a function of temperature, providing insights into the thermal properties of liposomes. In this project, liposomes were selected to investigate the mechanical behaviour in relation to cholesterol concentration using an indirect method involving citrate-capped gold nanoparticles, as developed by Caselli et al [185]. Additionally, liposomes were used to create SLBs. The citrate-capped gold nanoparticles serve as probes to indirectly measure the mechanical properties of the liposomes by interacting with the lipid bilayers, allowing for detailed analysis of how varying cholesterol levels affect membrane stability and fluidity. This approach not only provides insights into the biophysical properties of the liposomes but also aids in the development of optimized model systems for further research.

2.7 Supported lipid bilayers (SLBs)

SLBs are biomimetic membranes that closely mimic the physical and chemical properties of natural plasma membranes. These structures are characterized by their planar conformation on a solid support, typically mica or glass. The formation of SLBs usually begins with liposomes, and their composition can be tailored to replicate specific types of membranes, such as those from healthy or diseased cells, with a variety of lipid components [92,93]. Due to the architecture of SLBs, the upper lipid monolayer is exposed to the aqueous medium. This unique feature allows SLBs to be used not only for characterizing the chemical interactions between two free monolayers but also for providing various tools for surface- specific analyses. Several methods can be used to produce SLBs, but the most common is the vesicle fusion method. In this approach, liposomes are broken and subsequently fuse onto the substrate, interacting through Van der Waals forces or electrostatic interactions [94]. The success of this process relies on three critical factors: proper vesicle preparation, the choice of surface for adsorption, and the strength of interaction between the vesicles and the artificial substrate (mica or glass). The substrate plays a crucial role, as it must enable the vesicles to rupture and adsorb onto its surface. If the deposition process is flawed, the vesicles may remain physically unchanged. Given that the physical properties of the vesicles—such as lipid composition, concentration, structure, and environmental conditions—affect supported lipid bilayer formation, careful control of these variables is essential. As reported in several studies, the reconstitution of supported lipid bilayers has been crucial for investigating lipid raft formation. The use of Atomic Force Microscopy has illuminated the dynamics of lipid rafts and their interactions with various membrane proteins. For instance, Paba et al. (2023) investigated the mechanism of vesicle fusion processes onto lipid rafts through the reconstitution of SLBs. Their findings highlighted that cholesterol levels and changes in membrane

fluidity play key roles in vesicle uptake. This underscores the importance of SLBs as a model system for studying membrane dynamics and protein interactions in a controlled environment. However, these systems are not suitable for studying the properties of transmembrane proteins due to the physical limitation posed by the adsorption surface, which prevents the insertion of such molecules (Jackman and Cho, 2020). Additionally, SLBs exhibit a higher degree of stiffness compared to native membranes. This increased stiffness depends on parameters such as the saturation level of phospholipids and their transition temperature, as discussed previously. Specifical, lipids with unsaturated chains have higher lateral mobility, in the range of $\mu m^2 \cdot s^{-1}$, and a lower transition temperature. In contrast, lipids with saturated chains exhibit lower lateral mobility, less than 10^{-3} $\mu m^2 \cdot s^{-1}$, and increased packing. In the context of this work, the reconstitution of supported lipid bilayers has been utilized to assess the role of cholesterol in modulating lipid raft dynamics. This approach also enabled the quantification of membrane fluidity and other critical properties, such as stiffness. It is crucial to recognize that the choice of model systems depends on the specific measurements being conducted. For instance, techniques such as atomic force microscopy and cryo-electron microscopy (cryo-EM) necessitate a solid substrate; therefore, supported lipid bilayers are particularly well-suited for these applications. Conversely, when employing techniques like calorimetry, which require samples to be in solution, liposomes are the more appropriate choice. This consideration ensures that the selected model system aligns with the methodological requirements of the measurement technique.

2.8 Giant Unilamellar Vesicles (GUVs)

GUVs are micrometer-sized with a diameter between 1 to 100 μm, formed when phospholipids organize into a closed-sheet structure upon contact with an aqueous medium. One of the features of GUVs is their suitability for investigation using optical microscopy techniques, as their shape and curvature radius resemble that of cells [95]. From a morphological standpoint, the lipid bilayer of GUVs encloses an aqueous medium with the hydrophilic heads of the lipids exposed to the external solution. GUVs can be made from natural or synthetic lipids and are widely used to study lipid phase separation, membrane protein interactions, and the formation of pore-spanning membranes [96]. These membranes are typically created by suspending the lipid bilayer from GUVs over substrates that have small holes, usually around 1μm in diameter. This setup allows researchers to reconstitute functional membrane systems in a controlled environment, offering insights into membrane dynamics and protein-lipid interactions at the molecular level. Various methods are employed to produce GUVs including water oil emulsion transfer method [97] and electroformation [98]. for its ability to yield higher quantities of homogeneous GUVs by applying an electric field during vesicle formation, thereby enhancing their uniformity and yield. This technique, pioneered by Angelova and Dimitrov [99], involves the application of an external electric field during lipid swelling, that can be modified in dependence of the desired dimension of the GUVs and depending on the starting lipid composition. In contrast, the natural swelling method, first introduced by Reeves and Dowben in 1969, starts with

a lipid solution deposited on a surface and dried to form a lipid film. Upon rehydration, gentle stirring induces vesicle formation driven by osmotic pressure as the aqueous solution permeates between the lipid bilayers. The closure of the hydrophobic core of the lipid bilayer into vesicles occurs because exposure to the surrounding aqueous medium is energetically unfavourable for the hydrophobic lipid tails. To generate these vesicles, electrodes such as indium tin oxide (ITO) or platinum wires, initially introduced by Angelova and Dimitrov, can be used. The electroformation temperature is a critical factor and must be kept well above the transition temperature of the lipid with the highest melting point in the mixture. Studies have demonstrated that increasing the temperature during electroformation leads to the production of larger GUVs. It's important to avoid excessively high temperatures during GUVs electroformation, as prolonged exposure can accelerate lipid degradation. Additionally, careful control of the cooling process is essential. Cooling too quickly can lead to vesicle rupture or result in non- equilibrium states. On the other hand, if cooling is too slow—especially Lo and Ld phases coexist—it may cause the Ld phase to separate from the parent GUV, potentially introducing experimental artifacts. Maintaining the right balance between temperature control and cooling speed is critical for producing reliable results. In this work to produce GUVs has been maintained a constant temperature of 60°C, as DSPC had the highest transition temperature among the phospholipids used.

2.9 Pore Spanning Membranes (PSMs)

PSMs also known as free-standing lipid bilayer membranes, serve as model platforms that combine the accessibility of both sides of the membrane with the stability provided by solid- supported lipid bilayers [100]. In this work, PSMs were started to optimize, and the process is still ongoing. PSM are suitable to suspend lipid bilayers derived from giant vesicles, aiming to integrate important membrane receptors, involved in disease as breast cancer. We collaborated with the nanofabrication facility at the CNR-IOM in Trieste, to develop ad-hoc substrates of varying geometries and materials. PSMs have been developed for the first time by Janshoff and Steinem, that proposed different strategies to functionalize the substrates based on the physicochemical properties of the lipid membrane [101]. Depending on the functionalization strategy of the porous substrate, hybrid pore-spanning membranes can be categorized. Typically, these membranes involve hydrophobic or hydrophilic self-assembled monolayers (SAMs) chemisorbed on gold-covered porous substrates. PSM are particularly suitable for studying interactions involving membrane proteins, especially integral membrane proteins, since the presence of a second aqueous compartment. These approaches offer two significant advantages: increased space between the lipids and the substrate, and more importantly, preservation of protein activity, which prevents denaturation. However, analysing these platforms requires non-invasive detection techniques, as the stability of lipid assembly is typically lower compared to classic supported lipid bilayers. From a manufacturing perspective, these systems require tailored geometry, including the diameter, depth, and spacing of patterns, as well as the choice of nanofabrication material. Depending on the required surface chemistry and technique, these substrates can be made

from materials such as silicon nitride, which offers advantages for measurements with inverted optical fluorescence, or silicon oxide. For our purposes, we aimed to functionalize the substrates by making them hydrophilic. This can be achieved by creating a self-assembled monolayer of 6-mercaptohexanol in n-propanol, resulting in a hydrophilic terminated monolayer. Another strategy to obtain a hydrophilic surface involves depositing a thin silicon monoxide (SiO) layer, followed by treatment in 55°C hot water. This treatment results in a mixture of SiO and SiO_2 ($SiO_1 \leq x \leq 2$) . In general, the main techniques used to investigate PSMs are AFM and fluorescence microscopy. AFM provides topographical information and high lateral resolution, allowing for detailed imaging of the membrane surface. Fluorescence microscopy complements AFM by enabling the study of membrane chemistry and interactions with proteins. This combination of techniques allows for a comprehensive analysis of the structure, composition, and functional interactions within the membrane, providing valuable insights into membrane behaviour and protein integration.

2.10 Extracellular vesicles (EVs): An overview

EVs are are nanosized structures released by all types of eukaryotic and prokaryotic cells under both pathological and physiological conditions into the extracellular space [103,104]. These vesicles are integral to cell-to-cell communication, transporting molecular cargo that mirrors the composition of the originating cell. EVs can encapsulate a diverse array of functional cargo, including genetic materials, lipids, proteins, and various metabolites. Delimited by a lipid bilayer, they are classified into three primary subtypes: microvesicles, exosomes, and apoptotic bodies. These subtypes differ in their size, composition, mechanisms of formation, release processes, and functions [105]. EVs carry a diverse cargo, including lipids, nucleic acids, and proteins—especially those related to the plasma membrane, cytosol, and lipid metabolism [106].

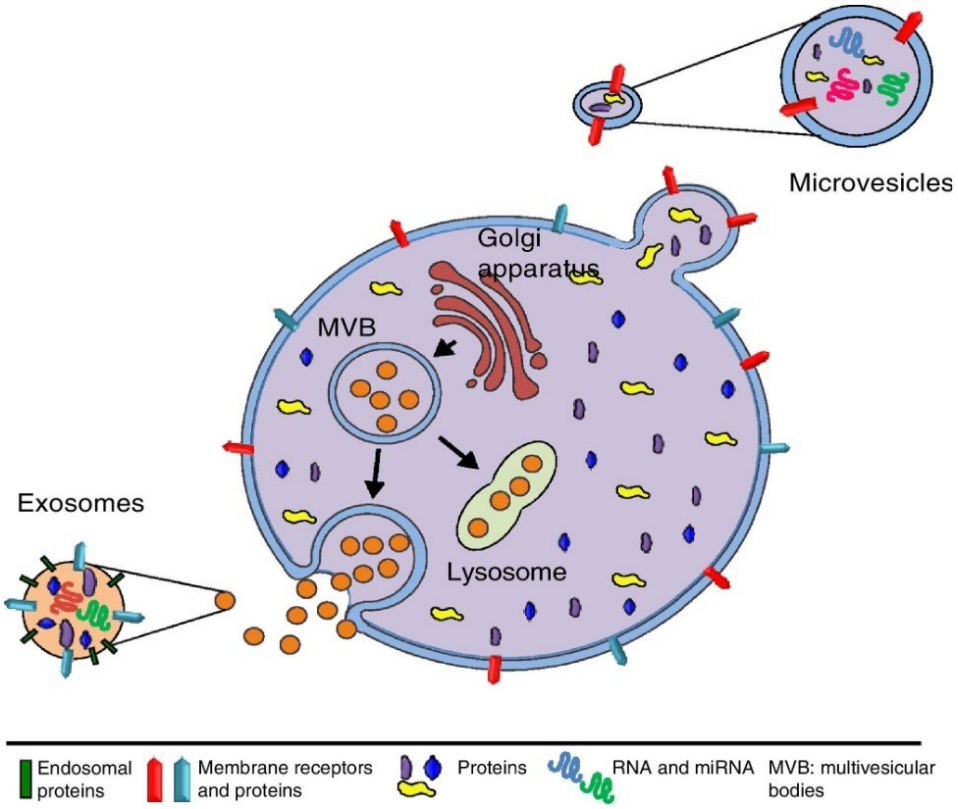

Figure 2.7 Origin and composition of extracellular vesicles. Figure adapted from [107].

Vesicle size is a crucial factor that affects the regulation of EVs and their interactions with recipient cells. Consequently, extensive research has been conducted to determine optimal methods for isolating and storing EVs in order to preserve their size and integrity [108,109]. Exosomes or small extracellular vesicles are a subtype of extracellular vesicles that are formed through an endosomal pathway, with a typical diameter of 30 to 150 nm. They arise from the inward budding of the limiting membrane of early endosomes, which then develop into multivesicular bodies during this maturation process. The biogenesis of exosomes is crucial for understanding their proteomic composition, particularly concerning the role of ESCRT (endosomal sorting complexes required for transport) proteins. These proteins, along with their accessory proteins—such as Alix, TSG101, HSC70, and HSP90—are integral to the formation and sorting processes that lead to exosome release [110,111]. These proteins are consistently identified in exosomes from various cell types, marking them as key exosomal marker proteins that help characterize these vesicles. Recent research suggests that exosome release may occur through mechanisms that do not involve the endosomal sorting complexes required for transport (ESCRT). Instead, these processes can involve enzymes such as sphingomyelinase. Tetraspanin proteins, including CD63, CD9, and CD81, are commonly found in exosomes and are enriched compared to their corresponding levels in cell lysates. Although initially believed to be exclusive to exosomes, tetraspanins are also present in microvesicles and apoptotic bodies. Exosomes typically have a higher glycoprotein content than their parental cells, while microvesicles are known to contain proteins that often undergo extensive post-translational modifications, including glycosylation and phosphorylation. These distinct characteristics are useful for differentiating

between the two types of vesicles. Additionally, emerging research is challenging the long-held belief that organelle-specific proteins, such as those from mitochondria or the nucleus, are absent in exosomes. While proteins originating from the Golgi apparatus and endoplasmic reticulum may be present in exosomes, they are generally found at lower levels compared to cell lysates and are not regarded as specific markers for exosomes [112]. EVs were once considered simple byproducts of cellular activity, primarily associated with waste disposal. However, this perspective has shifted dramatically. Small extracellular vesicles, including apoptotic bodies released during programmed cell death, play a crucial role in eliminating cellular debris, such as fragmented organelles and nuclear material, which helps to reduce the risk of damage and inflammation. Additionally, EVs can arise from cell membrane turnover or stress responses, shedding excess proteins and lipids to maintain cellular homeostasis. While it is true that EVs can carry waste materials, including oxidized lipids and dysfunctional proteins, their significance extends far beyond waste management. They are vital players in intercellular communication, capable of transferring bioactive molecules and mediating various physiological processes [113]. The molecular content of EVs can provide crucial insights into the states of cells and the presence of disease conditions, making them valuable tools for diagnostics and therapeutic applications. Their ability to reflect the molecular signatures of their cells of origin makes them promising non-invasive biomarkers for diagnosing and monitoring diseases, including cancers, cardiovascular disorders, and neurodegenerative conditions. Studying EVs can enhance our understanding of disease mechanisms, particularly in relation to inflammation, immune responses, and cancer metastasis.

2.11 SLBs as a platform to study the EVs Uptake

Model membrane systems are crucial for advancing our understanding of EVs-membrane interactions. These systems offer a simplified yet highly informative environment to dissect the intricate mechanisms underlying vesicle fusion and uptake, which are otherwise obscured by the complexity of the cellular milieu. By replicating key aspects of the eukaryotic PM, model membrane systems enable precise manipulation and observation of the factors influencing vesicle behaviour. This approach allows for detailed analysis of the molecular interactions, lipid dynamics, and protein functions involved in vesicle-membrane fusion processes. Utilizing these platforms not only facilitates a clearer understanding of fundamental cellular processes but also provides valuable insights into the development of therapeutic strategies for diseases related to vesicular transport and membrane dynamics. Thus, our use of model membrane systems is instrumental in bridging the gap between basic research and clinical applications, offering a powerful tool for unravelling the complexities of vesicle-mediated cellular functions. Our group has a rich history of investigating membrane-EVs interactions, and our application of biophysical approaches has effectively clarified the chemical and physical factors that influence EVs uptake (Paba et al.). In this context, optimized multicomponent SLBs have emerged as a crucial tool. These advanced SLBs are instrumental not only in exploring how

small extracellular vesicles modulate membrane properties but also in identifying the key lipids involved in mediating membrane-EV interactions.

In this thesis SLB were designed to closely mimic the complex composition of biological membranes, offering a comprehensive framework for investigating how cell membrane fluidity and the transient disruption of lipid raft integrity by EVs impact vesicle interactions. By employing multicomponent SLBs, we can discern how varying lipid compositions affect sEV uptake and the subsequent impact on membrane integrity. This involves understanding how EVs induce or alter lipid redistribution in the target membrane and evaluating any potential adverse effects on membrane stability. Furthermore, the versatility of these multicomponent SLB platforms by integrating a diverse array of lipids and proteins beyond cholesterol, provide a broader understanding of vesicle- membrane dynamics. This expanded approach facilitates the study of complex lipid interactions and functional modifications, thereby advancing the development of more effective and targeted drug delivery systems.

Chapter 3: Materials and methods

3.1 Chemicals

Lipids, 1,2-dioleoyl-sn-glycero-3-phosphocholine (DOPC) (≥98.0%), 1,2-distearoyl-sn- glycero-3-phosphocholine (DSPC) (≥98.0%), Sphingomyelin (Brain, Porcine, SM) and cholesterol (ovine wool) (≥99.5%) were provided by Avanti polar lipids. Chloroform (≥99.9%), NaCl (≥99.5%), HEPES, Tris and CaCl2 (99.999%) were provided by Sigma Aldrich (St. Louis, MO, USA). To prepare buffer solutions has been used ultrapure Milli-Q grade water. Fluorescent probe,18:1 NBD-DSPE1,2-dioleoyl-sn-glycero-3-phosphoethanolamine-N-(7-nitro-2-1,3-benzoxadiazol-4-yl) (ammonium salt), was provided by Avanti Polar Lipids. Fluorescent probe ATTO 655-DOPE was provided by ATTO-TEC GmbH Martinshardt 7 D- 57074 Siegen Germany. A gold (III) chloride solution, Trisodium citrate tribasic dihydrate was purchased from Sigma-Aldrich Chemical Co. (St. Louis, MO, USA).

3.2 Liposomes and SLBs preparation

First, stock solutions of lipids in chloroform were prepared at a concentration of 1 mg/mL. Then, the lipids were mixed in the following ratio: DOPC: DSPC: SM at 35:20:12 (w/w), with 7% and 33% cholesterol (w/w). The mixture was dried to form a lipid film under a nitrogen flow, and subsequently hydrated with a buffer solution. Three different buffers were prepared:

1. 10 mM HEPES, 150 mM NaCl (1:10), pH 7.4: This buffer was used for all experiments, as it represents a physiological condition [114].

2. 10 mM HEPES, pH 7.4: This buffer was used to study the impact of buffer composition on membrane formation.

The final lipid concentration was maintained at 1 mg/mL. Three freeze-thaw cycles were then performed. The resulting multilamellar liposomes were extruded through a polycarbonate membrane (Whatman by Cytiva) with a pore size of 100 nm to achieve a monodisperse liposome size distribution. The liposomes were utilized for two key purposes: first, to produce SLBs, and second, to investigate the interaction between liposomes and AuNPs. This interaction was analysed to obtain qualitative information on the stiffness of the liposomes, following the protocol established by Caselli et al., with slight modifications to suit the experimental conditions.

3.3 Liposome-AuNPs Interaction Study

To prepare the liposome-AuNPs mixtures, 20 µL of liposomes were combined with 100 µL of a 3.2 nM aqueous dispersion of negatively charged citrate-capped AuNPs (with a diameter of 15 ± 0.6 nm). This produced a final liposome/AuNPs molar ratio of approximately 1:100. The interaction between the liposomes and AuNPs was monitored by observing changes in the SPR profile after a 15-minute incubation at room temperature using a UV-Vis spectrophotometer, as outlined in the literature [185].

3.4 SLB Preparation for AFM imaging

SLBs for AFM imaging were prepared using the vesicle fusion method, a widely recognized technique for lipid bilayer formation. Liposomes were fused onto freshly cleaved mica, which had been mounted on a glass coverslip, in accordance with established protocols [115,116]. To ensure vesicle rupture and the formation of continuous, stable lipid bilayers suitable for high-resolution imaging, a buffer solution containing 200 mM $CaCl_2$ and 100 mM NaCl was used. The ratio of $CaCl_2$ to NaCl was maintained at 1:10, with the solution prepared by mixing 90 µL of NaCl with 10 µL of $CaCl_2$. This buffer system promotes efficient SLB formation and stability, optimizing the sample for AFM analysis.

3.5 SLB Preparation for Fluorescence Microscopy imaging

SLBs for fluorescence microscopy imaging were prepared by fusing liposomes onto freshly cleaved mica. To study phase separation, two different dyes were used: 0.001 mol% 18:0 NBD- DSPE to label the Lo phase, and 0.001 mol% ATTO655-DOPE to label the Ld phase. The buffer used, as in AFM imaging, consisted of 10 mM HEPES and 150 mM NaCl (1:10 ratio), adjusted to pH 7.4. Liposomes were sonicated for 10 minutes until the solution became clear, then fused onto the mica, followed by incubation and multiple rinses with 10 mL of buffer. Finally, 200 µL of the sample was retained in the chamber for imaging.

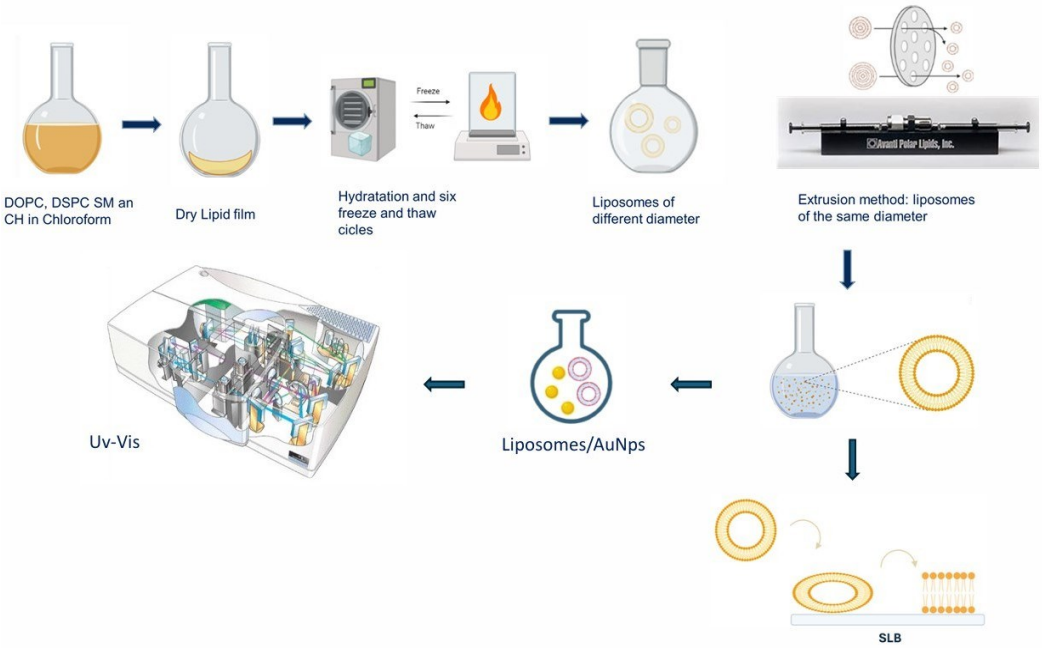

Figure 3.1 Schematic illustration of the thin film hydration method protocol that was employed to produce liposomes. Liposomes have been used both to reconstitute SLBs and to probe the mechanical properties through the interactions with gold nanoparticles monitored with Uv-Vis spectroscopy. (Created with Biorender.com).

3.6 Synthesis of AuNPs

AuNPs were prepared using the sodium citrate reduction method of $HAuCl_4$, following the protocol established by Turkevich et al. (1951) [117] and optimized by A. Alsadig, a formed Ph.D. student of our lab [118]. To prevent unwanted nucleation and the aggregation of AuNPs during synthesis, all glassware was meticulously cleaned with freshly prepared aqua regia (a 3:1 mixture of HCl and HNO_3), rinsed thoroughly with Milli-Q water, and dried in an oven at 100 °C before use. The synthesis was carried out in a 250 mL round-bottom flask, where 1.1 mL of 17.3 mM $HAuCl_4$ was added to 43.6 mL of Milli-Q water and brought to a boil under vigorous stirring on a magnetic stirrer hotplate. Once the solution reached boiling, 300 µL of a 72 mg/mL solution of trisodium citrate dihydrate was rapidly introduced. A series of color changes followed: from yellow to colourless, then to dark blue, and finally to a deep red within a few minutes, indicating the formation of AuNPs. The reaction was maintained at the boiling point for 30 minutes to ensure complete reduction of the gold salt. Afterward, the solution was allowed to cool to room temperature. The resulting gold colloid was protected from light and stored at 4 °C until further use.

3.7 GUVs preparation

GUVs were prepared with the same lipid composition used for SLB formation, using electroformation in PTFE chambers equipped with platinum (Pt) electrodes, following the method described by Kanwa et al. A 6 µL aliquot of a lipid mixture (2 mg/mL) dissolved in chloroform was carefully spread onto two Pt wires and left to dry in a desiccator for 20 minutes. The chambers were then filled with 350 µL

of sucrose solution (310 mOsm kg^{-1}), adjusted to be iso-osmolar with the imaging buffer. To induce vesicle formation, an alternating current (AC) electric field of 2 V (rms) was applied at a frequency of 10 Hz for 1 hour, followed by 2 Hz for 45 minutes, at a temperature of 50°C. After this process, the samples were gradually cooled to room temperature over 4 hours before being used for imaging.

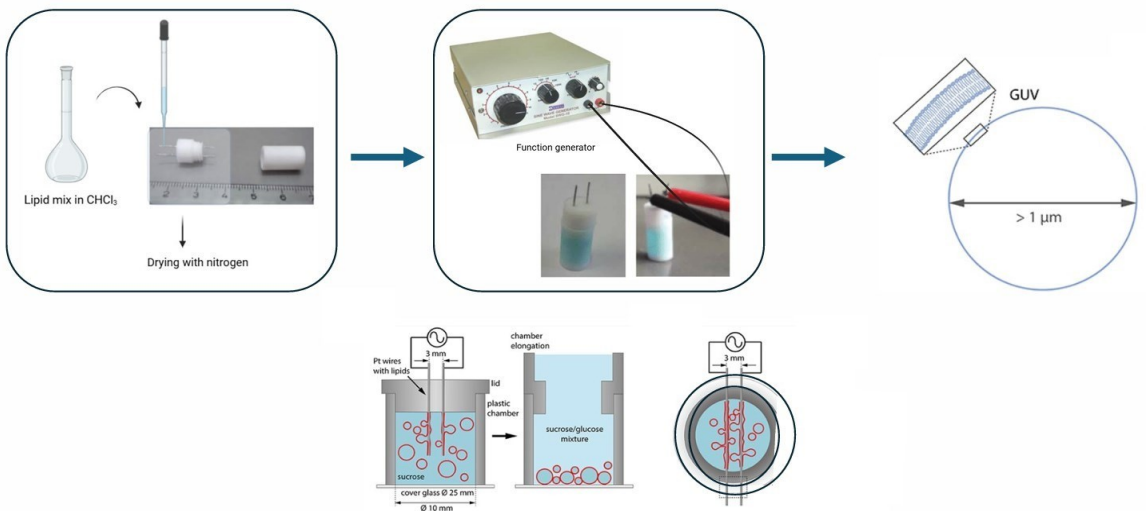

Figure 3.2 Vertical chamber setup used for GUVs preparation. A lid containing two platinum (Pt) wires, coated with a lipid mixture, is placed on top. When an alternating current (AC) electric field is applied, GUVs form as the lipids swell and detach from the wires. After vesicle formation, the lid can be replaced with an elongated chamber. If sucrose is used as the swelling solution, glucose can be added to the observation buffer, causing the GUVs to sink to the bottom for easy observation and harvesting. Readapted from [119].

3.8 PSMs optimization

Substrates composed of two distinct materials were utilized for the experiments: 1) silicon oxide (SiO) and 2) silicon nitride (Si_3N_4). The Si_3N_4 substrates were surface modified with a 20 nm gold layer, deposited via sputtering. The nanofabrication of these substrates was expertly carried out by Simone dal Zilio at the CNR IOM nanofabrication facility in Trieste, Italy. Although substrates with various hole diameters were tested, only those with a diameter of 1 micron, which showed the most promising results, are detailed here.

To functionalize the substrates, two distinct strategies were employed, in line with methodologies outlined by C. Steinem. The first strategy involved the functionalization of the Si_3N_4 substrates. This was achieved by creating a self-assembled monolayer (SAM) of thiol groups on the surface, specifically using 6-mercaptohexanol. For the SiO substrates, the second strategy was employed. This method involved oxidizing the surface at 55°C to create a SiO/SiO_2 mixture, which was then further functionalized by incubating the substrates overnight in a 1 mM 6-mercaptohexanol solution in n-propanol at room temperature. This process led to the formation of a hydrophilic terminated SAM. For the preparation of pore- spanning lipid bilayers, substrates were first rinsed with n-propanol and buffer A (10 mM Hepes, 100 mM KCl, 10 mM $CaCl_2$, pH 7.4). They were then mounted on glass

coverslips and pre-heated to 55°C. A 10 μL suspension of giant unilamellar vesicles (GUVs) was carefully deposited onto the substrates. To ensure a more uniform bilayer formation, the substrates were incubated at 55°C for 2 hours.

3.9 Atomic force microscopy (AFM)

Atomic Force Microscopy is one of the main techniques that have been used in this work. It is a near-field surface microscopy technique first developed by Gerd Binnig and his colleagues in 1986, as an evolution of Scanning Tunneling Microscopy [120].It operates by scanning a sharp nanometric probe or tip across the surface of a sample, detecting interactions between the tip and the sample to provide high-resolution maps of diverse physico-chemical properties of the sample surface, alongside topography, thus turning out to be a highly versatile tool [121]. AFM tips, typically made of silicon or silicon nitride, are attached to a flexible cantilever, which can be effectively approximated as an ideal spring [122]. These tips function as force sensors, probing the interaction forces acting between the tip apex and the surface being examined. Tips can vary in dimension and shapes, ranging from micrometric to nanometric apex radii and spherical to pyramidal, conical or customized geometries, depending on the application. Their sharpness can allow for extremely fine resolution, in some conditions even reaching the atomic scale. In most cases, lateral resolution can be nanometric and is typically defined by convolution effects between the tip apex size and the size of surface topographical features, whereas vertical resolution is sub-nanometric, basically depending only on instrument-related features as the vertical resolution of the piezoelectric actuator and the noise-to-signal ratio. This technique is particularly valuable for biological research due to its unique ability to work in every kind of environment, including physiological ones, such as liquid or buffer solutions under controlled temperature and humidity, which is crucial for studying biological samples in their native state [123-124]. Indeed, unlike other microscopy techniques that require samples to be dried or frozen, AFM can image different biological samples in physiological conditions and minimizing invasiveness. Moreover, its high versatility on both spatial and temporal scales can allow AFM to map simultaneously topographical and diverse surface properties of these samples, such as mechanical properties, ranging from cells and tissues to lipid bilayers mimicking the cellular membrane, or even single macromolecules like DNA or proteins, eventually probing their dynamics (high-speed AFM). As previously mentioned, this versality stems from AFM capability to accurately and quantitatively measure tip-sample forces, which can hide relevant information on diverse physico-chemical properties of the sample under investigation [125-127]. The forces detected by AFM are typically attractive forces acting at distances up to a few hundreds of nanometers (i.e. Van der Waals forces), combined with repulsive forces becoming dominant when the tip is in hard contact (within a few angstroms) with the surface). The main features of the tip-sample interaction can be modelled by the well-known Lennard- Jones potential reported in figure 3.3. This potential includes both attractive and repulsive components, illustrating the typical forces experienced by the AFM tip when interacting with the sample' surface at different proximities.

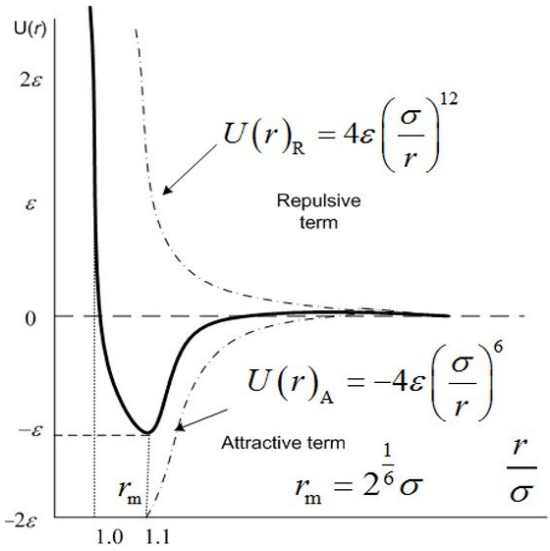

Figure 3.3 Potential Lennard-Jones [126]

The force detected by the tip leads to the bending of the cantilever: the cantilever deflection d is, in first approximation, proportional to the tip-surface force F according to the Hooke's law: F=- kd, where k is the is the cantilever elastic constant. K values typically vary in the range 0.01-50 N/m, depending on the cantilever material and geometry. During a AFM scanning, cantilever static deflection or oscillation amplitude, dependent on the chosen operational mode, is monitored using a laser directed onto the back of the cantilever, which is then reflected onto a four-quadrant photodiode detector. This detection system is known as "optical lever system". As the tip interacts with the sample surface, the cantilever deflects, causing a shift in the laser spot's position on the photodiode. The corresponding measured voltage variation ΔV is converted into cantilever deflection (in nm) through a user- calibrated parameter (dependent on the tip-cantilever type as well as on the working environmental conditions) which is known as deflection sensitivity or invOLS (units: nm/V). Another relevant part of the AFM is represented by the piezoelectric motors, which are voltage- dependent actuators, enabling precise sub-nanometric displacement control and resolution. In the tip-sample direction (z), fine adjustment of the relative distance is provided by the z scanner, while in x-y plane the scanner allows the movement of the tip above the sample surface (or, depending on the instrument's configuration, the substrate below the stationary tip) for imaging in a raster-scan motion [128].

For topographic imaging, AFM is typically operated in three different modes, according to the sample characteristics and the needed resolution: contact mode, semi-contact (also known as tapping mode or alternate contact mode) and non-contact mode. For all imaging modes, the key point to scan and reproduce the topographical features of the sample surface lies in monitoring a proper variable (i.e. cantilever deflection), dependent on the tip-sample distance, which is kept constant by an electronic

feedback loop system, acting almost instantaneously by adjusting the eventual distance variations. Maintaining a constant tip-sample vertical distance while scanning over the sample surface allows to track its topographical features; in other words, as reported by Butt et. al [129], a topographic image of the sample can be obtained plotting point by point the height adjustments of the piezo scanner. In contact mode, tip- sample distance is set in a range where repulsive forces are predominant, and the static cantilever deflection is monitored and provided as input for the feedback loop system In this mode, the AFM tip is kept in constant "hard" contact with the sample surface while scanning over it, and the ensemble cantilever-tip can be mathematically modelled as a point-mass static loaded spring This modality is quite simple and can be run at relatively high scanning frequencies, but at the same time it is characterized by high lateral friction forces, which in turn can easily lead to wearing of both tip and samples, particularly in the case of soft and fragile samples. Therefore, contact mode is not commonly used to image a large majority of biological samples. Non-contact mode and tapping mode are similar "dynamic" modes in which the AFM cantilever is forced to oscillate close to its resonance frequency, thus being mathematically modelled as an externally driven damped single harmonic oscillator. In this case, the distance- dependent variable exploited as input for the feedback loop system is the oscillation amplitude, which is typically reduced, when the approaching tip starts feeling the surface forces, with respect to the "free" oscillation amplitude measured when the AFM tip is far away from the sample surface and no net forces are experienced. More in detail, true non-contact mode is used in a minority of cases, for example by working in ultra-high vacuum conditions, i.e. when sensitive attractive long range forces, such as Van- der-Waals forces, can be detected, and the cantilever is forced to oscillate at very low amplitudes (~1 nm) in this purely attractive force regime, thus never touching the sample surface. In this way truly atomic resolution can be achieved also on the lateral dimensions, since the convolution effects between AFM tip and surface features are avoided. In most cases, as for our measurements, tapping-mode, where the AFM tip experiences both attractive and repulsive forces for each oscillation cycle, is exploited. Typical amplitude oscillations are larger compared to the non-contact mode, and the AFM tip is "tapping" the surface during each oscillation cycle. The real behaviour of the system in this modality can be quite complex [130,131].

Despite this, in first order approximation the amplitude oscillation is always reduced compared to the starting "free" amplitude, regardless of the net attractive or repulsive character of the interaction forces experienced by the AFM tip during each oscillation cycle. Additionally, this AFM modality greatly reduces the intensity of lateral friction forces, thus allowing to image also soft and delicate biological samples such as supported lipid bilayers.

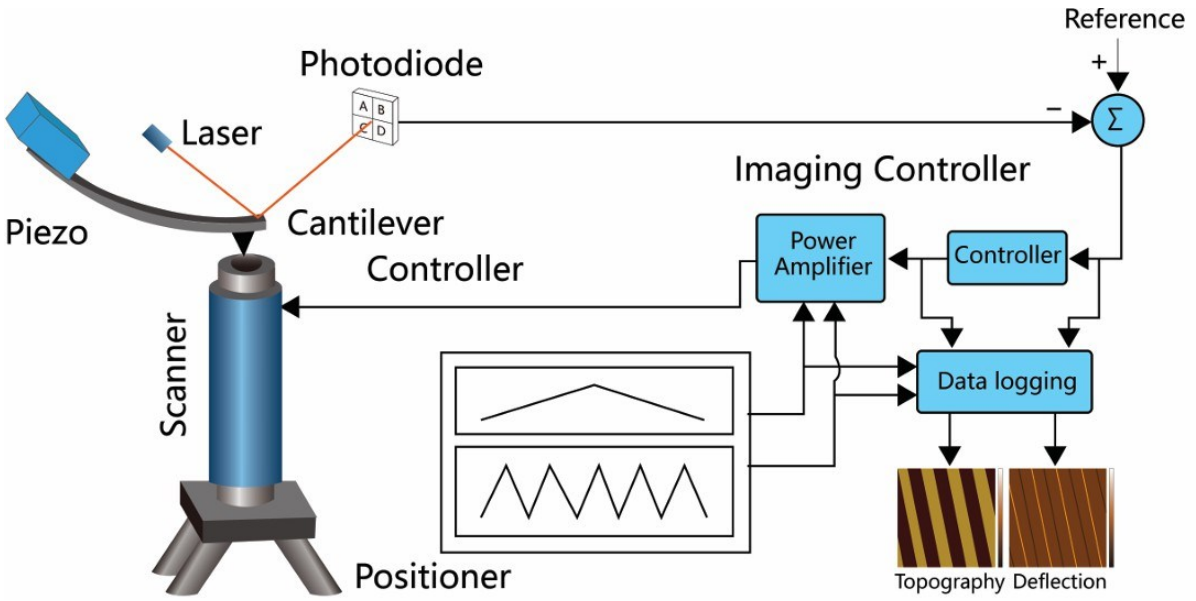

Figure 3.4 Schematic presentation of atomic force microscope. Adapted from [130]

As previously highlighted, AFM can be a valuable tool for mapping, alongside topographical properties, the mechanical properties of biological samples through the acquisition of force- distance (FD) curves. This operational mode, usually referred as "force mapping", is a "quasi- static" approach where, differently from the previously described modes, the AFM tip approaches the sample along the z-axis and the cantilever deflection is measured at each point of the vertical axis being subsequently converted into a force value through the cantilever elastic constant and the equation for a point-mass loaded static spring. The maximum applied force value, selected by the user, is exploited as input for the feedback loop system in order to obtain the topographic map. After reaching the maximum set force value, the tip is retracted back to its original position, so that two force curves, named respectively approaching and retracting force curves, are measured for each point on the x-y plane. The acquired force curve can be then analysed by proper mathematical model to extract the parameters of interest, thus building additional physico-chemical maps of the sample' surface in one-to-one correspondence with the topographic map. Force curves can vary and deviate from the simple model according to the specific sample, environment, and selected AFM probe, and consequently to the diverse tip-sample forces experienced, thus potentially allowing to extract a rich landscape of information and greatly contributing to the AFM versatility [132]. This method has been used in combination with tapping mode to investigate the mechanical properties of our supported lipid bilayers. For topographic imaging MFP-3D Stand Alone and Cypher VRS1250 AFM from Asylum Research (Santa Barbara, CA) have been used, employing dynamic tapping mode in liquid (droplet) environment. Cypher VRS1250 has been used for measurements performed under controlled temperature and humidity. In both cases, we employed microcantilevers from Olympus (BL-AC40TS), with nominal spring force elastic constant k=0.09 N/m and equipped with sharp silicon tips characterized by a nominal curvature radius R= 8 nm. Typically, we acquired 10x10 μm2 topographic maps with 512x512 points&lines resolution, at frequencies ranging from 1 to 4 Hz. Image post-

processing procedures such as flattening (i.e. removal of relative tilts between AFM tip and sample surface), height profiles extraction and surface evaluation has been performed using an open-source software named Gwyddion (v. 2.63, http://gwyddion.net/).

3.10 AFM Nanomechanics: Force spectroscopy mode

Recent innovations have significantly enhanced the capability of the AFM to probe the mechanical properties of supported lipid bilayers and other complex membrane structures. By utilizing specially designed cantilevers and optimized experimental setups, researchers can effectively assess the mechanical behaviour of these complex systems. Among them, AFM- based force spectroscopy (AFM-FS) has become an important technique for studying the nanomechanical stability of supported lipid bilayers. Force spectroscopy can be seen as a "subset" of force mapping or force-distance curves approaches, described previously. Basically, it refers to the identification and analysis of "sharp" events sometimes appearing inside the force curves and related to specific molecular interactions between the sample and the AFM tip, such as rupturing events, also often referred to as "jumps", or pulling events, also named "tethers" [133, 134]. In the case of very thin (5-7 nm) and soft samples like SLBs, in most of cases, upon making mechanical contact, the cantilever deflection initially increases as the AFM probe locally compresses the sample elastically Eventually, the probe breaks through the bilayer, making direct contact with the underlying substrate. When the AFM tip breaks the bilayer, this phenomenon appears as a sudden slope change in the force-distance curve. The force value at which this penetration occurs represents the maximum load the bilayer can withstand before it breaks, known as the breakthrough force (Fb). Typical values are observed in the range of a few nN to several tenths of nN, strongly depending on the chemical composition as well as environmental condition, like temperature and ionic strength of the buffer solution. In a minority of cases, a peculiar behaviour in the force-distance curves can be observed, suggesting rather a slow penetration of the tip in the bilayer accompanied by its lateral compression. In these situations, typically breakthrough events are not observed [135]. In experiments designed to measure mechanical properties, the sample's Young's modulus is typically measured, by fitting the starting elastic compression in the approaching force curve with proper contact mechanics models, such as the Hertz model, schematically described in fig. 13 (61H. Hertz, J. Reine Ang. Math. 92, 156 (1881) [137]. However, these models usually make strict assumptions that are rarely satisfied. Despite the rigid assumptions, these models still provide good approximations for mechanical measurements on the microscale for cells and tissues, whereas their validity for nanomechanical measurements on more complex samples like SLBs is still strongly debated. For this reason, along with the fact that often SLBs exhibit behaviours that strongly deviate from the predictions of these models, we chose to evaluate breakthrough forces (Fb). Fb are not "direct" elasticity parameters as the Young's Modulus, yet they are strongly correlated to it.

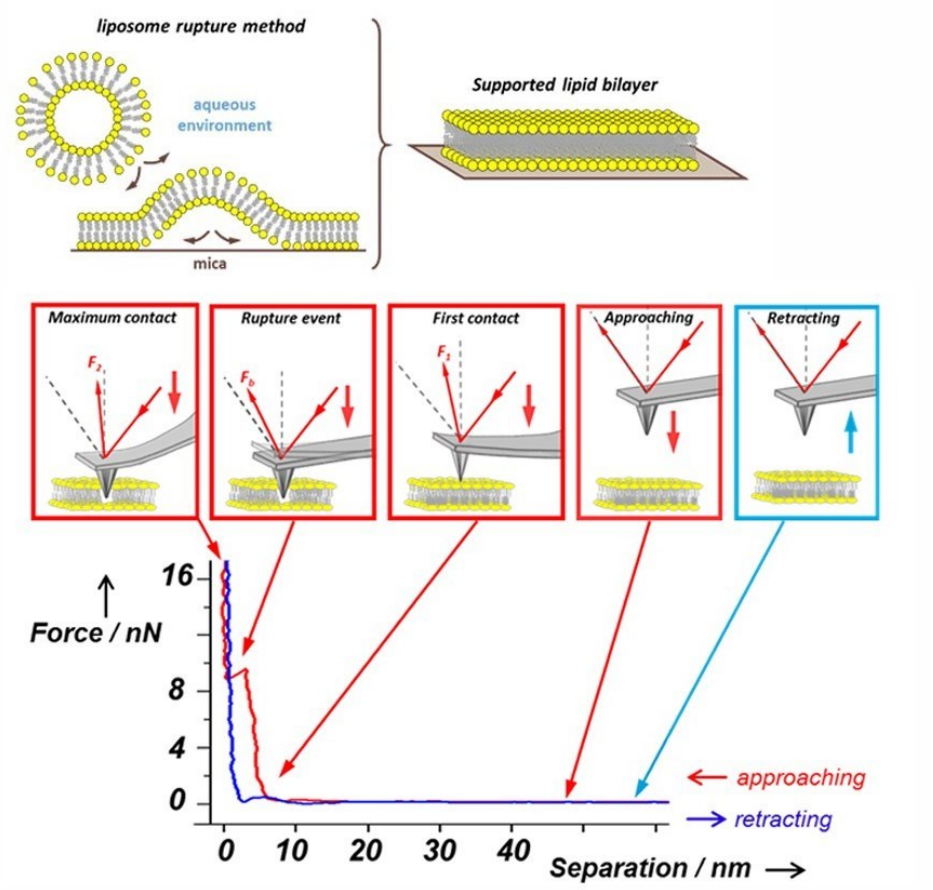

Figure 3.5 Formation of supported lipid bilayers (SLBs) via the vesicles fusion method (a), along with the SLB indentation process using AFM-FS (b). The force–separation curve demonstrates a typical discontinuity in the approach curve, which occurs when the bilayer is punctured. The various stages in the indentation process and the corresponding features of the force curve are linked by arrows. Figure adapted from [136].

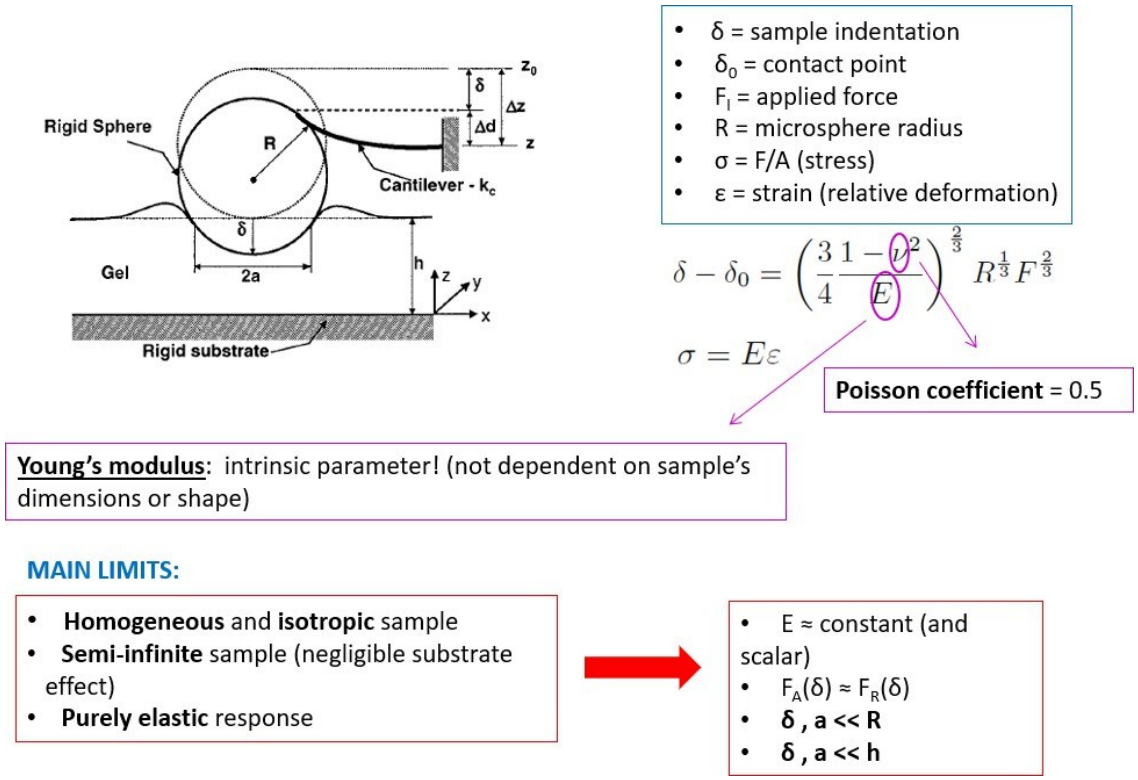

Figure 3.6 Hertz Model Theory for Force-Distance Curve Fitting. (Courtesy of L.Puricelli).

In order to discriminate among the different coexisting phases (Lo & Ld), we acquired force distance curves on a few selected spots over the different phases per each topographic image. Again, we chose this technique, more commonly known as "Point&Shoot", due to technical reasons related to the peculiar mechanical response of the Lo phase in the 7% mol. cholesterol concentration samples, dropping more statistically high-throughput and less time-consuming techniques as the previously described Force mapping. A second topographical map has been measured on the same region after the acquisition of the force curves, to verify that the selected spots were still belonging to the same original phase, given the dynamic nature of SLBs.

For what concern the technical specification of these measurements, topographic maps, employing dynamic tapping mode in liquid (droplet) environment, along with Point&Shoot- based force curves have been acquired under controlled temperature and humidity, using the Cypher VRS1250 AFM from Asylum Research (Santa Barbara, CA). In this case, we exploited ultra-short cantilevers USC-F0.3-k0.3 provided by NanoWorld, with a nominal elastic constant k=0.3 N/m and equipped with sharp diamond-like carbon (DLC) tips characterized by a nominal apex curvature radius R<10 nm. The choice of this probes has been based on the need to measure relatively high breakthrough forces without reaching the photodetector non- linear response region, as well as the need to keep the AFM tips clean, avoiding the formation of lipid bilayers on them. Indeed, DLC tips shows a significantly larger "lipophobic" character compared to standard silicon tips, which gets easily covered by lipids, making the analysis of the acquired force curves quite difficult and ambiguous [138].

Force curves have been acquired on both 7 mol% and 33 mol% cholesterol samples with the following parameters: closed loop mode, ramp length L=500 nm, approaching and retracting velocity v=200 nm/s, trigger point V=1-3 Volts, sampling rate f=33 kHz. More accurate values for cantilever elastic constants k have been evaluated using the GetReal calibration method provided by the Cypher software, which combines Thermal Noise and Sader methods (refs.), whereas invOLS has been calibrated directly from the acquired force curves, by linearly fitting the region of the curve where the tip is pressed against the rigid and undeformable mica substrate, following the bilayer breakthrough. Data analysis of force curves, including automated detection of breakthrough forces, has been carried out using custom routines developed in Matlab.

3.11 Confocal fluorescence microscopy

Confocal microscopy was conceptualized by Marvin Minsky in 1955 and patented in 1957. Minsky's design introduced key innovations, including pinhole apertures and point-by-point illumination of the specimen. In the early 1970s, Davidovits and Egger built the first mechanically scanned confocal microscope using laser illumination, specifically for biological research [139,140]. Advances in computers, lasers, and digital imaging software over the following decades greatly enhanced the technology. By the late 1980s, these improvements made confocal microscopes commercially available. The most crucial components of a confocal microscope are the spatial filters known as pinholes. These pinholes are essential for eliminating out-of-focus light from fluorescently labelled specimens that extend beyond the focal plane. By blocking this unwanted light, pinholes enable the acquisition of high contrast, bidimensional images at various focal planes or depths within the sample. These images can then be stacked to reconstruct a detailed three- dimensional representation of the specimen. This optical sectioning capability is valuable for both reflection and fluorescence modes, providing clear, focused images of complex structures within the sample [141]. The elimination of out-of-focus light in confocal microscopy significantly enhances image resolution, especially for samples labelled with multiple fluorophores, making it highly suitable for studying complex biological systems. In contrast, conventional (widefield) light microscopy illuminates the entire depth or volume of a specimen uniformly and simultaneously, collecting emitted light from all planes [142]. This results in out-of-focus blur from regions above and below the focal plane, which diminishes both contrast and resolution. Confocal microscopy, however, operates on the principle that both the illumination and detection optics are precisely focused on the same diffraction-limited spot. This selective focus allows for the capture of sharp, high-resolution images with minimal out-of-focus interference, providing clearer and more detailed views of the specimen [143]. In confocal microscopy, a focused spot is scanned across the sample to build a complete image on the detector. Only fluorophores located at the exact positions aligned with both the illumination and detection pinholes are detected, which enhances contrast and resolution. Confocal microscopes can be classified according to their scanning techniques. The image is formed by systematically moving the illumination point across the sample, with various strategies employed to accomplish this. In a stage-scanning system, like the Minsky

configuration, the optical components remain fixed while the microscope stage moves to scan the specimen. In our study, we utilized LSCM. In a LSCM a laser beam is scanned across the sample using galvanometer mirrors. Initially, the laser is directed onto a set of scanning mirrors that move the beam in the x and y directions, covering a specific field of view. This process allows for systematic movement of the laser across the entire sample, generating images of each optical section or slice. To create a z-stack, the focal plane is adjusted after capturing the initial slice, and the scanning process is repeated for each successive layer. This technique enables the reconstruction of three-dimensional images, offering detailed insights into the sample's structure.

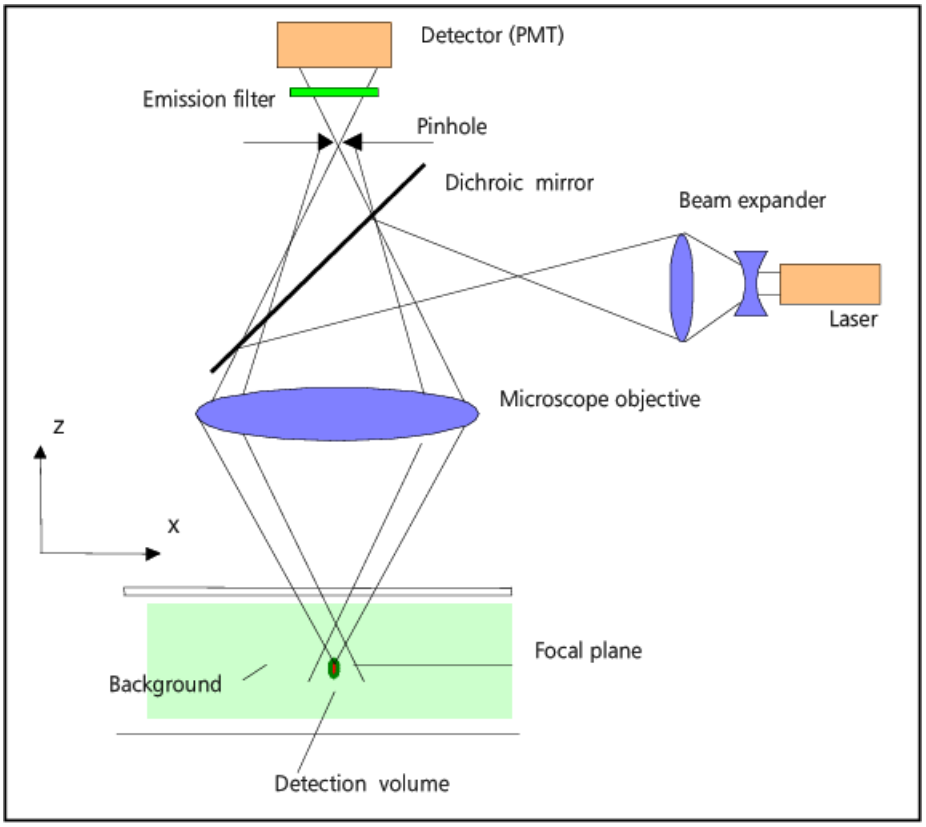

Figure 3.7 Ray path in a confocal LSM. Adapted from [144]

The optical sectioning capability of a confocal microscope depends on the size of its pinhole, which controls how effectively out-of-focus light is excluded. A smaller pinhole improves

optical sectioning by minimizing out-of-focus blur but also reduces the amount of light reaching the detector, which can decrease the signal-to-noise ratio. To counteract this, increasing the fluorescence from the sample can help, but too much excitation light can harm the specimen and degrade the fluorophores. The optimal pinhole size is usually near to the radius of the first zero of the Airy disks; beyond this point, further size reduction offers minimal improvements in optical sectioning. With the use of more sensitive photodetectors with high quantum efficiency, the confocal imaging has been improved by enhancing the ability to detect photons and providing more accurate measurements.

All the CLSM experiments in this work have been carried out using a LSM780 confocal laser scanning microscope with a 20x objective lens (Carl Zeiss, Germany).

3.12 Fluorescence recovery after photobleaching (FRAP)

FRAP is a fundamental technique in cell biology and biophysics, primarily employed to assess molecular mobility and transport. First developed in the 1970s, FRAP was originally used to investigate diffusion within cellular membranes using organic dyes [145]. This method allowed researchers to study protein dynamics by tracking the rate at which fluorescence returns to a bleached area [146]. Today, FRAP remains a powerful tool for both qualitative and quantitative analysis of biomolecular behaviour in live cells and biomimetic systems. This technique involves irreversibly bleaching a defined region within a sample using intense light, followed by tracking the gradual return of fluorescence in that area over time. This recovery occurs as unbleached, fluorescently labelled molecules from surrounding regions diffuse into the bleached zone. The speed and extent of fluorescence recovery provide key insights into the dynamics, mobility, and diffusion rates of the labelled molecules, offering valuable information about molecular interactions, membrane fluidity, and protein movement within living cells or biomimetic membranes.

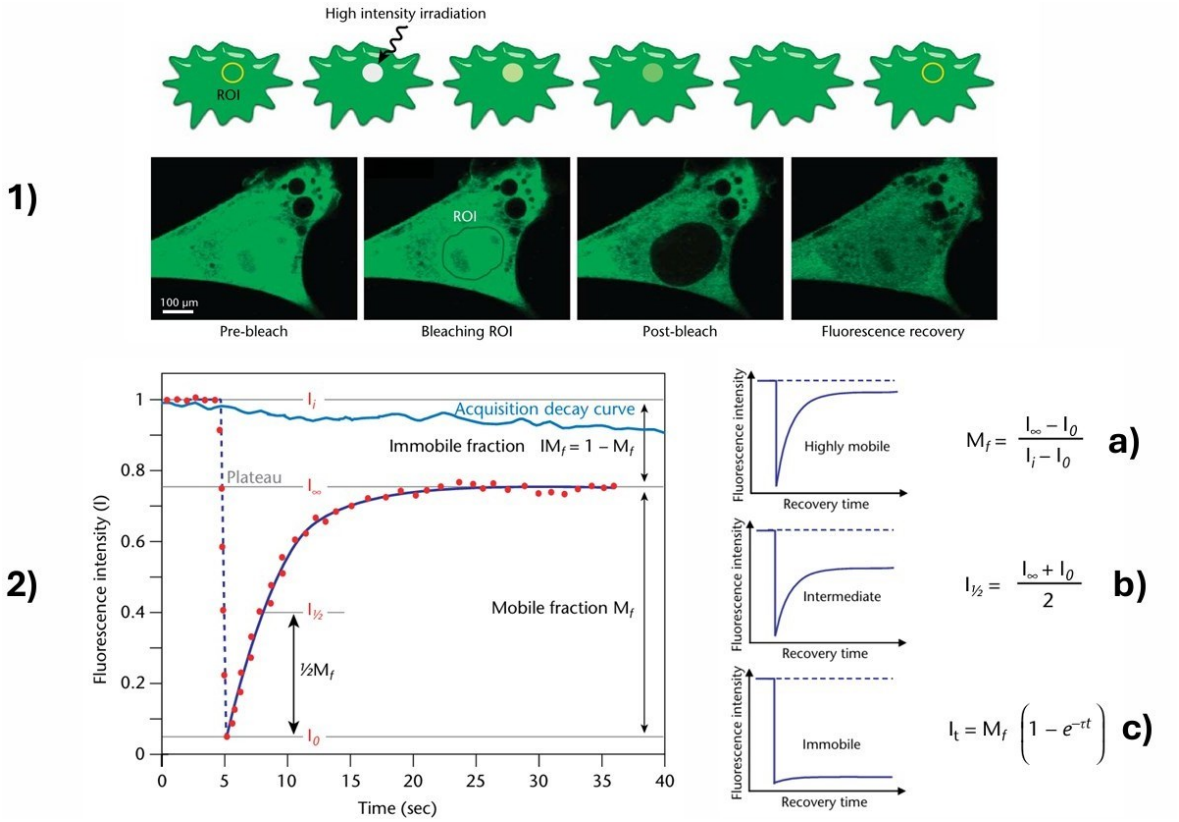

Figure 3.8 A region of interest (ROI) is selected, bleached using a high-intensity laser, and the fluorescence recovery within the ROI is monitored over time. Below is an example from an actual experiment in a myoblast cell line (myo3) homogeneously expressing GFP-Myosin III before bleaching. (2) Initially, the fluorescence intensity starts at a pre-bleach level (Ii), then sharply decreases to a low value (I0) when the intense laser bleaches the fluorophores in the ROI. Over time, the fluorescence signal recovers from I0 to a maximal plateau

value (IN). From this recovery curve, along with equations (a) and (b), key parameters such as the mobile fraction (Mf), immobile fraction (IMf), and the half-time of recovery (I1/2) can be determined. A reference photobleaching curve (light blue line) is included to correct for fluorescence loss during data acquisition. The recovery curve (I0 to IN) provides critical information to calculate the diffusion constant and assess the binding dynamics of fluorescently labeled proteins. A more precise method for obtaining the half-life and immobile/mobile fractions, suitable for automation, involves nonlinear curve fitting of the experimental data using the simple exponential model described by equation (c). Readapted from [146].

In a typical FRAP experiment, a specific region of interest (ROI) is carefully selected for photobleaching. This ROI contains fluorescently labelled molecules whose dynamics are under investigation. A critical parameter in FRAP is the precise definition of the ROI's diameter, as it directly influences the spatial resolution and accuracy of diffusion measurements. Once the ROI is established, it is subjected to high-intensity laser illumination, causing photobleaching, which is the irreversible loss of fluorescence due to high-energy excitation [147,148]. This process destroys the fluorescent properties of molecules within the targeted area. After photobleaching, the recovery of fluorescence is monitored over time by illuminating the sample with a low-intensity laser, which excites the remaining fluorescent molecules outside the bleached area. These intact molecules then diffuse into the bleached ROI, and their fluorescence emission is measured using a photodetector. The resulting fluorescence recovery curve provides a temporal profile of how quickly fluorescence returns to the bleached region. The recovery curve is analysed to extract key parameters, such as the diffusion coefficient, which quantifies the mobility of the fluorescent molecules. This analysis provides valuable insights into the dynamics of molecular interactions, diffusion rates, and mobility of proteins, lipids, or other biomolecules in the sample. Several factors influence the dynamics of fluorescence recovery, including the diffusion characteristics of the molecules, their concentration in surrounding unbleached regions, and potential barriers or obstacles that may hinder diffusion, such as membrane structures or cytoskeletal elements [149]. FRAP is often employed to investigate the phase behaviour of supported lipid bilayers, offering insights into the fluidity of distinct membrane phases, such as the liquid-ordered (Lo) and liquid-disordered (Ld) phases. By utilizing fluorescent dyes that selectively partition into these phases, FRAP experiments provide detailed information on the dynamics and organization of these membrane domains. In this study, FRAP was used to calculate the diffusion coefficients of the Lo and Ld phases, allowing for a deeper understanding of their respective fluidity and membrane properties. The diffusion coefficient (D) in a FRAP experiment can be derived by analysing the recovery of fluorescence over time in the bleached region. We used a Function: Diff_2D_InfiniteReservoir_Circle, developed at the MPI of Biochemistry (MPI of Biochemistry,Schwille Laboratory, Martinsried, Munich, Germany). Briefly, this function models FRAP in a two-dimensional (2D) system or in a prolate bleach region within a three-dimensional (3D) environment. The primary application is for analysing FRAP experiments where the diffusion of fluorescent molecules occurs within a plane (e.g., cell membranes) or for certain cases of 3D diffusion where the geometry approximates a prolate spheroid. The function is characterized by four

parameters, which control aspects such as the diffusion coefficient and other relevant variables specific to the system being analysed. This is a user-defined function, designed to accommodate specific experimental setups that fall under FRAP-based diffusion models, and it is represented as an expression, allowing for flexible fitting of experimental data, such as fluorescence intensity recovery curves over time. The function involves one independent variable, typically time, which serves as the axis along which the fluorescence recovery is monitored and measured. There is one dependent variable, usually representing the fluorescence intensity or recovery ratio over time as the unbleached fluorescent molecules diffuse back into the bleached region. The function operates as an explicit model, meaning the output (dependent variable) is directly calculated from the input (independent variable) and parameter values, making it suitable for fitting FRAP recovery curves and extracting diffusion coefficients. The normalized fluorescence intensity is plotted as a function of time to produce a recovery curve characteristic of FRAP. The final fluorescence intensity generally remains slightly lower than the pre-bleach level because a portion of the molecules in the sample is permanently photobleached. The diffusion rate of molecules in the sample is quantified by fitting the recovery curves to a theoretical FRAP model. The Soumpasis equation (Equation A) is commonly used to accurately describe fluorescence recovery in circular regions of interest (ROIs) [150].

$$f(t) = A\left\{exp\left(-\frac{2\tau_D}{t}\right)\left[J_0\left(\frac{2\tau_D}{t}\right) + J_1\left(\frac{2\tau_D}{t}\right)\right]\right\}$$

Equation A

where t is time, A is the fluorescence recovery level, τD is the characteristic recovery time, and J0 and J1 are modified Bessel functions of the first order. The diffusion coefficient (D) can be calculated from the recovery times and the radius of the bleached region (ω) using the equation B.

$$D = \frac{\omega^2}{4\tau_D}$$

Equation B

In this work, a FRAP experiment was performed using a time series of 200 cycles, with 7 iterations of bleaching applied. A Plan-Apochromat 20x/0.8 M27 objective was utilized. The pixel dwell time was set to 0.70 microseconds, resulting in a scan time of 121.02 milliseconds per frame. The imaging field had dimensions of 42.5 µm × 42.5 µm, corresponding to a pixel size of 0.17 µm. The region of interest (ROI) selected for bleaching was 5 µm. The experiment employed a 488 nm argon laser and a 633 nm HeNe laser. Bleaching was initiated after the 5th scan in the series of 200 scans.

3.13 Differential scanning calorimetry (DSC)

DSC is a thermodynamic technique that measures the heat energy absorbed by a sample as its temperature changes under controlled conditions. This method is particularly useful for investigating bilayer membranes, as it allows for the precise monitoring of lipid phase transitions, which are critical for understanding membrane stability and functionality [151]. Through DSC, it is possible to obtain insights into the thermal behaviour of lipids, helping to characterize phase changes that occur during temperature variations. DSC has become an essential tool in membrane biophysics, since it allows to study lipid interactions, phase diagrams, and the effects of various additives on membrane properties [152]. This technique's ability to provide detailed thermal profiles makes it invaluable for developing new biomaterials and understanding membrane dynamics in biological systems. In a typical DSC experiment, the energy is applied to two identical sealed capillary cells simultaneously: one containing the sample and the other serving as a reference. The key principle is that the energy required to elevate the temperature of the sample to match that of the reference reflects the heat absorbed or released by the sample during phase transitions [153]. For endothermic processes, the sample absorbs heat, resulting in a positive energy differential, whereas, in exothermic processes, the sample releases heat, leading to a negative differential. This energy exchange provides valuable insights into the thermal properties of the sample, allowing researchers to characterize phase transitions and thermal stability effectively. What is measured in a DSC experiment is the specific heat capacity (Cp) of a sample as a function of temperature [154]. As the temperature changes, the specific heat capacity reflects how much heat energy is required to raise the temperature of the sample by one degree Celsius. This capability is particularly important for assessing phase transitions, such as melting or crystallization, which can provide insights into the structural and dynamic properties of the material being studied, especially in lipid bilayers. In this context, key thermodynamic parameters that can be derived from the DSC data include the enthalpy change (ΔH), that quantifies the heat absorbed or released during a phase transition, providing insights into the thermodynamic stability of the sample, the transition temperature (Tm), at which a phase change occurs, the entropy change (ΔS), that represents the degree of disorder associated with the phase transition, and finally the heat capacity (Cp) that measured specific heat capacity provides a direct measure of how the material responds to changes in temperature. The primary information obtained from DSC analysis is the first order phase transitions of the system. This is typically identified at the peak of the DSC curve, corresponding to the characteristic transition temperature of the sample. In addition to determining Tm, integrating the area under the peak allows for the calculation of the enthalpy change (ΔH) associated with the transition. This value is essential for understanding the energy dynamics of the phase change. Furthermore, the entropy change (ΔS) can be approximated using the relationship $\Delta S = \Delta H/Tm$, providing further insight into the thermodynamic properties of the system [155].

These thermodynamic parameters—enthalpy and entropy changes—are crucial for elucidating the stability and behaviour of lipid bilayers and other complex systems under varying temperature

conditions. The DSC experiments were conducted in collaboration with Prof. Valeria Rondelli from the University of Milano's Biometra research center. This collaboration enabled us to investigate the phase behaviour and transition temperatures of supported lipid bilayers at two different cholesterol concentrations (7 mol% and 33 mol%). The goal was to gain insights into how cholesterol influences the phase behaviour of the optimized model systems. To provide further details, we investigated with this technique the two samples studied in this work, composed of DOPC:DSPC:SM and two different cholesterol concentration namely 7 mol% and 33 mol%. In table 4.1 of the experimental results section are reported the molar ratio of the lipids. As a first step have been prepared the liposomes using the thin film hydration method and hydrated to a 2% concentration (0.02 g/mL) using PBS buffer. The samples were then subjected to freeze-thaw cycles and stored at 40°C until use, without extrusion or additional processing. Each sample was sealed separately in DSC-specific glass capillaries, measuring 9 cm in length and 2 mm in diameter. The calorimeter used for the measurements consisted of two identical cells, each containing a glass capillary. One cell held the sample solution, while the other contained water as a reference. The specific heat capacity was determined by measuring the difference in power supplied to the two cells during controlled temperature changes over time. The model membrane samples were analysed through temperature cycles ranging from 5°C to 60°C at a scan rate of 1°C per 3 minutes, in both cooling and heating modes. At the beginning of the experiment, an isothermal hold at 60°C was applied for 1 hour to ensure thermal equilibrium between the sample and the instrument. Subsequently, intermediate isothermal holds of 3600 seconds were introduced before each cooling and heating cycle.

Chapter4: Experimental Data

4.1 Optimization and characterisation of 4- components model SLBs in physiological buffer

The primary aim of this research was to develop multicomponent SLBs that accurately mimic the outer leaflet of eucaryotic cell membranes. As already stated, there is an extremely rich variability of lipid species in plasma membranes (500-1000 different molecules), which depends on cell type and phase of the respective cell cycle. They concur to grant the membrane a high degree of lateral heterogeneity, with distinct sub-compartments either in gel or liquid phase, that vary in their biophysical properties and composition. The idea here is to develop simple mimics, by selecting the most representative lipid building blocks, able to reproduce both disordered and gel or ordered liquid phases, maintaining the relative ratios among species close to the ones in the external leaflet of eukaryotic cell membranes. Achieving a good degree of variability of the parameters (e.g. cholesterol concentration) and reproducibility in these models is crucial for understanding how different molecular players interact within the membrane and contribute to molecular trafficking through eukaryotic membranes. The most abundant lipids in the external membrane leaflet have a phosphatidylcholine (PC) head group and are known to reach 60-80% of total lipids [156]. Another well represented lipid is sphingomyelin (SM), which is characterized by saturated alkyl chains (18 carbons long) and is therefore in gel phase at RT (Tm = 37 ° C). Therefore, a composition consisting of the unsaturated 1,2-dioleoyl-sn-glycero-3-phosphocholine (DOPC), brain-SM and cholesterol has been identified and used in many works as particularly effective simple model to mimic the plasma membrane. In this framework, researchers at the NanoInnovation Lab before this work had optimized SLBs composed of DOPC and SM in ratio 2:1, plus various molar ratios of cholesterol. A careful characterization of the membrane, obtained via a combination of complementary microscopy, spectroscopy and scattering techniques, allowed to highlight the role of the degree of lipid order and membrane fluidity in the uptake of extracellular vesicles (Paba et. al.; Perissinotto et. al.,) [157,158]. Such SLBs were also used as effective models for investigating how iron affects the binding and interaction of α-synuclein with lipid raft domains, simulating the lipid environment of neuronal cell membranes (Perissinotto et. al.). [159] The SLB model developed by C. Paba bore the limitation of being stable only up to a cholesterol molar concentration of about 20%, below the physiological ones, which are exceeding 30%. This limitation should be attributed to the the ratio of unsaturated lipids (DOPC) to saturated sphingomyelin (SM) in the model. In Paba's mimic, the DOPC:SM ratio was maintained at 2:1, whereas studies in the literature that explore cholesterol variation typically use an unsaturated/saturated lipid ratio close to 1 [160].

Therefore, we decided to introduce a model richer in PC and with a saturated/unsaturated lipid ratio close to 1. We introduced DSPC, a saturated phospholipid with a strong affinity for cholesterol, that

shares the same acyl chain length (18 carbons) as DOPC and SM. The addition of DSPC not only increases the diversity of phosphatidylcholine (PC) groups but also promotes the formation of lipid rafts due to its saturated nature. By maintaining the 1:1 balance of saturated to unsaturated lipids, this model closely reflects the natural lipid distribution and provides a robust framework for studying the effects of cholesterol on membrane formation. In Figure 3.1 the lipids used in the new model membrane are reported, together with their relative Tm. An unpredicted advantage of this mimic is that phase-separated membrane domains form already at RT (25±1°C), i.e. well below the transition temperature of both DSPC (Tm = 55 ° C) and SM (Tm = 37 ° C), for both the conditions of cholesterol exploited here. In the study by Paba et al. instead, the development of phase separated domains was obtained only upon maintaining the system at a temperature above the SM melting temperature for about 30 minutes. The reasons for this behaviour will be discussed in detail in the next sections.

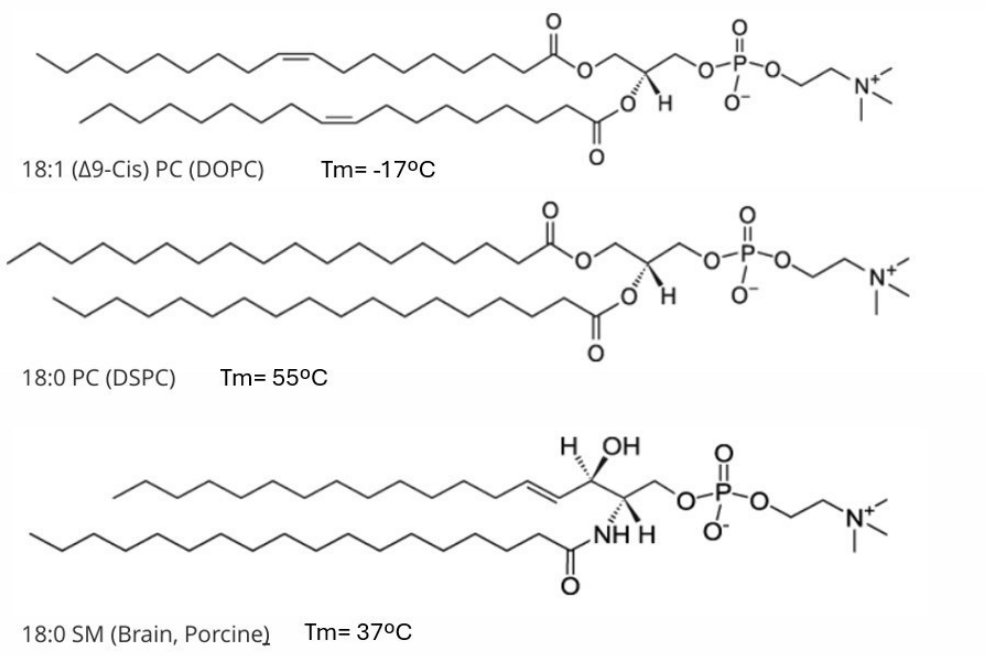

Figure 4.1 Molecular structures of three phospholipids used in this work: 18:1 (Δ9-Cis) PC (DOPC), 18:0 PC (DSPC), and SM (Sphingomyelin, Brain, Porcine). DOPC is an unsaturated phosphatidylcholine with one double bond, while DSPC and SM are saturated lipids with 18:0 fatty acid chains. These lipids are critical components of membrane models due to their distinct interactions with cholesterol and their roles in modulating membrane fluidity and raft formation. Image source: Avanti polar lipids website.

SLB	% DOPC	% DSPC	% SM	% Cholesterol
Low Cholesterol	48.6	27.8	16.6	7
High Cholesterol	35	20	12	33

Table 4.1 Percentage of lipids (m/m) used to reconstitute SLBs at two different cholesterol concentrations (7 mol % and 33 mol%). The molar ratio of DOPC:DSPC: SM is kept constant to evaluate the effect of cholesterol in determining LRs behaviour.

Two distinct SLBs were optimized by varying the cholesterol concentration from 7% to 33% while keeping the lipid ratios (DOPC: DSPC:SM) constant (Table 4.1). In particular, the model containing 33 mol% cholesterol, was specifically designed to replicate the lipid composition of the plasma membrane outer leaflet. This concentration is known to be critical for preserving the membrane's structural integrity, regulating fluidity, and supporting key functional properties, including the formation of lipid rafts and protein-lipid interactions [161-162].

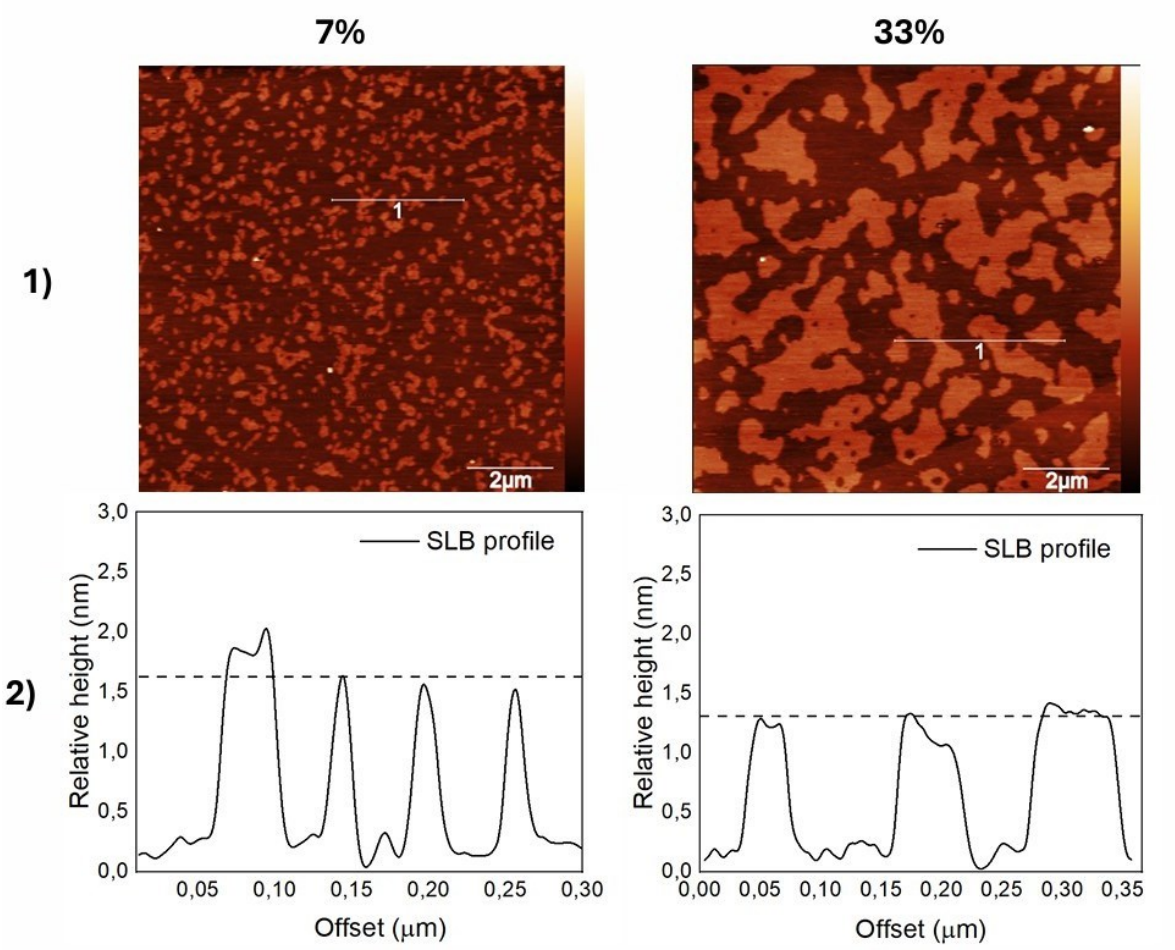

Figure 4.2 AFM topography images (1) of SLBs reconstituted with constant ratio of DOPC:DSPC:SM at two different cholesterol concentrations (7% mol% (low) and 33% mol % (high)) in HEPES/NaCl (10mM, 150mM) buffer. Panel 2 displays the relative height profiles highlighting the mismatch between the lipid rafts and the liquid-disordered phase (Ld) of the membrane.

The morphology of lipid rafts was studied through atomic force microscopy topography images (Figure 4.2, Panel 1). In the AFM images we observe bright islands protruding with respect to a homogeneous phase, lower in height. We attribute the bright islands to Lo phase (or LRs), since their height suggest that these assemblies are more ordered and tightly packed than the surrounding bilayer, which in contrast we attribute to the Ld phase [163]. The size and the relative height of such Lo islands (with respect to the summit of the Ld phase) depend strongly on cholesterol concentration. At a 7 mol% cholesterol, the LRs are smaller in size than those in membranes with 33 mol% cholesterol, while the relative height decreases as cholesterol concentration increases. Specifically, the

relative height decreases from 1.84 ± 0.3 nm at 7% cholesterol to 1.03 ± 0.2 nm at 33%, as illustrated in Figure 4.3 , panel 2, which presents a statistical analysis of multiple datasets obtained from different experiments. At the same time, as cholesterol levels increase, the area occupied by lipid rafts expands, from 22 ± 3.7% at 7% cholesterol to 34.7 ± 5.6% at 33% cholesterol, as illustrated in Figure 4.3, panel 1.

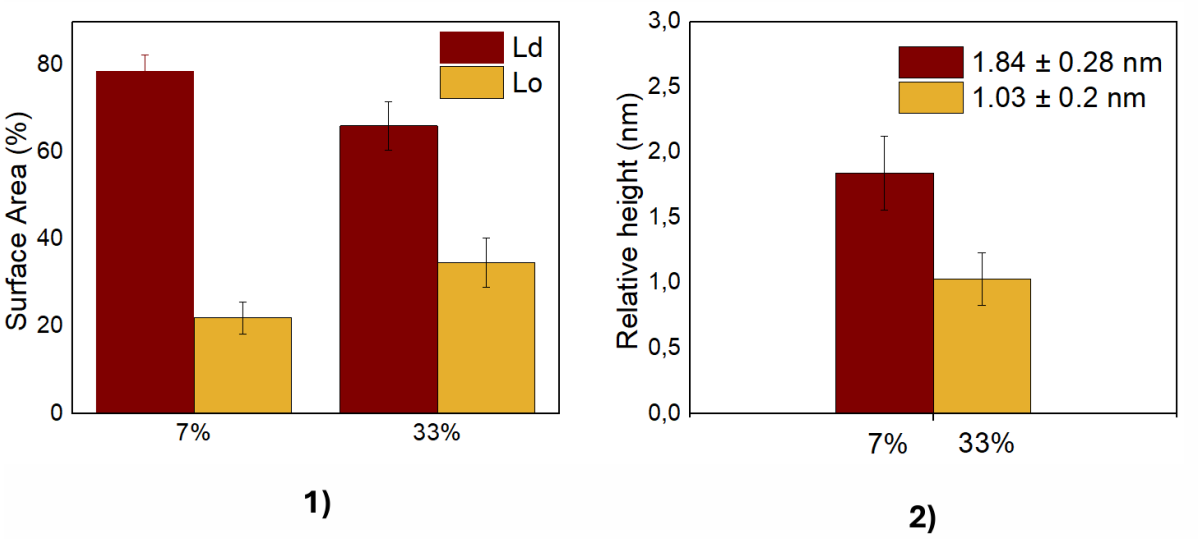

Figure 4.3 Statistical analysis of LRs relative height variation with cholesterol concentration is presented in the panel 1. Panel 2 displays the statistical analysis of the surface area (%) at the two different cholesterol concentrations.

This cholesterol-induced effect on the height of ordered domains is consistent with findings reported in other studies in the literature and is attributed to cholesterol's tendency to preferentially interact with saturated lipids [164-166], specifically in our case DSPC and SM. Van der Waals and hydrophobic forces play a pivotal role in decreasing lipid rafts height and increasing the local fluidity of the ordered (Lo) phase. Also in the Ld phase, cholesterol has a role in tuning the lipid disorder. In our membrane model at room temperature (25 ±1 °C), DOPC exists in the Ld phase due to its transition temperature (Tm) of -17°C. In contrast, the saturated lipids, DSPC and SM, which have transition temperatures of 37°C and 55°C, respectively, are in gel (or solid ordered, So) phase in the absence of cholesterol, or in liquid ordered phase when cholesterol is introduced, respectively. Consequently, without cholesterol, we expect to observe gel phase islands surrounded by DOPC.

By labelling the different phases in our SLBs and by combining confocal laser scanning microscopy and atomic force microscopy imaging, we confirmed the contribution of each lipid species to the different phases. In Figure 4.4 we report confocal microscopy (Panel a) and AFM images (Panel b) relative to a zero cholesterol SLB. To visualize the gel phase phase via fluorescence microscopy, we employed NBD-DSPE, a probe that preferentially binds to saturated lipids like SM and DSPC. In this experiment, we maintained a constant lipid ratio of DOPC:(DSPC+SM) at 0.9, These gel-phase islands are protruding approximately 2 nm in height (measured with the AFM) from the surrounding DOPC,

labelled with ATTO655-DOPE. ATTO655-DOPE preferentially partitions into the disordered phase due to its association with a DOPE characterized by a melting temperature (Tm) of -15°C, similar to that of DOPC (-17°C)[167, 168]. As a result, it inevitably localizes within the disordered phase. Without cholesterol, the system forms gel-phase domains, meaning the phase should be defined as So (solid-ordered) rather than Lo (liquid-ordered). The Lo phase—associated with lipid rafts—emerges only in the presence of cholesterol. In the So phase, lateral mobility is highly restricted, as gel domains inherently exhibit minimal lateral movement when cholesterol is absent and are surrounded by a disordered matrix composed of DOPC in this case. The relative height between So and Ld phases is higher with respect to what measured in the presence of cholesterol, as reported in Figure 4.4, panel b), confirming the role of cholesterol in disrupting the tightly packed arrangement of saturated lipids in the So phase. As previously discussed, cholesterol has a dual role: it disrupts the highly structured So phase while simultaneously stabilizing the more fluid Ld phase.

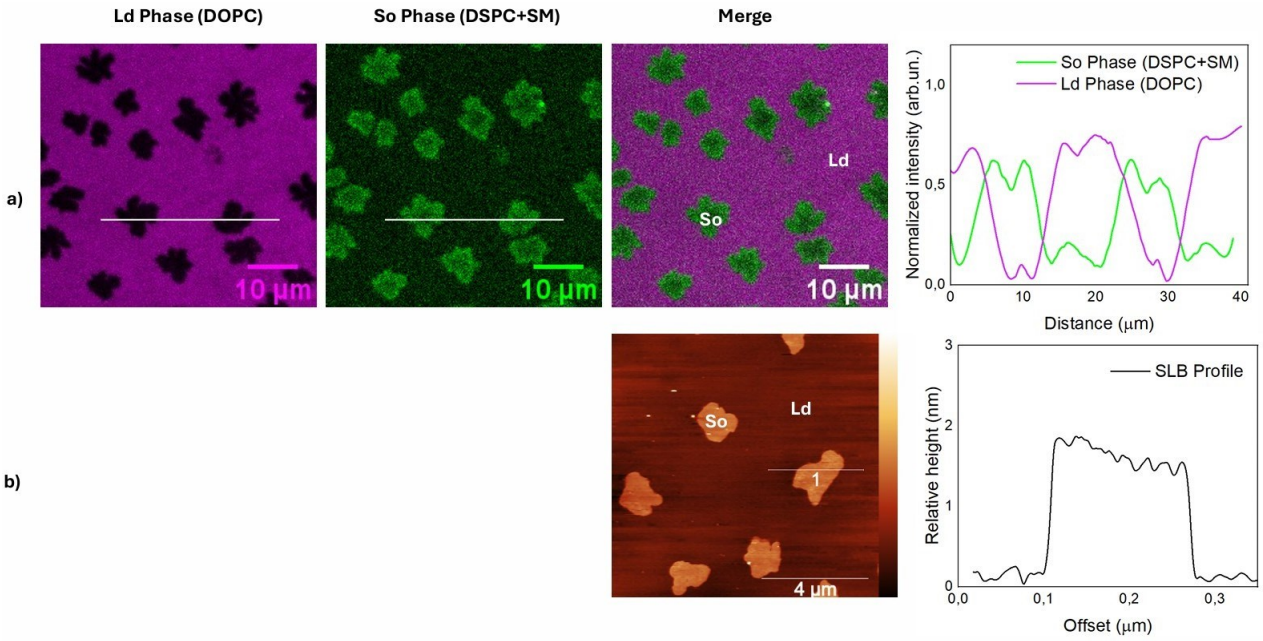

Figure 4.4 Visualization of the solid-ordered phase (So) formation in SLB Composed of DOPC, DSPC, and SM. This figure illustrates the distinct separation between Ld and So phase with measurable differences in fluorescence intensity. Panel a) display the CLSM images showing the phase separation between Ld-So. Panel b) display the AFM topography image in which the bright islands represent the thicker So phase, while the brown matrix is the Ld phase. The relative height profile taken along the white line in the AFM image, showing a clear height difference between the Ld and So phases, with the So phase protrude from Ld phase approximately 2 nm. Magenta: Ld phase, green: Lo phase.

In the presence of cholesterol, the So phase relaxes to a Lo one, significantly altering the membrane's physicochemical properties. Cholesterol induces the formation of small domains in membranes with low cholesterol concentration (7 mol%), which gradually expand as cholesterol level increases. This behaviour is likely due to the discontinuity at the boundary between the lipid phases. When both Ld

and Lo phases coexist in the membrane, the bilayer width discontinuity generates tension along the phase boundary [169-171].

This tension affects membrane curvature at the interface between the Ld and Lo phases and influences the kinetics of separation and the size of lipid domains. The observed decrease in raft height with increasing cholesterol concentration indicates a reorganization of lipid molecules, shifting from an ordered state in the gel phase to a locally disordered configuration. Literature confirms that cholesterol can order disordered phases while locally disordering gel phases, thereby facilitating the formation of the Lo phase. This effect occurs as cholesterol integrates into both phases, with a preference for the ordered phase, as evidenced by the progressive increase in the area occupied by this phase. In Figure 4.5, CLSM was used to follow the evolution of domains with increasing concentration of cholesterol.

We adopted a dual-labelling approach for targeting cholesterol (Bodypy- cholesterol probe) or the saturated lipids (NBD-DSPE) on one side, vs. unsaturated ones (ATTO655-DOPE) to facilitate a fluorescence-based exploration of phase separation process. In the presence of fluorophores, the domains increase in size as reported in figure 3.4. This can be attributed to several factors described in the literature [172,173]. Notably, the choice of fluorophore has been shown to influence raft morphology, as highlighted by previous studies, while substrate effects on domain formation are also recognized. In this study, we used mica as the substrate for both atomic force microscopy and fluorescence measurements, which minimizes substrate-related artifacts. In literature [174] has been investigated the dipole orientation angle (θ) of lipid molecules in relation to the membrane's normal, exploring how factors such as lipid head group structure, membrane composition, hydration level, and cholesterol content can influence this angle. This angle, θ, represents the orientation of lipid molecules in the membrane and is crucial for understanding membrane dynamics. The calculations assumed that the acyl chains (long fatty acid tails) of lipid probes are perpendicular to the chromophore, the part of the dye responsible for fluorescence. In the case of DiI, a commonly used dye, they observed that θ was 62° in liquid- disordered bilayers (such as those formed with POPC) and increased to 70° in more ordered bilayers (like those with DPPC/cholesterol at a 1:1 ratio). This change in θ as the membrane shifts from a disordered to an ordered state suggests a correlation between membrane order and the orientation of the dipole. This observation is further supported by examining the order parameter, which measures the degree of organization, or "order," within the membrane. A higher order parameter corresponds to a more ordered membrane state. For DiI, the order parameter was 0.34 in liquid-disordered POPC bilayers (θ = 62°) and increased to 0.65 in the more ordered DPPC/cholesterol bilayers (θ = 70°). This trend reflects how θ and the order parameter both rise with increasing membrane order, indicating that the orientation of lipid molecules aligns more predictably in ordered environments. In contrast, other dyes such as Rh-DOPE, Rh-DPPE, and NBD-DPPE have a single bond connecting the chromophore to the lipid molecule, allowing their dipole orientation angle θ to fluctuate more freely. This flexibility complicates the calculation of the order parameter for

these dyes, as their orientation is less stable compared to DiI. DiI, on the other hand, has a rigid linkage between the chromophore and its acyl chains, resulting in a fixed angle θ, which allows for more stable and reliable measurements of membrane order. Based on these observations, the authors concluded that differences in dye flexibility— particularly between dyes like DiI and those with single-bond flexibility (Rh-DOPE, Rh-DPPE, NBD-DPPE)—impact membrane morphology. Flexible dyes interact differently with the membrane structure than dyes with fixed orientations, influencing properties such as membrane organization and potentially the overall morphology of the bilayer. Given these observations and the use of NBD-DSPE as a dye for the Lo phase and ATTO655 for the Ld phase in this study, it's possible that the dyes themselves may be influencing the morphology of membrane domains. In fluorescence imaging, we observe larger domains than those detected with AFM, suggesting that the presence of the dyes might be contributing to an apparent increase in domain size. This discrepancy makes reasonable the hypothesis that the dyes may alter the membrane's structure in ways that affect the observed domain morphology in fluorescence techniques. However, the reasons for the expansion of Lo/Ld domains in model membranes to a microscopic scale, in contrast to the nanometer-scale domains found in physiological plasma membranes, remain an area of ongoing investigation [175,176]. The discrepancies between AFM and fluorescence findings can be attributed to the resolution limits inherent in fluorescence techniques. AFM can resolve nanoscale domains, while fluorescence lacks the resolution to identify domains smaller than 1 μm due to background noise and intrinsic limitations in optical resolution. However, as we can see in figure 4.5, the presence of micron-scale domains is primarily related to how the lipids organize themselves. With AFM, we can distinguish not only micron-scale domains but also those on the nanometer scale, as AFM has the resolution capability that confocal fluorescence microscopy cannot achieve. To further elucidate the localization of cholesterol within these phases, we employed Top-Fluor cholesterol as a selective labelling agent. The results indicated that cholesterol preferentially intercalates into the Lo phase, corroborating our earlier findings that the area of the Lo phase increases with higher cholesterol concentrations.

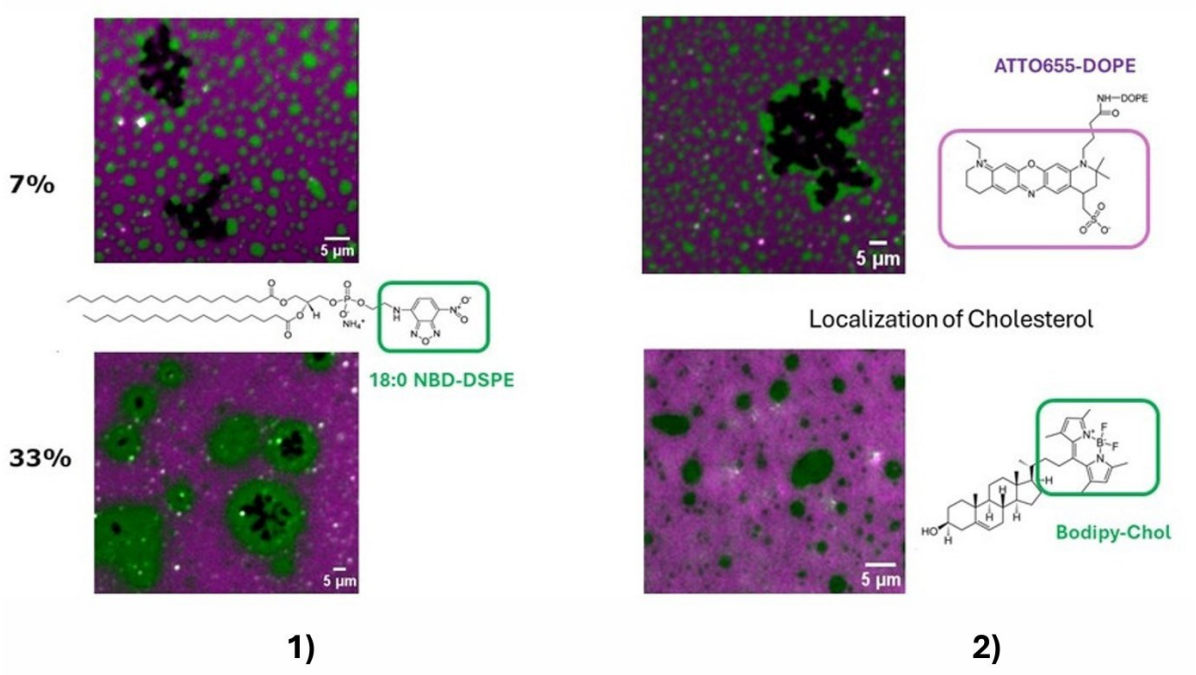

Figure 4.5 CLSM images of SLBs in which has been fluorescently labeld the entire Lo phase with 18:0 NDB-DSPE 1) and cholesterol with Bodipy-Chol dye 2) (green). The Ld phase (magenta) has been fluorescently labeld with ATTO-655-DOPE in both cases. The scale bar is 5 µm.

4.2 Evaluation of SLBs thickness

To evaluate the thickness of the optimized SLBs composed of constant ratio of DOPC:DSPC:SM at two different cholesterol concentrations (7% mol% and 33% mol %) in physiological buffer HEPES/NaCl, we created defects in the SLBs by applying targeted pipetting, which induced localized defects in the lipid membrane. These defects expose the substrate beneath the bilayer, allowing for a precise measurement of the bilayer height [177].

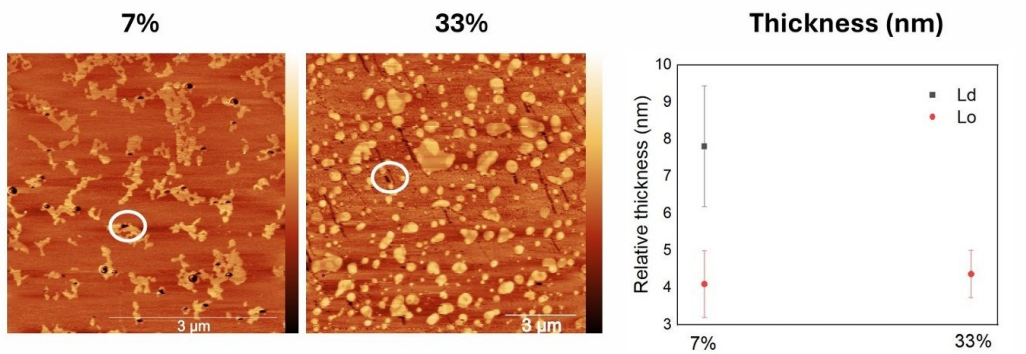

	Thickness Lo (nm)	Thickness Ld (nm)
7%	7.8 ± 1.6	4.1 ± 1
33%	-	4.4 ± 0.6

Figure 4.6 AFM images and thickness analysis of SLBs with 7 mol % and 33 mol % cholesterol concentrations. The AFM images on the left show the surface of SLBs at the two cholesterol levels, with circled regions indicating

defects used to measure the thickness of the lipid bilayers. The graph on the right displays the relative thickness of the Ld and Lo phases at 7 mol % and 33% cholesterol. The table below summarizes the measured thickness values for each phase.

Our AFM images are reported in Figure 4.6, for both 7 and 33% cholesterol. In the case of 7% cholesterol, we were able to scratch both the Lo and Ld phases, obtaining separated measurements of their relative height. There, we found that the Lo phase is significantly thicker (7.8 ± 1.6 nm) than the Ld phase (4.1 ± 1 nm), indicating a structured, ordered lipid region likely due to tighter packing of the lipids in the Lo domains. In the case of the 33 mol% cholesterol, we were able to directly scratch only the Ld phase finding a thickness of 4.4 ± 0.6 nm, similar to the one of the Ld phase at 7 mol % cholesterol, and in line with the average values of 4-5 nm typically reported in the literature [177,178]. The fact that in SLBs with 33 mol % cholesterol the scratches attempted in the Lo phase were closing fast, suggests that higher cholesterol concentrations alter the lipid packing, increasing lipid mobility. In this case, the observed difference in height compared to Figure 4.3 can also be attributed to the intentional perturbation of the membrane to create defects. These defects were necessary to measure the bilayer thickness, and as a result, the lipids may not have fully reorganized.

4.3 AFM Study of SLB Morphology and LRs Organization

As previously discussed, the formation of the SLBs is strongly influenced by temperature. The observed decrease in height with increasing cholesterol concentration implies a reorganization of lipid molecules, transitioning from an ordered state to a locally disordered configuration. It is well established in the literature that cholesterol can increase order disordered phases and locally disorder the ordered ones, promoting the transition of So to Lo phase. In our system, given the progressive increase in the area occupied by the LRs, we assume that it preferentially locates in the Lo phase. With respect to the system developed by Paba, the ordered phase in our SBL mimic is in fact more extended, having a 1:1 mol/mol ratio between saturated/unsaturated lipids (against the 1:2 of Paba). This result suggests that the model membranes used exhibit a different fusion and organizational dynamic compared to those in previous studies. This also justify the fact that in Paba's model in order to promote phase separation the system required to reach a temperature above the Tm of SM, and then cooled down to RT, while in the present case it forms already at 25 °C. To better understand this phenomenon, further investigations were carried out to study the effect of temperature on membrane formation and the potential impact on the stability and organization of lipid rafts under various thermal conditions.

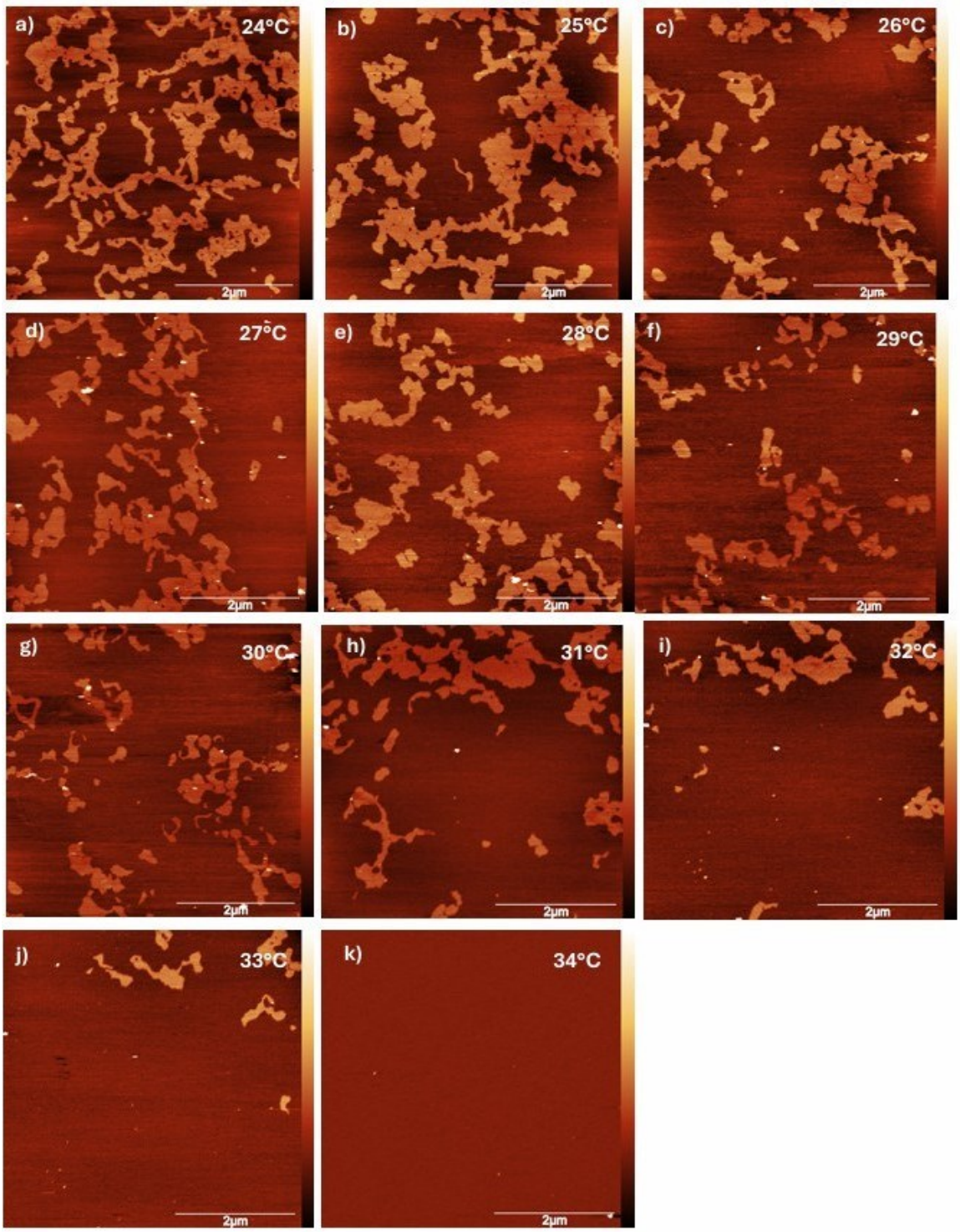

Figure 4.7 AFM topography images of the SLB composed of DOPC: DSPC:SM (48.6:27.8:16.6) and 7 mol % Cholesterol, fused on mica, illustrating the effect of temperature on lipid raft formation dynamics. Lipid rafts are protruded from the liquid-disordered phase, composed primarily of DOPC, and their morphology is highly temperature-dependent. The images represent different temperatures: (a) 24°C (b) 25°C, (c) 26°C, (d) 27°C, (e) 28°C, (f) 29°C, (g) 30°C, (h) 31°C, (i) 32°C, (j) 33°C, (k) 31°C. Each frame has been acquired after 5 min. Image size = 5x5 µm, with a scale bar of 2µm.

SLB 7% Cholesterol	Temperature (°C)	Relative Height LR (nm)
	24	2.3± 0.08
	25	1.8 ± 0.3
	26	2.0 ± 0.3
	27	1.7 ± 0.3
	28	1.6 ± 0.3
	29	1.6 ± 0.1
	30	1.2 ± 0.2
	31	1.0 ± 0.1
	32	1.0 ± 0.1
	33	1.1 ± 0.2

Table 4.2 Statistical height values of LRs at various temperatures for the supported lipid bilayer with the 7 mol % cholesterol concentration. The data reveal a distinct trend: as the cholesterol concentration increases, the height of the lipid rafts decreases. However, it is important to note that some data points deviate from this general trend. These anomalies may be attributed to the dynamic nature of lipid rafts, which can experience fluctuations and rearrangements due to changes in temperature. Such variations can affect the raft height and lead to outliers in the data.

SLB 7% Cholesterol	Temperature (°C)	Area Ld phase (%)	Area Lo phase (%)
	24	76± 3.2	24 ± 3.0
	25	78 ± 2.4	22 ± 2.4
	26	81 ± 2.4	19 ± 2.5
	27	84 ± 6.5	16± 6
	28	82 ± 2.6	18 ± 2.7
	29	83 ± 4.0	17 ± 3.4
	30	89 ± 4.2	11 ± 4.4
	31	96± 1.55	4.0 ± 2.05
	32	98 ± 0.7	2 ± 0.7
	33	99.5 ± 0.3	0.5 ± 0.3

Table 4.3 Statistical percentage of membrane area occupied by the two distinct lipid phases, liquid-disordered and liquid-ordered, at various temperatures for the SLB at the lowest cholesterol level. As temperature increases, the proportion of membrane area covered by lipid rafts, decreases. At 34°C, specific values for the areas of the Ld and Lo phases are not provided due to the observation of complete phase mixing, which results in a uniform distribution of lipid molecules and the absence of distinct phase separation.

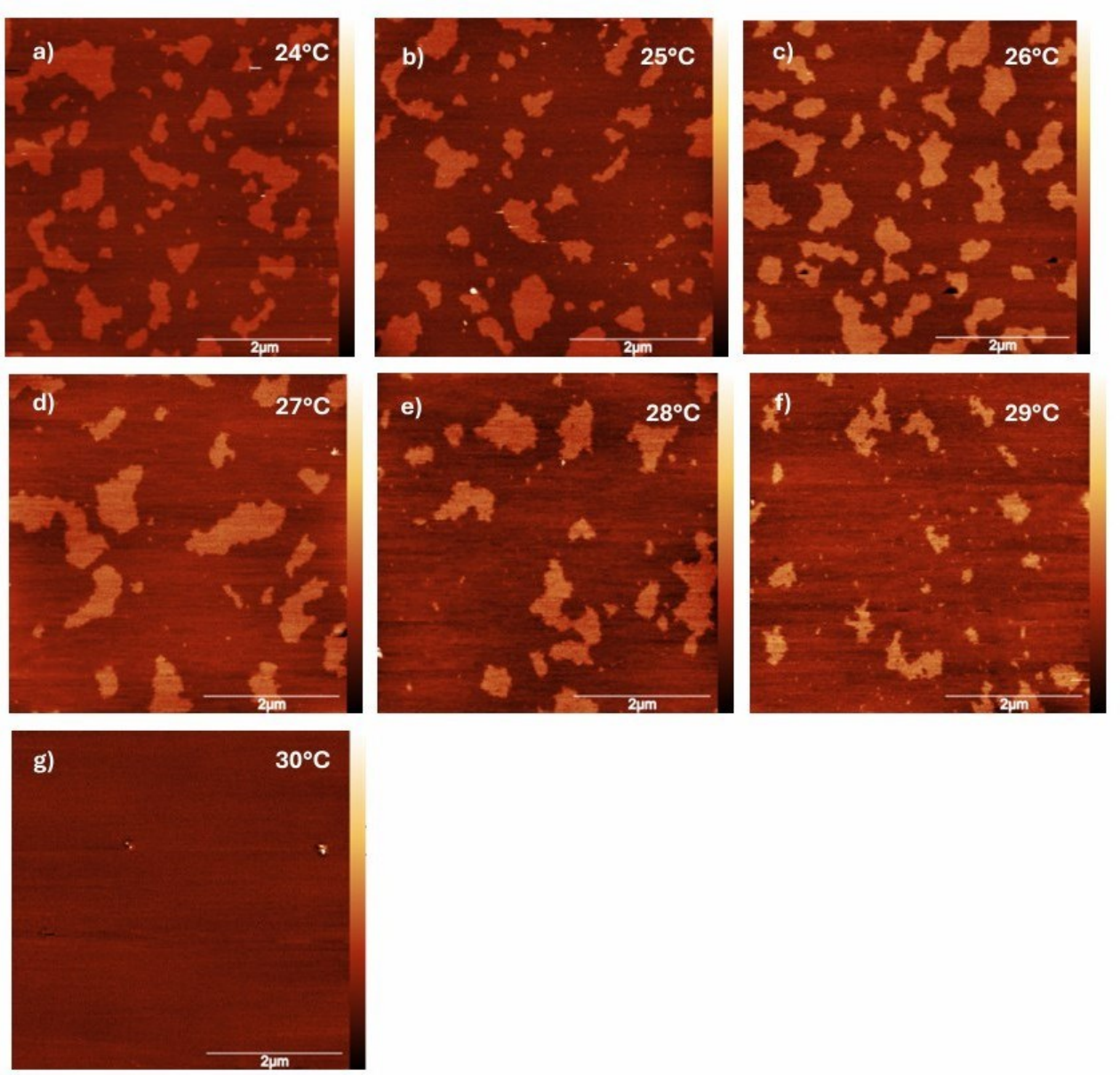

Figure 4.8 AFM topography images of the SLB composed of DOPC:DSPC:SM (35:20:12) and 33 mol % Cholesterol, fused on mica, illustrating the effect of temperature on lipid raft formation dynamics. LRs protruded from the liquid-disordered phase, composed primarily of DOPC, and their morphology is highly temperature-dependent. The images represent different temperatures: (a) 24°C, (b) 25°C, (c) 26°C, (d) 27°C, (e) 28°C, (f) 29°C, (g) 30°. Each frame has been acquired after 5 min. Image size = 5x5 µm, with a scale bar of 2 µm

SLB 33% Cholesterol	Temperature (°C)	Relative Height LR (nm)
	24	0.8± 0.08
	25	0.7± 0.01
	26	0.8 ± 0.02
	27	0.7 ± 0.1
	28	0.6 ± 0.01
	29	0.5 ± 0.04

Table 4.4 Height values of LRs at various temperatures for the SLB with 33 mol % cholesterol concentration. As cholesterol concentration increases, the height of the LRs decreases. This trend suggests that higher

cholesterol levels lead to a reduction in the height of the lipid rafts, likely due to increased packing density and altered membrane fluidity.

SLB 33% Cholesterol	Temperature (°C)	Area Ld phase (%)	Area Lo phase
	24	76 ± 5	24 ± 5
	25	77± 3	23 ± 4
	26	75 ± 1.4	25 ± 1.4
	27	81 ± 3.2	19 ± 3.3
	28	78 ± 4.1	22 ± 4.2
	29	93 ± 1.7	7 ± 1.7

Table 4.5 Percentage of membrane area occupied by the two distinct lipid phases, liquid-disordered and liquid-ordered, at various temperatures for the SLB at the 33 mol% cholesterol level. As temperature increases, the proportion of membrane area covered by LRs, or the Lo phase, decreases. At 30°C, specific values for the areas of the Ld and Lo phases are not provided due to the observation of complete phase mixing at this temperature, which results in a uniform distribution of lipid molecules and the absence of distinct phase separation.

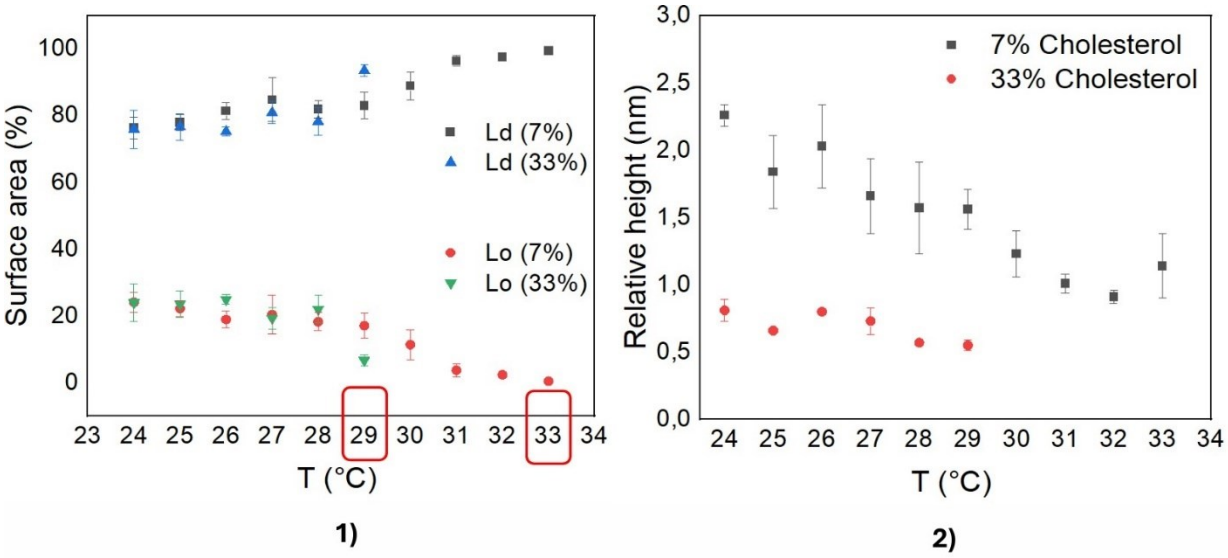

Figure 4.9 Scatter plots depicting the variation in surface area of the two phases as a function of temperature under the two cholesterol conditions investigated. In the case of SLBs with 7 mol % cholesterol, complete mixing between the two phases occurs at 34°C. However, as cholesterol content increases (33 mol %), the mixing between the two phases takes place at a lower temperature (30°C). This suggests a different degree of membrane fluidity, which, as expected, is closely dependent on temperature. 2) Scatter plots illustrating how the relative height of the LRs at the two different cholesterol concentrations changes with temperature. The trend in both cases point to a decrease in the relative height as the temperature increases.

We observed that phase mixing within the membrane begins at 29°C for the SLB with the 7 mol% cholesterol, with a complete mixing between the two phases at 34 °C. (Figure 4.7) The complete mixing is achieved at 30°C for the SLB with the 33 mol% cholesterol (Figure 4.8).

In both cases investigated, we observed a consistent behaviour characterized by a gradual disappearance of rafts. Based on evidence in the literature [179] we can associate that thermal fluctuations influence the orientation and packing of lipids, resulting in a more disordered state at

elevated temperatures. We found that increasing temperature has a significant impact on the phase transitions of lipid membranes, particularly affecting the transition between liquid-ordered (Lo) and liquid-disordered (Ld) phases. This effect is strongly dependent on the presence of cholesterol, which plays a crucial role in modulating membrane fluidity and stability. AFM experiments reveal that cholesterol modulates lipid bilayer transition temperatures, with phase mixing starting at 29°C for 7 mol% cholesterol and completing at 30°C for 33 mol%, temperatures destabilize lipid packing, shifting membranes to a liquid-disordered state.

As observed from the AFM measurements (both figures 4.7 and 4.8) conducted at varying temperatures, this parameter plays a pivotal role in modulating phase separation. The lipids in our membrane exhibit distinct transition temperatures, which mark the point at which they shift between different physical states. To gain deeper insights into the thermotropic properties of the complex SLBs developed at two different cholesterol concentrations, Differential Scanning Calorimetry (DSC) was employed to investigate their phase behaviour and transition temperatures, enabling us to differentiate between their phase characteristics. This technique is particularly useful since cholesterol concentration can significantly alter the membrane's structure and phase behaviour. Furthermore, cholesterol induces changes in the overall melting temperature of the membrane. Samples have been hydrated with PBS buffer to the final concentration of 20 mg/mL and sealed in glass capillaries for investigation. The scan rate was set to 3°C/min and measurements have been performed while cooling and heating the sample along more cycles. No difference emerges in the themograms related samples to heating and cooling, and none effect of annealing was observed when comparing repeated measurements.

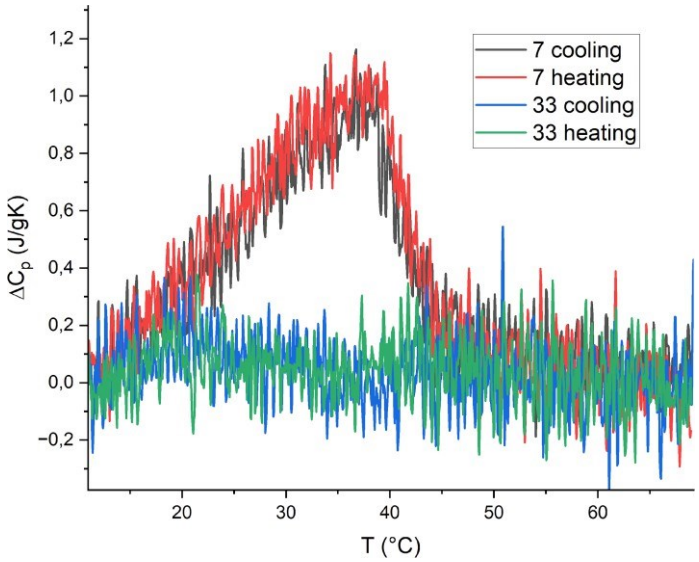

Figure 4.10 Differential Scanning Calorimetry (DSC) thermogram showing the heat capacity change (ΔCp) as a function of temperature (T) for lipid bilayers at two different cholesterol concentrations (7 mol % and 33 mol %) during both heating and cooling cycles. The red and black curves represent the heating and cooling processes for the sample with 7% cholesterol, respectively, while the blue and green curves represent the cooling and heating processes for the sample with 33% cholesterol. The presence of a pronounced peak around 40°C in the

7% cholesterol sample indicates a phase transition, while the 33% cholesterol sample shows a much more subdued transition, reflecting the impact of cholesterol concentration on the thermotropic behaviour of the membrane.

The thermogram, as reported in figure 4.10, measured for membrane with high cholesterol content shows no enthalpic peak, indication that the membrane does not undergo a phase transition over the investigated temperature range. This behaviour is expected for membranes with high cholesterol content, the cholesterol imposing a disordered phase to the lipids that, therefore, even at low temperatures, keep a disordered phase. On the other hand, the membrane with lower content of cholesterol undergoes a broad gel-to-fluid lipid chains phase transition around 35°C, likely to be associated to membrane regions with lower cholesterol content. The transition enthalpy is as low as 21+0.5 J/g, as expected for membranes with relatively high content of low-melting temperature lipids and cholesterol. These results are consistent with the surface area analysis we performed using AFM while varying the temperature. In fact, as shown in Figure 4.9, panel 1, we observe a significant change in the surface area occupied by the lipid rafts at the lower cholesterol concentration, which aligns with the phase transition observed in the DSC thermogram. On the other hand, for the higher cholesterol concentration, there is no significant change in the surface area of the lipid rafts as the temperature increases. This observation is also consistent with the DSC data, where no clear phase transition was detected in the thermogram at the higher cholesterol level. These findings suggest that the presence of higher cholesterol stabilizes the membrane structure, preventing major phase transitions even with increasing temperature. In order to be more aligned with the DSC analysis, we decided to investigate the structure and behaviour of the SLBs with AFM in an extended temperature range. We prepared SLBs with the two different cholesterol concentrations at 24°C and subsequently lowered the temperature to 16°C to assess the effects of cooling on SLB organization, and then increased T again to 24°C, in steps of 2 °C.

For the SLBs containing 7 mol % cholesterol, we observed no significant changes in the morphology of the lipid rafts, upon cooling and then warming-up the membrane. When the temperature was raised above 24°C, the SLBs retained the same characteristics that we had previously observed, indicating stability in the raft organization across the temperature range tested (Figure 4.11). However, in the case of SLBs with 33 mol % cholesterol (Figure 4.12) results were notably different. Cooling the system from 24°C to 16°C had a profound impact on the lipid raft organization. Upon reheating the sample to 24°C, we observed substantial changes in both the morphology of the lipid rafts and the area they occupied. Surprisingly, when the temperature was further increased to 28°C—a value slightly lower than the transition temperature identified in our earlier measurements—there was a complete mixing of the two membrane phases, indicating a disruption in domain segregation. Interestingly, when the temperature was lowered back to 16°C, the lipid rafts reformed, but with altered morphology and shape compared to their original state. This suggests a reversible but non-identical reorganization of lipid domains upon temperature cycling. These observations provide valuable insight into why DSC

results did not detect a distinct phase transition. The absence of a detectable transition does not necessarily imply a lack of lateral domain segregation. Rather, it suggests that at certain temperatures, the lipid domains may undergo dynamic reorganizations that prevent the detection of a clear transition by DSC. For instance, the complete mixing of phases observed at 28°C during our AFM investigation could explain the absence of a transition peak at that temperature. Our findings underscore the extreme sensitivity of SLBs to temperature changes, especially in cholesterol-rich systems. Cholesterol appears to play a crucial role in modulating the structural dynamics of the membrane, particularly in the organization and stability of lipid rafts.

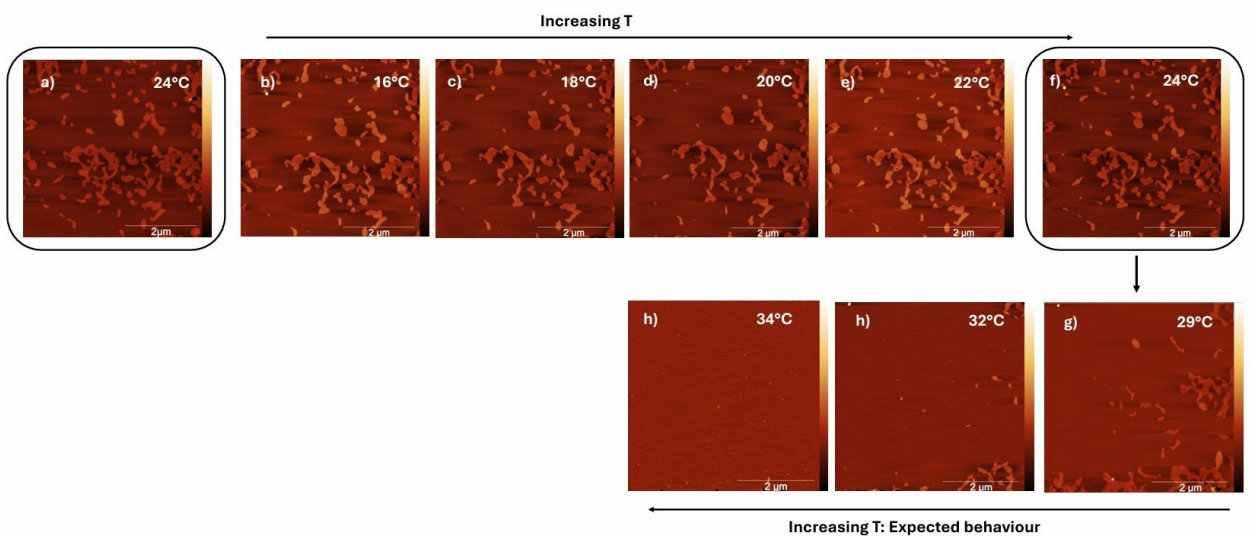

Figure 4.11 AFM images of SLBs composed of 7 mol % cholesterol at various temperatures. Images (a- f) show the formation and evolution of the LRs domains as the temperature is increased from 16°C to 24°C, with no significant changes in domain size and density. Panels (a) and (f) represent the system at 24°C before and after thermal cycling, showing reversible domain formation. Images (g-h) display the expected behaviour of the bilayer at higher temperatures (29°C, 32°C, and 34°C), where the lipid domains are dissolved, resulting in a smooth bilayer surface with no visible domains.

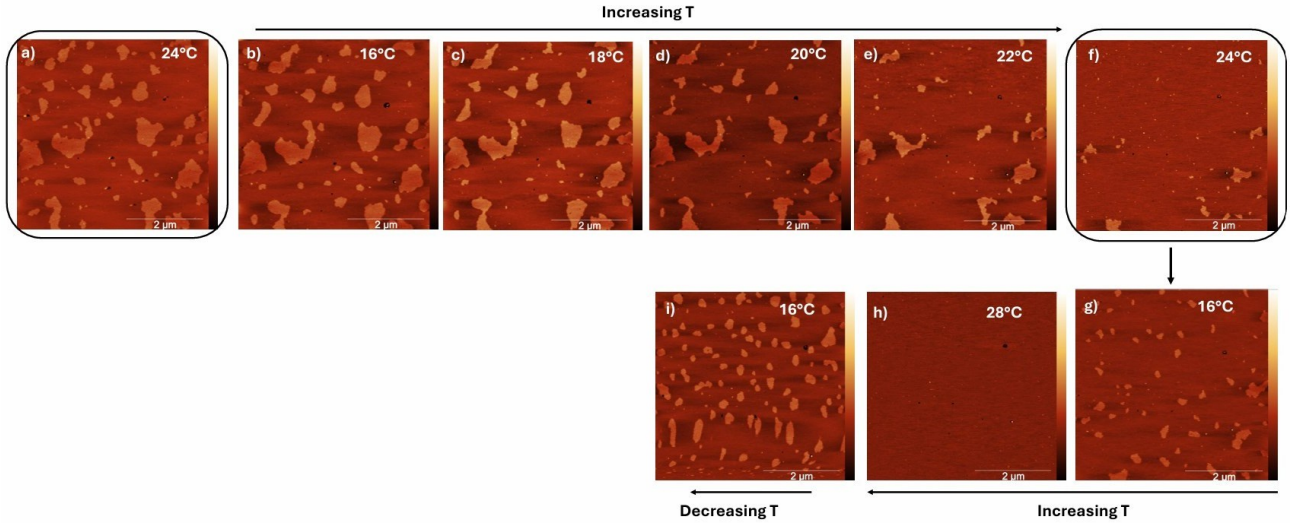

Figure 4.12 AFM images showing the temperature-dependent behaviour of SLBs with 33 mol % cholesterol. (a) SLB morphology at 24°C, showing well-defined lipid rafts. (b-f) Sequential heating from 16°C to 24°C with temperature increments of 2°C. The images demonstrate minimal changes in lipid raft morphology and area coverage as the temperature increases, indicating stability of the membrane phases up to 24°C. (g) Upon heating to 28°C, complete mixing of membrane phases is observed, with no distinct raft structures present. (h) After reheating to 16°C, the lipid rafts reorganize but exhibit different morphology compared to the initial state at 24°C, indicating a reversible but altered membrane phase organization. (i) The SLB shows raft formation at 16°C after the cooling process, demonstrating the temperature sensitivity and cholesterol's role in membrane phase behaviour. Scale bars: 2 μm.

The AFM results integrated with the DSC results, reveals two important features: firstly, cholesterol modulates the membrane's overall melting temperature, as reported in several studies. In our experiments, we found that cholesterol lowers the melting temperature, and this effect is more pronounced in SLBs with higher cholesterol levels. The second feature is that the ordered phase of the membrane with high cholesterol content appears more fluid, as phase mixing occurs more rapidly. In our complex systems, the inclusion of DSPC seems crucial for stabilizing lipid rafts. This is particularly notable since DSPC is the only additional component compared to the ternary lipid mixtures mentioned in the literature. Moreover, several studies report that cholesterol has a strong affinity for saturated phospholipids like DSPC. As demonstrated in a recent paper [180], the addition of cholesterol to a pure SLB composed of DSPC decreases the bilayer's mechanical stability in the gel phase. Structurally, it is well known that the substrate significantly influences SLB formation, impacting its dynamics and behaviour. This interaction between the substrate and SLB likely plays a role in the membrane's stability and phase behaviour, especially in the presence of cholesterol. Several studies in the literature have demonstrated that the buffer plays a crucial role in modulating raft morphology and certain membrane properties such as the stiffness and the fluidity. J. Tucker Andrews et al [181]. demonstrated the critical role of salt concentration in the formation of SLBs. Low concentrations of Group I chloride salts significantly influence the kinetics of SLB formation by affecting membrane assembly, surface coverage, and bilayer stability. The study shows that even small amounts of these salts can alter lipid-lipid and lipid- surface interactions, which are essential for determining the bilayer's morphology and integrity. Different salts impact the electrostatic interactions between lipid vesicles and the substrate, either facilitating or hindering bilayer formation depending on the ionic strength. From the other hand there is a strong impact regarding the ionic strength of the salt in the membrane formation. Madhurima Chattopadhyay et al. [182] demonstrated how sodium ions (Na^+) and water molecules work together to influence lipid mobility in model cell membranes. The study highlights the key role of sodium ions in promoting lipid dynamics, essential for various cellular processes. Na^+ ions interact with phospholipid headgroups, enhancing membrane fluidity and viscosity. Water molecules surrounding the Na^+ ions play a crucial role in this interaction, with the hydration shell helping to balance ion-lipid binding and maintain membrane fluidity.

This cooperative effect between sodium ions and water enhances lipid mobility, revealing a delicate balance between electrostatic interactions and hydration forces. Based on these considerations, we aimed to further investigate the role of NaCl in modulating SLB formation.

4.4 Effect of the buffer ionic strength in the morphology of the LRs

From the measurements conducted in a HEPES/NaCl buffer, a strong modulation in the formation of lipid rafts induced by cholesterol was observed. However, it is well-documented in the literature that ionic strength can significantly influence crucial membrane properties such as the fluidity and the stiffness. Previous measurements, which showed a decrease in the heights of the LRs (Figure 4.12), led to the hypothesis that the preferential incorporation of cholesterol into the rafts results in an increase in local membrane fluidity. This hypothesis is supported by evidence that the reduction in raft height correlates with decreased raft rigidity. This occurs because the acyl chains experience a local disturbance, resulting in a loss of their packing. Studies have shown that NaCl plays a significant role in modulating the phase behavior and morphology of SLBs. The presence of NaCl enhances phase separation, increasing the size and area occupied by ordered lipid domains within the disordered phase of the membrane [183]. This effect is attributed to the preferential interaction of Na^+ ions with the Lo phase, which fosters favourable interactions among saturated lipids, such as sphingomyelin. These interactions promote the clustering and merging of smaller lipid domains into larger, more distinct entities. To further investigate this phenomenon and considering the literature's indication that NaCl presence enhances this effect, we decided to reconstitute supported lipid bilayers in 10 mM HEPES, chosen because it is zwitterionic [184] and does not contribute to the system's ionic strength. In figure 4.13 the AFM topography results are reported.

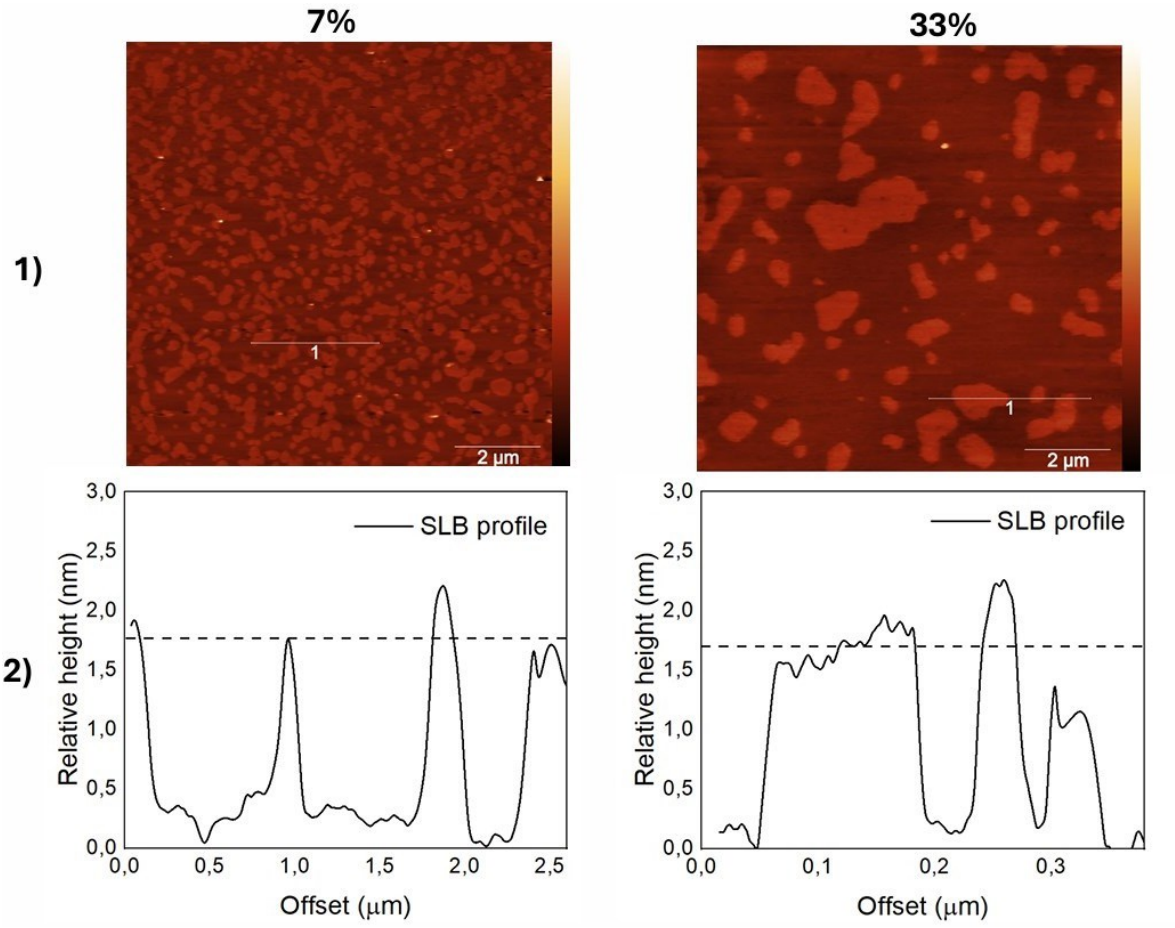

Figure 4.13 AFM topography images (1) of SLBs reconstituted with DOPC: DSPC:SM (35:20:12) in HEPES buffer (10mM) at two different cholesterol concentrations (7 mol% and 33 mol%) are presented. Panel 2 displays the height profiles highlighting the mismatch between the lipid rafts and the liquid- disordered phase of the membrane.

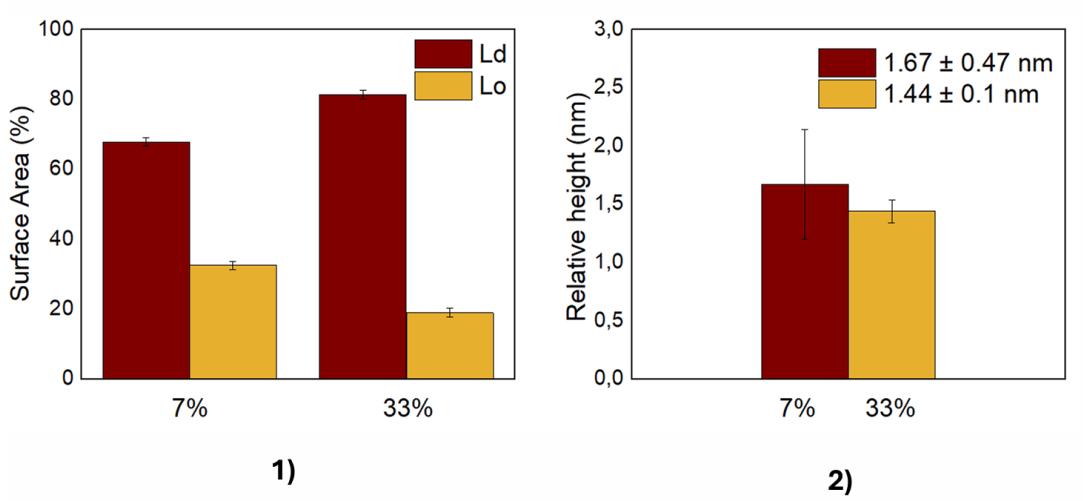

Figure 4.14 Statistical analysis (Panel 1) of the surface area percentage as cholesterol levels increase. Statistical analysis of lipid raft height variation with cholesterol concentration is presented in panel 2. Comparison with the SLBs reconstituted in HEPES/NaCl indicates that there is no significant decrease in height as cholesterol concentration increases. This suggests that the effect is enhanced in the presence of NaCl.

As shown in Figure 4.13, compared to previous results obtained with SLBs reconstituted in HEPES/NaCl buffer, the lipid rafts exhibit a more roundish morphology, especially at 33 mol% cholesterol. This change in morphology correlates with a significant difference in the raft- covered area. Under these conditions, the lipid rafts coverage for SLBs with 7 mol % cholesterol was 32.5 ± 1.18% in HEPES alone, whereas in the presence of NaCl, the coverage was reduced to 21.94 ± 3.73%. For SLBs containing 33 mol % cholesterol, the LR-covered area was 18.92 ± 1.27% in HEPES alone but increased to 34 ± 5.63% in the presence of NaCl. In figure 4.15 is reported the comparison of the LRs height in only HEPES and in the case of the presence of NaCl.

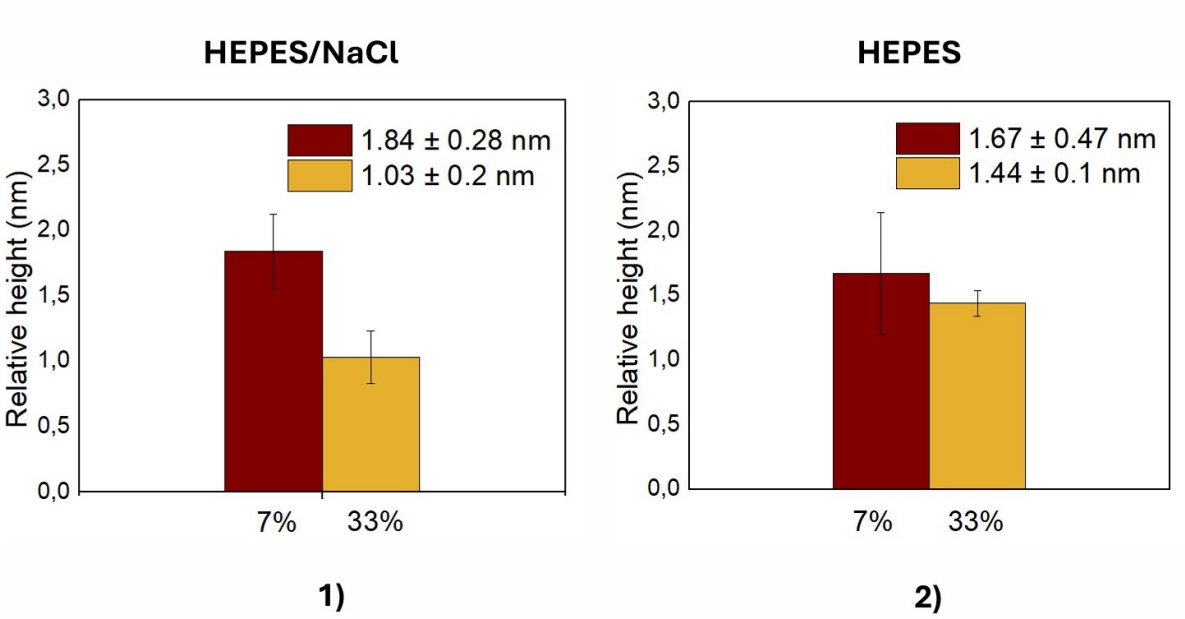

Figure 4.15 shows the comparison of LR heights under the two different buffer conditions clearly demonstrates the effect of NaCl on modulating lipid organization within the rafts.

The comparison of lipid raft heights reveals a decrease in LR height with increasing cholesterol concentration, an effect that is more pronounced in the presence of NaCl. This suggests that NaCl contributes to increased membrane fluidity, likely causing the lipids within the two phases to pack less tightly. Such findings point to a clear influence of ionic strength and buffer composition on the lipid structural organization, even when the buffer maintain the same physiological pH value of 7.4. According to existing literature, variations in buffer composition can significantly alter the properties of lipid bilayers [185], affecting parameters such as membrane curvature and domain morphology. Specifically, buffers with differing ionic strengths can modulate lipid-lipid interactions and the packing of cholesterol within rafts. On the other hand, it is essential to consider the role of $CaCl_2$, as it was used in all experiments to facilitate vesicle rupture on the substrates. Specifically, a 200 mM $CaCl_2$ solution was added to mica in a 1:10 ratio with the hydration buffer under the two different buffer conditions. The interaction between synthetic lipid vesicles and the substrate is predominantly electrostatic, with $CaCl_2$ playing a critical role in modulating these interactions. The presence of Ca^{2+} ions effectively screen the electrostatic forces, reducing their strength and stabilizing the vesicles,

which slows the rupture process. This behaviour underscores the significance of ionic strength in controlling vesicle stability and rupture dynamics during surface interaction, ensuring controlled membrane formation. Additionally, the role of buffers has been shown to be crucial in studying interactions involving the lipid bilayer. In fact, J.T. Andrews et al [181] demonstrates for instance that DNA-lipid interactions are significantly influenced by the ionic composition of the solvent. The thickness of the DNA layer adsorbed onto the lipid bilayer decreases in the order: citrate > phosphate > Tris > HEPES. The effect of cations on the thickness of the DNA layer follows the order: $K^+ > Na^+ > Cs^+ \approx Li^+$. In addition to this, in literature are reported studies in which the SLBs formation can follow different pathway, that depend on the physiological environment. In the formation of SLBs are involved two possible routes: the first mechanism involves an adsorption-rupture process, which includes an intermediate step where a critical vesicle density must accumulate on the surface before SLB formation occurs. The second mechanism involves the direct rupture of vesicles upon contact with the surface, without requiring intermediate steps. Specifically, it has been demonstrated that HEPES and Tris buffers follow the first mechanism, while the presence of NaCl facilitates the adsorption-rupture mechanism. In the NaCl-mediated process, the degree of interaction between vesicles and the surface is influenced by the salt concentration, which modulates electrostatic screening effects. For subsequent measurements, we opted to use a physiological HEPES/NaCl buffer, as it better mimics biological membrane conditions. The inclusion of NaCl in the buffer replicates the ionic environment of biological systems, which is essential for accurately modelling membrane behaviour.

4.5 From SLBs to equivalent composition liposomes: Qualitative evaluation of the membrane stiffness

Previous AFM results have shown that cholesterol modulates the formation of lipid rafts, and that physiological saline conditions plays a critical role in the modulation of the membrane structure. A reduction in raft height has been correlated with changes in properties such as stiffness and fluidity. Based on these findings, we hypothesize that increasing cholesterol concentration leads to an increase in membrane fluidity, an effect further enhanced by the presence of NaCl. As cholesterol concentration increases, the membrane's rigidity typically decreases, allowing for greater lateral movement of lipids, which in turn increases fluidity. This effect is especially pronounced in the presence of NaCl, as ionic interactions further modulate the lipid packing, stabilizing the more fluid phase. These findings suggest that both cholesterol content and ionic strength are key factors in determining membrane dynamics and organization. Earlier studies demonstrated that cholesterol alters membrane dynamics and raft formation, leading us to explore how it specifically affects the mechanical properties of liposomes, particularly their stiffness. In a study published by Caselli et al. [186], the mechanical properties of both synthetic and natural liposomes were examined by exploiting the interaction between the liposomes and gold nanoparticles synthesized using citrate as a reducing agent. These

measurements take advantage of the fact that gold nanoparticles aggregate to varying degrees depending on the stiffness of the liposomes involved. More specifically, liposomes that exhibit high fluidity, such as pure DOPC liposomes, promote the aggregation of nanoparticles on their surface. In contrast, as the rigidity of the liposomes increases, this aggregation is inhibited. Therefore, this method allows for indirect analysis of the mechanical properties of liposomes through UV-Vis measurements. The degree of aggregation is indicated by the red shift in the SPR spectrum of the gold gold nanoparticles and the appearance of a secondary absorption band, which intensifies with increased aggregation. As illustrated in Figure 4.16 of L. Caselli's paper.

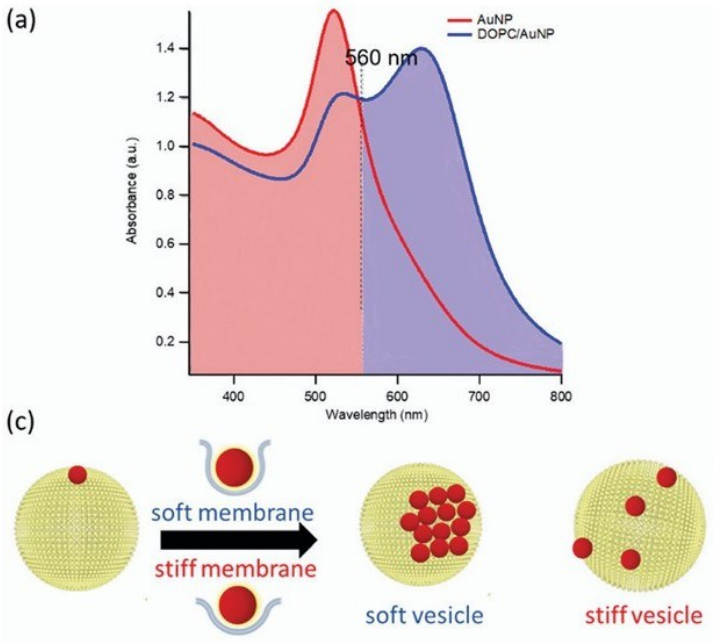

Figure 4.16 Panel a) shows the spectrum of citrate-capped gold nanoparticles (red) and, in blue, the spectrum of gold nanoparticles interacting with pure DOPC liposomes. Panel c) illustrates the interaction mechanism between AuNPs and vesicles with varying membrane stiffness. When AuNPs adhere to a soft membrane, they undergo significant wrapping by the membrane, leading to the aggregation of AuNPs on the vesicle surface. In contrast, when AuNPs dock on a stiffer membrane, the wrapping is less pronounced, preventing the clustering of AuNPs. Caselli et.all [186].

Measurements using this technique were conducted on liposomes with two different cholesterol concentrations (7 mol % and 33 mol %), reconstituted in both HEPES/NaCl and HEPES-only buffers. This indirect method was chosen to demonstrate that increasing cholesterol concentration leads to an increase in membrane fluidity, a property closely linked to stiffness (a softer, more compliant membrane is typically more fluid) and that this effect is further amplified in the presence of NaCl, suggesting that ionic strength plays a key role in modulating lipid packing and membrane dynamics.

The sample preparation method developed by Caselli et al. was followed, with some adjustments noted in the Materials and Methods section. Figure 4.17 the UV-Vis spectra obtained for liposomes at two different cholesterol concentrations and under two different buffer conditions. In the absence of

liposomes, the dispersion of gold nanoparticles (AuNPs) exhibits a well-defined surface plasmon resonance (SPR) peak at 521 nm (green curve). However, upon mixing with liposomes, a transition occurs as the cholesterol concentration increases from 7 mol % to 33 mol % for two investigated buffer conditions. The changes in the SPR profile correlate with a decrease in vesicle stiffness, revealing a gradual evolution in spectral characteristics. Specifically, as we move from the stiffest liposomes (7 mol % cholesterol) to the softest (33 mol % cholesterol), a high-wavelength shoulder emerges, eventually giving rise to a secondary plasmon peak around 596 nm. This new spectral feature indicates the aggregation of AuNPs, which occurs due to the spatial proximity of the nanoparticles, leading to the coupling of their individual plasmon resonances. Overall, we observe a clear increase in aggregation correlating with rising cholesterol concentrations in the liposomes, as evidenced by the pronounced alterations in the spectral features. Notably, in panel 1), (Figure 4.17) where liposomes were reconstituted in the presence of NaCl, the aggregation is more pronounced. This observation indicates that NaCl significantly influences the modulation of membrane stiffness, a finding that aligns with previous AFM results. Although these results are not quantitative, they support the hypothesis that the presence of NaCl contributes to alterations in membrane stiffness and fluidity. Specifically, the ionic strength provided by NaCl may enhance lipid interactions, leading to a more fluid membrane state and a corresponding decrease in stiffness.

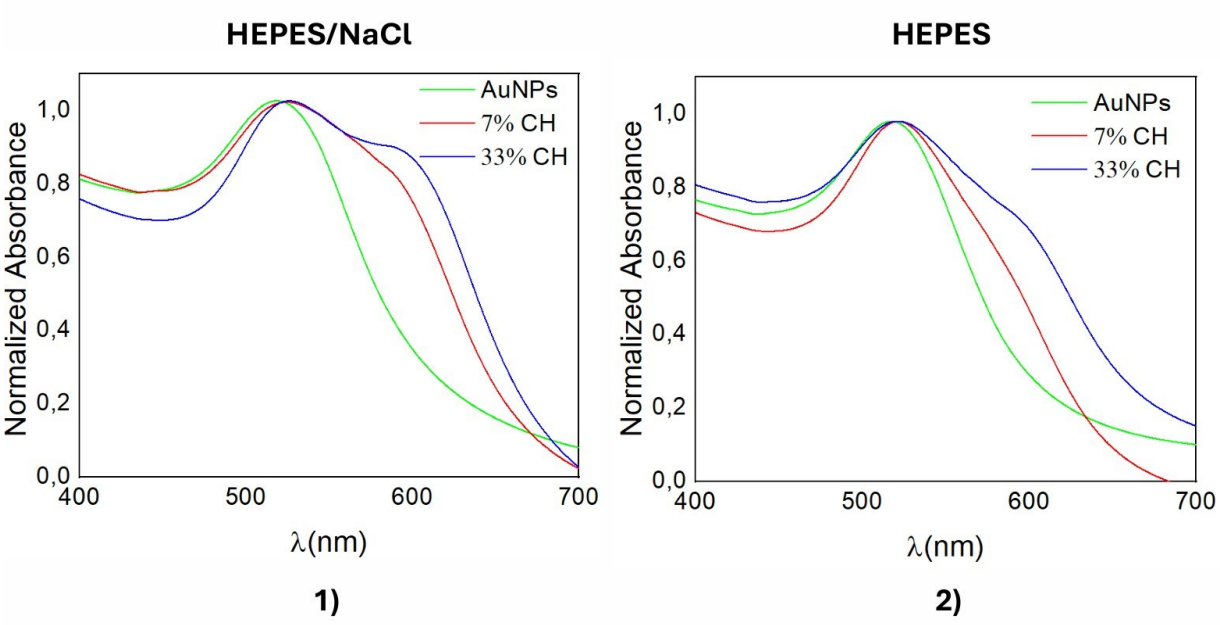

Figure 4.17 UV-VIS spectra of HCit@AuNPs (Green) and liposomes matching the concentrations of SLBs synthesized in HEPES 10mM/NaCl 150mM (1:10) buffer and HEPES 10mM, composed of 7% cholesterol (red) and 33% cholesterol (green), incubated with HCit@AuNPs. There is a SPR modulation effect induced by cholesterol and this effect is highlighted in presence of NaCl.

This experiment is qualitative in nature, and as such, we were unable to determine whether there is an increase in stiffness specifically with respect to the Lo or Ld (phases. At this stage, we couldn't discriminate which phase exhibits more pronounced nanoparticle aggregation. Various studies in the

literature have explored how stiffness varies with cholesterol concentration, as well as its effect on fluidity. According to these studies, increasing cholesterol in the membrane generally enhances membrane rigidity. However, this effect can vary depending on the specific type of system being investigated. Additionally, some research indicates that the impact of cholesterol on stiffness and fluidity is not straightforward; cholesterol can induce local ordering within disordered phases while simultaneously inducing local disorder within ordered phases. To acquire quantitative insights into these behaviours, further techniques are needed to provide precise parameters, thereby elucidating the role of cholesterol in modulating stiffness and fluidity within these systems.

4.6 Quantitative evaluation of membrane stiffness with nanometric resolution

As mentioned in the previous discussion, this work focused on deepening the understanding of how cholesterol modulates the formation of lipid rafts and its impact on altering properties such as stiffness and fluidity. In the previous data where we assessed stiffness, we did not obtain quantitative measurements and, as previously stated, we were unable to discriminate the stiffness of the two phases. For this reason, nanoindentation experiments were conducted to obtain quantitative data on the mechanical properties of the membrane in the form of SLBs. Membrane fluidity and lipid lateral mobility, are closely correlated with various mechanical parameters, including Young's modulus and breakthrough forces. These parameters can be measured with nanoscale precision using AFM mechanical mapping, as described in the materials and methods section [187,188]. AFM provides detailed insights into the mechanical properties of the membrane, allowing for a comprehensive understanding of how lipid dynamics and membrane stiffness are correlated. Figure 4.18 shows representative experimental AFM force curves acquired on the Lo phase for both samples with low and high cholesterol concentrations.

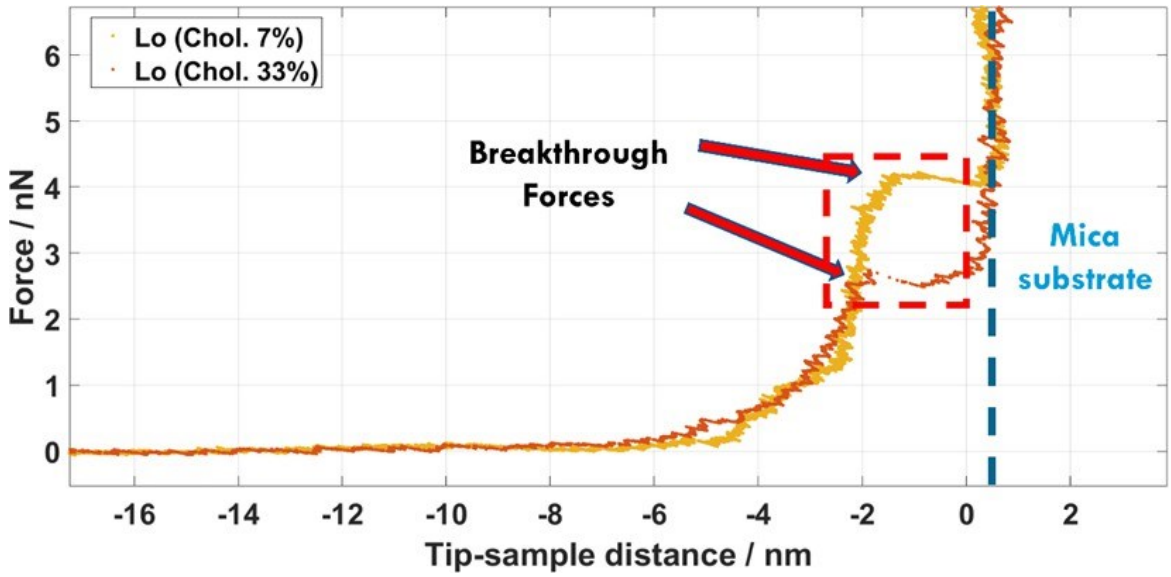

Figure 4.18 Representative experimental force curves acquired by AFM on the Lo phase of SLBs with 7% (yellow curve) and 33% (brown curve) mol cholesterol concentration, highlighting the breakthrough points, characterized by a sudden change in the curve slope, where the force applied by the tip overcome the mechanical resistance of the bilayer and break it, reaching the underlying rigid and undeformable substrate.

The different breakthrough forces are highlighted, with the lower cholesterol concentration sample exhibiting a larger resistance to the applied force, thus suggesting a larger rigidity, in agreement with expectations and literature data [189] . We decided to evaluate this parameter instead of the sample Young's Modulus, given the still open discussions related to the suitable contact mechanics model for the case of SLBs and the anomalous mechanical behaviour sometimes exhibited by these complex samples. On the contrary, breakthrough forces benefit of not needing a proper fitting model and being detectable in a faster and easier way by automated algorithms. Yet, they show a relatively high sensitivity to several parameters, such as AFM tip velocity (or loading rate), temperature, buffer ionic strength and environmental humidity, which in turn regulates the buffer droplet evaporation rate, and consequently its salt concentration. Besides temperature, buffer ionic strength looks to have a large impact on the absolute values of breakthrough forces, thus requiring the control of environmental humidity inside the AFM cell, which we obtained thanks to a technique based on the use of saturated salt solutions. Specifically, on the bottom of our AFM cell we inserted wipes soaked with NaCl saturated solution, providing a constant relative humidity around 75%. Another critical point regards the choice of the proper technique to perform nanomechanical measurements on these systems, and to clearly discriminate among the different coexisting lipidic phases. Again, for technical reasons, mainly related to the quite different dynamics and mechanical behaviour exhibited by the two analysed cases, and the subsequent need to find experimental parameters which could fit for both samples and allow a meaningful comparison, we had to drop the most common and high-throughput technique known as force mapping for the "Point and Shoot" technique shown in figure 4.19.

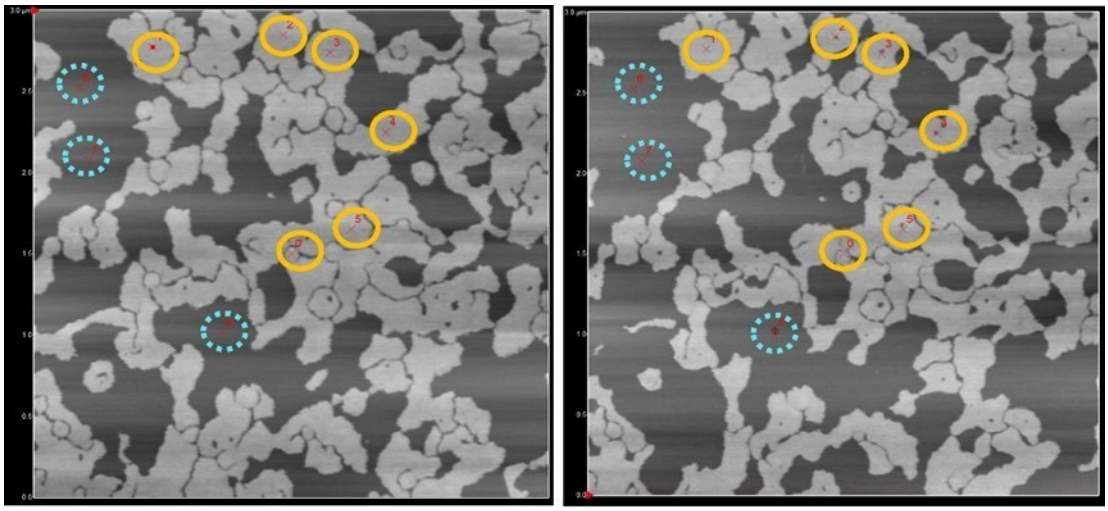

Figure 4.19 3x3 μm2 AFM topographic maps obtained on a SLB sample with 7% mol cholesterol concentration, acquired before (a) and after (b) performing single force curves on the selected spots, numbered and marked by red crosses. Yellow continuous circles and blue dashed circles highlight the spots selected on the Lo and Ld phases, respectively.

There here, we basically acquire a starting topographic map (fig 4.19 a), selecting a few spots for single force curves on both Lo and Ld phases, followed by a second fast topographic map (fig 4.19 b) on the same region to assure that the selected points still belong to the original phase after the force curves measurements, given the dynamic behaviour of LRs. Eventually, figure 4.20 summarizes the breakthrough forces measured on Lo and Ld phases for the two different cholesterol concentrations. Four-five different samples have been measured, collecting a total number of force curves comprised between one and two hundreds for each case. Median and median absolute deviation values have been evaluated in place of the most commonly used average and standard deviation, since they are known to be more robust against outliers, particularly in the case of relatively low data amounts.

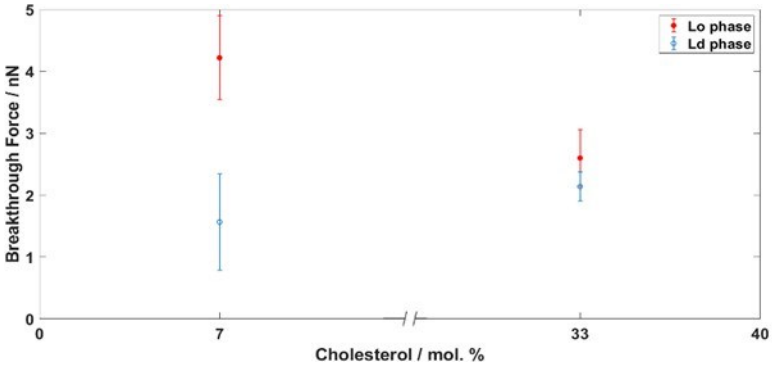

	Median +/- Mad
Lo phase (7%)	4.22 ± 0.68 nN
Ld phase (7%)	1.57 ± 0.78 nN
Lo phase (33%)	2.60 ± 0.46 nN
Ld phase (33%)	2.14 ± 0.24 nN

Figure 4.20 Overall statistics of the breakthrough force values for both phases and cholesterol concentrations, along with the corresponding median +/- median absolute deviation values. A total number of force curves comprised between one and two hundreds have been analysed for each case.

Overall, the obtained results are in good agreement with literature data acquired on similar systems, eventually improving their accuracy and reproducibility by carefully controlling the stability of the most impacting environmental conditions, such as temperature, humidity, and buffer ionic strength. Furthermore, AFM nanomechanical measurements confirm the hypothesis that an increase in cholesterol concentration, preferentially localizing inside LRs (Lo phase), strongly lowers their molecular ordering and increase their lateral mobility, thus decreasing their resistance to externally applied loads. Less significant changes are observed for the Ld phase, and a slight increase in the median value for the Ld phase, along with the increase in cholesterol concentration, agrees with the idea that a possible partial localization of cholesterol inside the Ld phase induces an opposite mechanical trend compared to LRs.

4.7 Evaluation of SLBs' fluidity

In previous AFM nanoindentation experiments of supported lipid bilayers at two distinct cholesterol concentrations (7 mol % and 33 mol %) we found that an increase in cholesterol concentration, which preferentially localizes within lipid rafts (Lo phase), significantly reduces molecular ordering and enhances lateral mobility. Interestingly, there is a slight increase in the median value for the Ld phase as cholesterol concentration increases, which suggests that a partial localization of cholesterol within the Ld phase induces a mechanical response that contrasts with that of the LRs. This differential effect highlights the complex role of cholesterol in modulating the mechanical properties of lipid membranes based on phase composition. The data indicate that increasing cholesterol concentration not only expands the area occupied by lipid rafts but also reduces their height and has an impact in the mechanical properties. Since cholesterol plays a complex, bidirectional role in modulating membrane properties such as fluidity and stiffness, as supported by extensive literature [189-191]. Specifically, cholesterol has the ability to induce local ordering in disordered lipid phases, thereby stabilizing them, while simultaneously introducing disorder into more ordered lipid phases [192]. This duality allows cholesterol to finely tune the membrane's structural dynamics. In addition, the lateral packing of lipids within the cell membrane is significantly influenced by the chain length and saturation of the fatty acid tails. These factors directly affect lipid mobility and, consequently, the overall fluidity of the membrane. Specifically, the presence of cis-double bonds in unsaturated lipids introduces a kink in the lipid tail, which hinders the lipids' ability to pack closely together. For instance, it has been demonstrated that cholesterol reduces the fluidity of membranes composed of unsaturated lipids like DOPC or POPC. In contrast, in saturated lipid environments such as those composed of DMPC, cholesterol enhances fluidity [193]. This selective modulation underscores the critical role of cholesterol in maintaining the balance of membrane dynamics, influencing both the mechanical properties and functional behaviours of cellular membranes. These effects are crucial in physiological contexts, as the fluidity of lipid membranes directly impacts processes such as membrane trafficking, signalling, and the formation of lipid rafts. Moreover, it has been demonstrated that membrane parameters, such as fluidity, play a crucial role in modulating and mediating interactions between the

membrane and key molecular entities, including small extracellular vesicles. In a recent study, Paba et al. provided evidence that cholesterol significantly impacts the modulation of membrane fluidity and the lateral organization of the lipid bilayer. Their findings highlight that the fluidity and structural arrangement of lipid raft domains are fundamental in determining the rate at which EVs interact with and integrate into these domains. Cholesterol, by altering membrane fluidity, directly influences the extent and efficiency of these interactions, underscoring its critical role in cellular communication and membrane dynamics. As previously mentioned, fluidity is a fundamental property in membrane modulation, with significant implications in various pathological contexts, making it a potential biomarker for disease states. To gain a deeper understanding of how cholesterol influences the fluidity of different membrane phases— specifically the Lo and Ld phases—FRAP experiments were performed. FRAP is a powerful technique used to measure the diffusion coefficient of fluorescently labelled molecules within a membrane. This is achieved by using a high-power laser to irreversibly photo bleach a specific region of the membrane, rendering the fluorescent molecules in that area non-emissive. Over time, unbleached fluorescent molecules from surrounding regions diffuse back into the bleached area, allowing for the measurement of their lateral mobility. The speed at which the fluorescence recovers in the bleached region is directly proportional to the diffusion rate: the quicker the recovery, the higher the diffusion coefficient. The relationship between cholesterol content and membrane fluidity is not only crucial for understanding basic cell biology but also has significant implications for the development of therapies targeting cholesterol-related disorders. For instance, an abnormal increase in cholesterol concentration within cellular membranes has been shown to decrease membrane fluidity, which can disrupt normal cellular functions and contribute to the development of various diseases, including breast cancer and hepatocellular carcinoma. In the FRAP experiments conducted, the impact of cholesterol on membrane fluidity was assessed by comparing the diffusion coefficients in membranes with low (7 mol%) and high (33 mol %) cholesterol content (Figure 4.21). The results demonstrated that higher cholesterol levels led to a more pronounced increase in the diffusion rate within the Lo phase, suggesting enhanced fluidity in these more ordered regions. Conversely, in the Ld phase, the diffusion coefficient remained relatively unchanged, indicating that cholesterol's effect was more significant in stabilizing the Lo phase rather than modulating the inherently more fluid Ld phase. To calculate the diffusion coefficients, the supported lipid bilayers were meticulously prepared as outlined in the materials and methods section. FRAP measurements were performed at a carefully controlled temperature of 25°C to ensure consistency across experiments. NBD-DSPE, a fully saturated phospholipid, was used to label the ordered phase, as it preferentially localizes within lipid rafts, which are more ordered regions of the membrane. For the disordered phase, ATTO 655 DOPE, a dye that preferentially integrates into the more fluid, disordered regions of the membrane, was selected. These fluorophores were used at a concentration of 0.001 mol%, that has been validated in previous studies to ensure high selectivity and minimal perturbation to the membrane's natural state. FRAP experiments involved irradiating a specific region of interest (ROI), having a circular shape in both the ordered and disordered phases of the SLBs with

a high-intensity laser to induce photobleaching. The recovery of fluorescence in the bleached area, driven by the lateral diffusion of unbleached fluorophores, was monitored over time. The resulting FRAP curves were then analysed using specialized software (provided by the MPI of Biochemistry), which provided a quantitative assessment of the diffusion coefficient. The analysis revealed a distinct behaviour in the diffusion dynamics between the ordered and disordered phases when comparing SLBs with low and high cholesterol content. In the ordered phase, the diffusion coefficient increased significantly with higher cholesterol levels from 0.215 μm²/s to 1.19 μm²/s, corresponding to a decrease in diffusion time, indicating faster recovery dynamics.

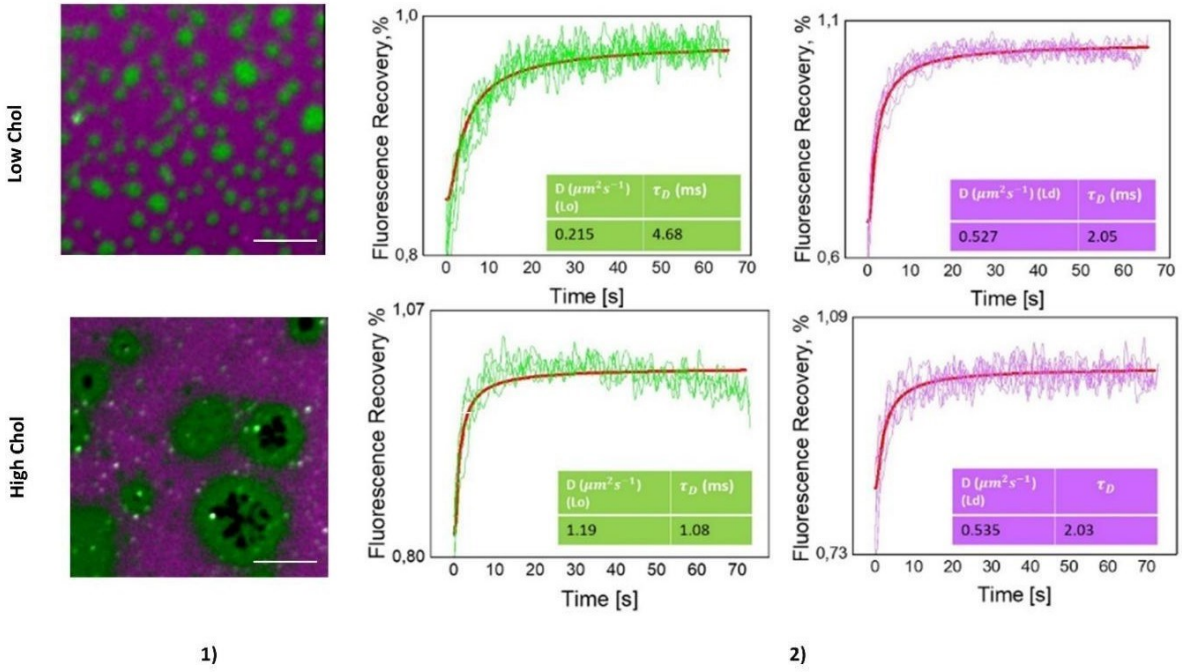

Figure 4.21 FRAP data for supported lipid bilayers (SLBs) are shown. The liquid-ordered (Lo) phase is fluorescently labelled with NBD-DSPE (green), and the liquid-disordered (Ld) phase is labelled with ATTO 655-DOPE (magenta). The scale bar represents 10 μm. At low cholesterol levels, the diffusion coefficient of the Lo phase is 0.215 μm²/s, with a diffusion time (τ) of 4.68 seconds. As cholesterol levels increase, the diffusion time decreases to τ=1.08 seconds, and the diffusion coefficient rises. This trend indicates that the dynamics of fluorescence recovery accelerate with higher cholesterol levels, reflecting increased lipid mobility and enhanced fluidity in the Lo phase.

In contrast, the diffusion coefficients within the disordered phase showed no significant variation between low and high cholesterol samples. This observation is consistent with the fact that the overall composition of DOPC, DSPC, and SM was maintained constant, with only the cholesterol concentration being varied. The small change in diffusion coefficient suggests that cholesterol predominantly associates with the ordered phase, exerting minimal influence on the fluidity of the disordered phase, where unsaturated lipids like DOPC dominate. This selective localization of cholesterol reinforces its role in modulating the biophysical properties of the membrane in a phase-specific manner, with significant implications for the understanding of membrane organization and

function in different cholesterol-rich environments. This conclusion is further supported by the observation that, as cholesterol content in the membrane increases, there is a significant expansion in the size of lipid rafts. This indicates that a higher percentage of cholesterol is preferentially localizing within the lipid rafts. In the literature, a FRAP diffusion study conducted by Zhang et al. explored the diffusion characteristics of membrane systems composed of phospholipids and varying concentrations of cholesterol. The study found that when cholesterol was introduced into a membrane system composed solely of DOPC, there was a gradual decrease in diffusion coefficients: from 0.73 ± 0.16 $\mu m^2/s$ at 10 mol% cholesterol, to 0.42 ± 0.14 $\mu m^2/s$ at 20 mol%, and further down to 0.28 ± 0.13 $\mu m^2/s$ at 30 mol%. This decrease in diffusion suggests that cholesterol induces a local ordering effect within the otherwise disordered DOPC membrane. However, in our study, where cholesterol localizes predominantly within the ordered phase of the membrane, it appears to create local disorder within these more structured regions. This behaviour can be explained by the "umbrella model" of cholesterol-lipid interactions. According to this model, cholesterol, with its small polar headgroup and bulky hydrophobic body, causes neighbouring phospholipids with larger headgroups to "shield" its nonpolar regions from the aqueous environment. This shielding effect reduces the unfavourable free energy associated with exposing cholesterol's hydrophobic body to water. In the process, hydrogen bonds form between the hydroxyl group of cholesterol and the phosphate oxygens of the phospholipids, which typically increases the overall activation energy of the membrane. However, in our study, the opposite effect is observed: cholesterol intercalates into the lipid rafts, decreasing the activation energy and thereby expanding the raft area, which leads to increased fluidity within these ordered domains. Zhang et al. also observed a similar phenomenon in DPPC+ Chol membranes. At room temperature, DPPC is in a gel phase with high activation energy. The study showed that adding cholesterol to the DPPC bilayer led to an increase in diffusion coefficients, with values increasing from approximately 0 $\mu m^2/s$ at 0 mol% cholesterol, to 0.24 ± 0.16 $\mu m^2/s$ at 10 mol%, and 0.45 ± 0.18 $\mu m^2/s$ at 20 mol%. This increase in diffusion is attributed to the fact that cholesterol weakens the van der Waals interactions between lipid chains, thereby reducing the activation energy and enhancing the fluidity of the DPPC bilayers. However, when cholesterol levels reached 30%, the viscosity of the system became more pronounced, slightly offsetting the fluidizing effect. In our study, even though our system includes multiple components within the liquid-ordered (Lo) phase, we still observe a consistent increase in membrane fluidity with higher cholesterol content. This suggests that cholesterol's impact on membrane dynamics is complex and highly dependent on the specific lipid composition and phase behaviour of the membrane.

Chapter 5 Membrane- vesicles interactions

5.1 SLBs to Elucidate the Uptake Mechanisms of Small Extracellular Vesicles (EVs)

To validate SLBs as a tool for studying EVs -membrane interactions, EVs provided by the Paracelsus Medical University (PMU) of Salzburg were used in this study. These EVs were derived from umbilical cord mesenchymal stem cells (UC-MSC) cultured under standardized and optimized conditions, ensuring high experimental reproducibility. Two distinct populations of EVs were investigated in their interactions with the optimized SLBs with 7 mol % and 33 mol % cholesterol. EVs uptake mechanisms are now understood to be highly heterogeneous, influenced by a wide range of factors and cell membrane characteristics (e.g., membrane composition, fluidity, and temperature) [194-195]. In this respect, SLBs offer a controlled and simplified biophysical platform for investigating the specific variables that regulate the EVs uptake. Unlike cellular environments, where various factors can complicate the analysis of EV-membrane interactions, SLBs are versatile tools to systematically isolate and assess critical biophysical parameters, such as membrane fluidity and lipid composition [196]. This streamlined approach is particularly valuable for studying the uptake mechanisms of small EVs, that are small in size (30-100nm) and this approach is particularly valuable since the difficulty to study EVs due to their small size, providing an accessible framework for high- throughput experimentation. Furthermore, SLBs serve as a promising model system for exploring EV fusion kinetics, facilitating a deeper understanding of the underlying mechanisms of EV uptake. This level of investigation would be significantly more challenging within the complex milieu of a living cell. By leveraging SLBs, researchers can gain important insights into the dynamics of EV interactions, paving the way for advancements in the field of small EVs research. We tested two distinct samples of EVs: the first sample consisted of EVs isolated and resuspended in Milli-Q water (referred to as serum-free EVs), while the second sample contained EVs dissolved in Ringer buffer (designated as Ringer-EVs). These two vesicle populations differ based on the buffer in which they are resuspended. Vesicles in the serum- free condition are resuspended in Milli-Q water, while the other population is resuspended in Ringer's lactate buffer. To study the interaction between EVs and the SLBs, the same experimental conditions were employed for all samples. SLBs were prepared as previously described in materials and methods, utilizing a physiological HEPES/NaCl buffer. Following the formation of the membrane, 10 μL of vesicles, diluted 1:1 in HEPES/NaCl buffer, were injected onto the SLB. After a 5-minute incubation period, time-lapse imaging was conducted to assess how the vesicles interact with the membrane and influence its morphology. This approach allows for real-time observation of EVs behaviour, including adhesion, fusion events, and potential changes in the lipid bilayer structure. By monitoring these interactions over time, we aimed to elucidate the mechanisms by which vesicles modulate membrane characteristics, providing insights into their functional roles in cellular processes.

5.2 Mechanisms of EVs (Serum free) Uptake

The topographic images presented in Figure 5.1, captured five minutes after the introduction of serum-free vesicles to SLBs containing 7 mol % cholesterol, illustrate preferential interactions with the LRs. Notably, over time, a modification of the membrane morphology is observed, which is induced by the uptake of the EVs. As the vesicles interact with the lipid rafts, we did not observe any defect formation in the Ld phase. Rather, we observed that the interaction started from the edges of lipid rafts. This are if fact regions where thermodynamic stability is lower, creating favourable conditions for vesicle docking and subsequent fusion events. The presence of lipid rafts, characterized by height mismatches between distinct lipid phases is believed to enhance preferential interactions at the boundaries of lipid domains, thereby facilitating vesicle attachment and interaction dynamics, the functional outcomes of EV uptake, including potential lipid mixing and cargo delivery into the target membrane. What we observe from the sequence of images in Figure 5.1, is that upon interaction with the EVs the lipid raft area decreases. EVs preferentially interact with the Lo phase.

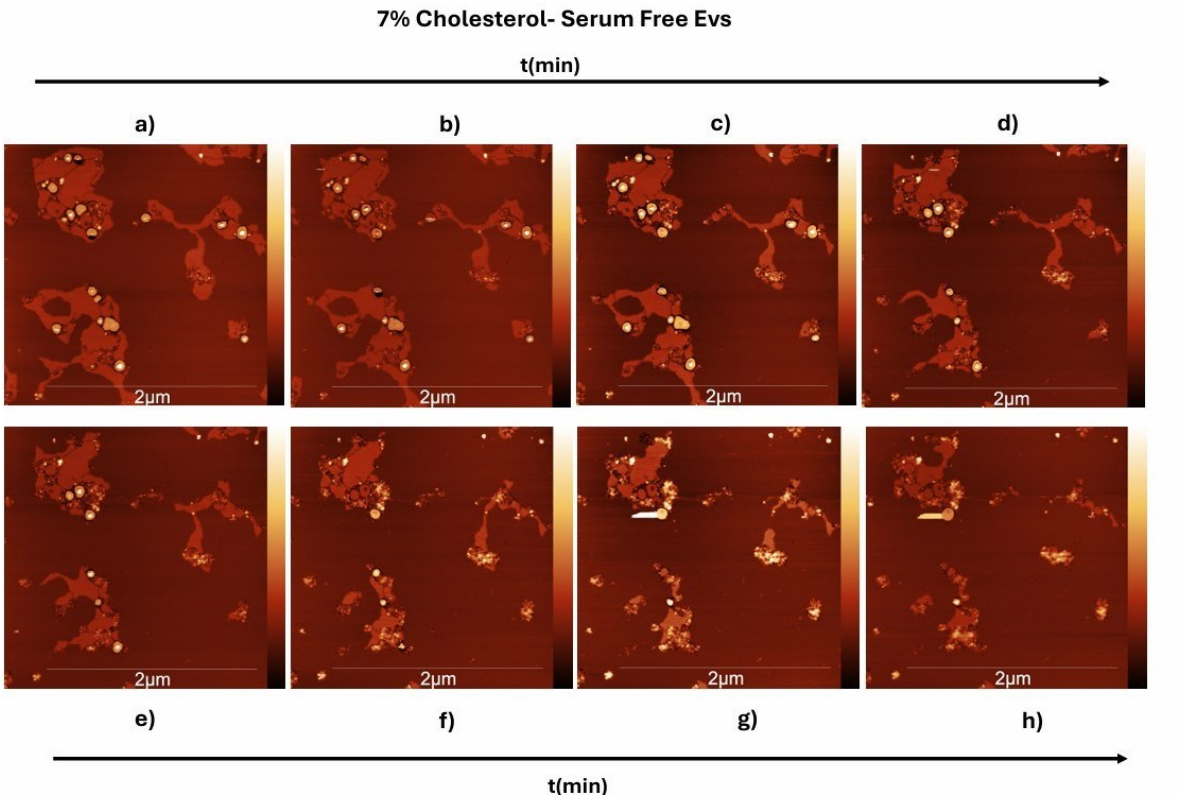

Figure 5.1 AFM Topography Images of SLBs Composed of 7 mol % Cholesterol interacting with Serum- free EVs. The images depict the temporal evolution of the SLB surface morphology during a 1-hour interaction with EVs. The time points highlight key stages in the interaction process, capturing the dynamic changes occurring at the nanometer scale. a) t_0 = after 5 min of incubation min b) t_2: Further evolution in the surface morphology is observed, indicating progressing interaction. c) t_3: A continued shift in topography d) t_4 e) t_5, f) t_6: Intermediate phase of interaction, illustrating significant morphological adaptations. g) t_7 h) t_8 = After 1 hour. A final time point showing the rapid response of the SLB, capturing smaller, rapid shifts. Each time point

provides a snapshot of the lipid bilayer's response to EV exposure, contributing to an overall understanding of the interaction kinetics and potential mechanisms involved in SLB-EV binding or fusion processes.

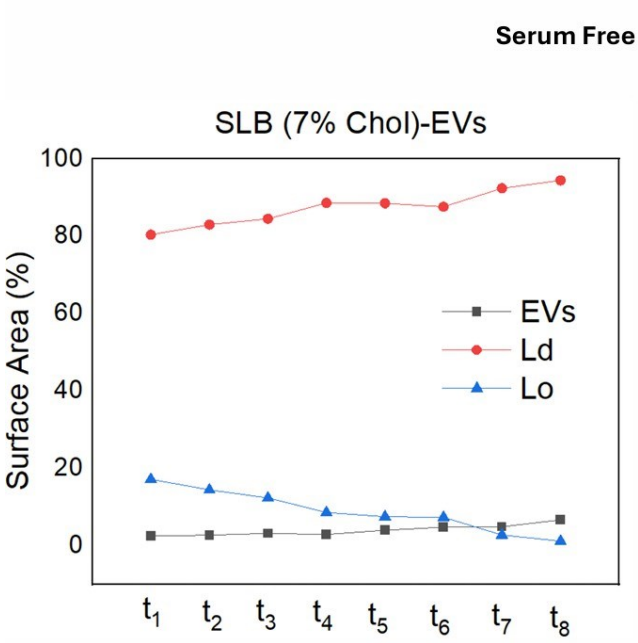

Time (min)	Surface Area (%) EVs	Surface Area (%) Ld	Surface Area (%) Lo
t1	2.4	80.6	17
t2	2.7	83	14.3
t3	3.2	84.5	12.3
t4	3	89	8
t5	4.1	88.5	7.4
t6	4.7	88.1	7.2
t7	5	92	3
t8	6.5	92.3	1.2

b)

Figure 5.2 a) graph depicting changes in surface area (%) over time for EVs the liquid-disordered phase (Ld), and the liquid-ordered phase (Lo) of SLBs containing 7% cholesterol, and b) a table providing the corresponding numerical surface area data for each component at different time points.

This mixing can be attributed to the influence of vesicles on membrane fluidity. EVs have the capacity to modify the physicochemical properties of the membranes they interact with, an effect that has been well documented in the scientific literature. For instance, studies have shown that EVs can alter membrane fluidity by increasing lipid mobility and facilitating fusion with cellular membranes [197] (Lai et al., 2013). This interaction not only modifies the structure of the membrane but can also influence important biological processes, such as nutrient uptake and cell signalling. On the other side, the interaction mechanisms depend on the complex organization of the membrane, including lipid composition, physiological conditions, temperature, and the protein content of the EVs. It is therefore assumable that the pronounced height disparity between the Lo and Ld phases may create a thermodynamically advantageous pathway for lipid-protein interactions and vesicle integration, which could account for the tendency of serum-free EVs to preferentially embed at the peripheries of lipid domains, as we see in Figure 5.1.

This observation is supported by the calculation of areas occupied by topmost Lo phase, topmost Ld phase, EVs defined as a new protruding area with respect to the original SLB. Figure 5.2 summarized the area covered by Lo, Ld and the EVs, as just defined, as a function of time, calculated from the average of different areas obtained from 3 different experiments in the conditions of the Figure 5.1. The data in figure 5.2 indicate that the surface area occupied by the EVs exhibits a continuous upward

trend, increasing from 2.4% at t1 to 6.5% by t8 (i.e. after 1 h from the initial interaction). This progressive increase suggests an ongoing interaction between EVs and the SLBs, where vesicles are gradually covering more of the bilayer surface. In parallel, the surface area of the Ld phase shows a consistent and steady expansion, growing from 80.6% at t1 to 92.47% at t8. This increase in the Ld phase implies a reorganization of the lipid bilayer structure over time, driven by the incorporation of EVs into the bilayer and the resulting destabilization of other lipid domains. Conversely, the liquid-ordered phase, which corresponds to lipid rafts, exhibits a significant reduction in surface area, decreasing from 17.1% at time point t1 to a 1.2 % at time point t8. The vesicles are positioned on top of the raft, and only the areas without vesicle coverage have been considered part of the Lo phase. This decline indicates the near-complete disappearance of lipid rafts as the experiment progresses. The data suggest that as EVs interact with the SLBs, their surface coverage increases, possibly through a mechanism that disrupts the structural integrity of lipid rafts. Changes in the height of the EVs and lipid rafts were not reported, as no significant variations were observed during the period in which we studied the interaction. The preferential interaction likely occurs at the domain boundaries between the Ld and Lo phases, where defects in lipid packing may serve as docking sites for the vesicles. The interaction between the serum free-EVs and the SLBs at the 33 mol% cholesterol is shown in Fig. 5.3. Data reveal that EVs preferentially interact with the Ld phase of the membrane starting, also in this case, at the edges of the lipid rafts (more visible in region 2), causing its expansion over time. In contrast, the Lo phase, steadily decreases in surface area as the interaction progresses. We examined two distinct regions to determine if the interaction effects were consistent across both areas. In both the investigated regions, the surface area occupied by EVs increases gradually, while the Ld phase shows a consistent and marked expansion. Meanwhile, the Lo phase undergoes a continuous decline in both regions indicating the progressive breakdown of lipid rafts during EV interaction. This suggests that the EVs which preferentially target the Ld- Lo domain boundaries, disrupt the structural integrity of lipid rafts, while drive the expansion of the Ld phase. The differences between region 1 and region 2 highlight potential heterogeneity in membrane composition or organization, which could result in region-specific interaction dynamics. Since no significant changes in the height of the vesicles or rafts were observed during the interaction, a representative height profile image is shown in figure 5.9.

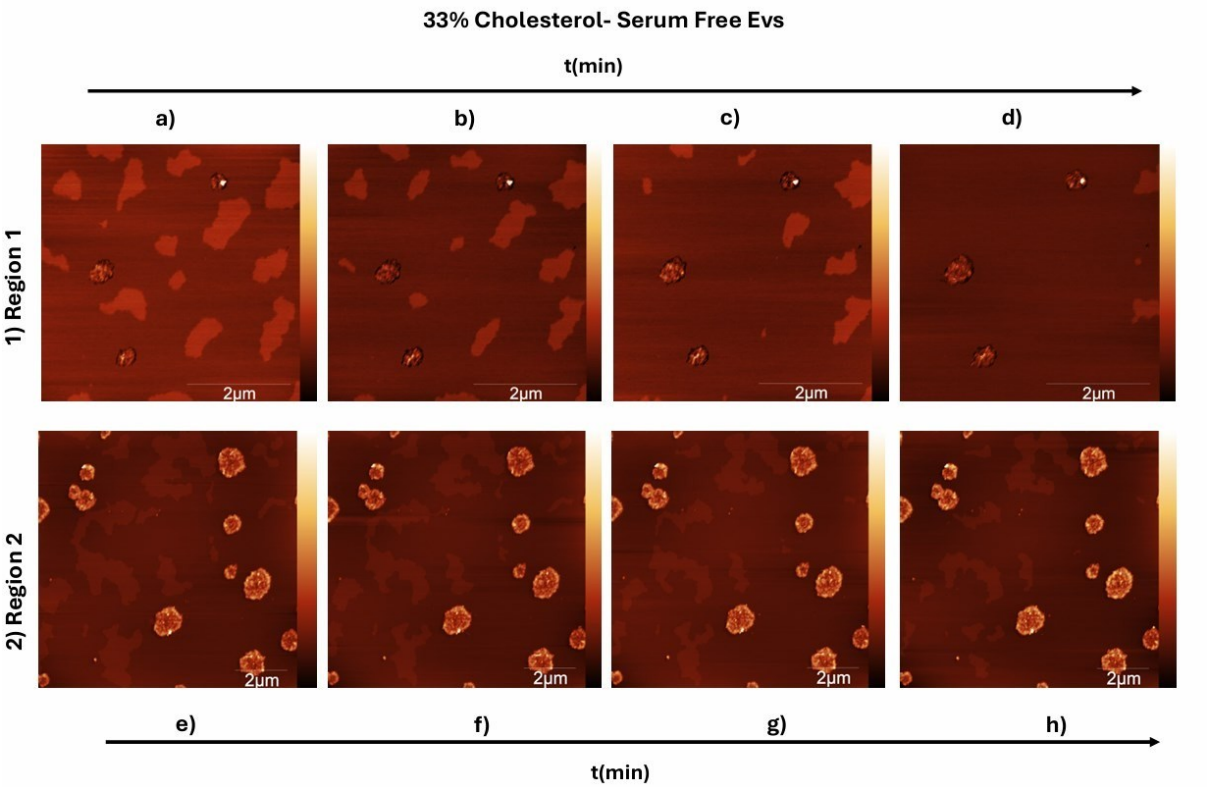

Figure 5.3 AFM Topography Images of SLBs Composed of 33% Cholesterol Interacting with EVs in Serum-Free Conditions across two distinct regions (Region 1 and Region 2). These images capture the evolution of SLB surface morphology during a 1-hour interaction with EVs. a) and e) t_1 = 5 min: Initial interaction stage, showing early surface modifications and the onset of lipid reorganization or EV-SLB binding. b) and f) t_2 = 10 min: Continued surface development indicates progression in the interaction, with potential differences in responses between the two regions. c) and g) t_3 = 12 min: More pronounced topographical changes reflect deeper interactions and ongoing binding or fusion processes. d) and h) t_4 = 19 min: Significant structural alterations indicate deeper integration of EVs into the SLB, with variations in modifications observed between the regions.

Figure 5.4 presents the temporal analysis of the surface area associated with the three phases of the membrane (Lo, Ld, EVs). We chose to report on two different regions of the membrane where imaging was performed to demonstrate that even in cases where there is a lower population of vesicles in the membrane, the trend remains consistent and does not directly depend on the number of vesicles present. To calculate the area occupied by the vesicles, the Lo phase, and the Ld phase, we used Gwyddion data analysis software. By masking the specific regions, it was possible to obtain their respective percentages.

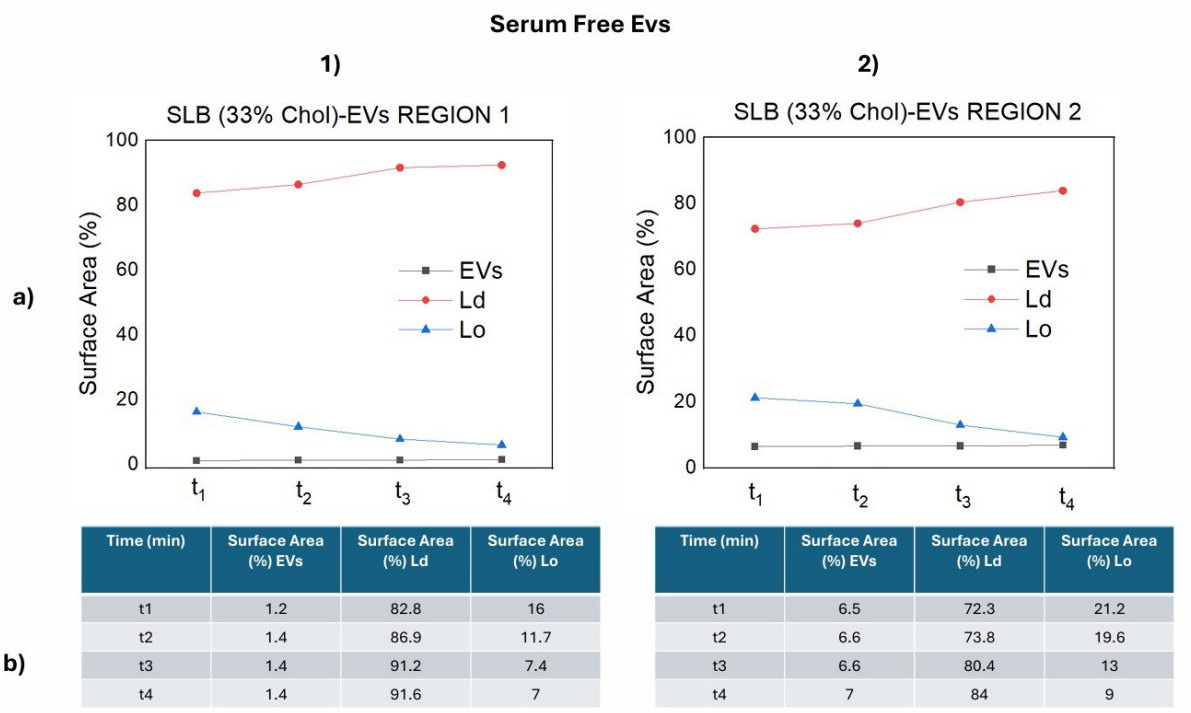

Time (min)	Surface Area (%) EVs	Surface Area (%) Ld	Surface Area (%) Lo
t1	1.2	82.8	16
t2	1.4	86.9	11.7
t3	1.4	91.2	7.4
t4	1.4	91.6	7

Time (min)	Surface Area (%) EVs	Surface Area (%) Ld	Surface Area (%) Lo
t1	6.5	72.3	21.2
t2	6.6	73.8	19.6
t3	6.6	80.4	13
t4	7	84	9

Figure 5.4 Interaction of EVs serum free with SLBs composed of 33% cholesterol in two regions, labelled Region 1 and Region 2. Panel a) shows graphs depicting the temporal changes in surface area (%) occupied by EVs, the liquid-disordered phase (Ld), and the liquid-ordered phase (Lo) in each region. Panel b) includes tables with numerical values for the surface area (%) occupied by EVs, Ld, and Lo phases at each time point (t_1 to t_4). In both regions, the Ld phase steadily increases in surface area, while the Lo phase gradually decreases, indicating lipid raft disruption. EVs also show a consistent increase in surface area, reflecting ongoing interaction with the SLBs.

Interestingly, when comparing the SLB-EVs interaction at the two investigated cholesterol concentrations (7 mol% and 33 mol%) we see that, in both cases, the trend indicates that the lipid rafts disappear over time. This agrees with previous work of F. Perissinotto et al. who explained this behaviour by suggesting that local redistribution of membrane components plays a crucial role, accompanied by an overall thinning of the membrane as vesicles mix with the bilayer. No significant changes in height were observed, so the full set of line profiles has not been reported. However, what does change significantly over time is the surface area associated with the raft domains. This reduction in raft-covered surface area suggests that the vesicles exert an effect in this direction, possibly promoting membrane fluidization. Such fluidization could facilitate mixing between the Lo and Ld phases, potentially leading to a more dynamic membrane environment as the distinct phases interact and merge under the influence of vesicle interactions.

5.3 Mechanisms of EVs (Ringer) Uptake

To better rationalize the interaction between EVs and SLBs, we studied EVs of the same origin (UC-MSC) but isolated in Ringer's buffer. Ringer buffer is normally used to maintain a physiological conditions and it helps maintain the stability and integrity of the EVs during experimental procedures. This isotonic solution, composed of salts and sometimes glucose, mimics the ionic environment of extracellular fluids, creating an optimal medium for preserving the biological activity of EVs. By maintaining membrane integrity and functional characteristics during isolation and experimentation, Ringer's solution is essential for accurately assessing the properties and interactions of EVs. Its isotonic nature allows these vesicles to engage with target cells or membranes without inducing osmotic stress, thereby simulating more physiological conditions in vitro. This environment is then particularly conducive to investigating various biological functions of EVs, including their uptake by recipient cells, signalling pathways, and roles in intercellular communication. The comparison between EVs in Ringer buffer and those in serum-free conditions underscores the importance of the ionic environment in sustaining EV functionality and facilitating interactions, ultimately enhancing our understanding of EV biology and their potential applications [198,199].

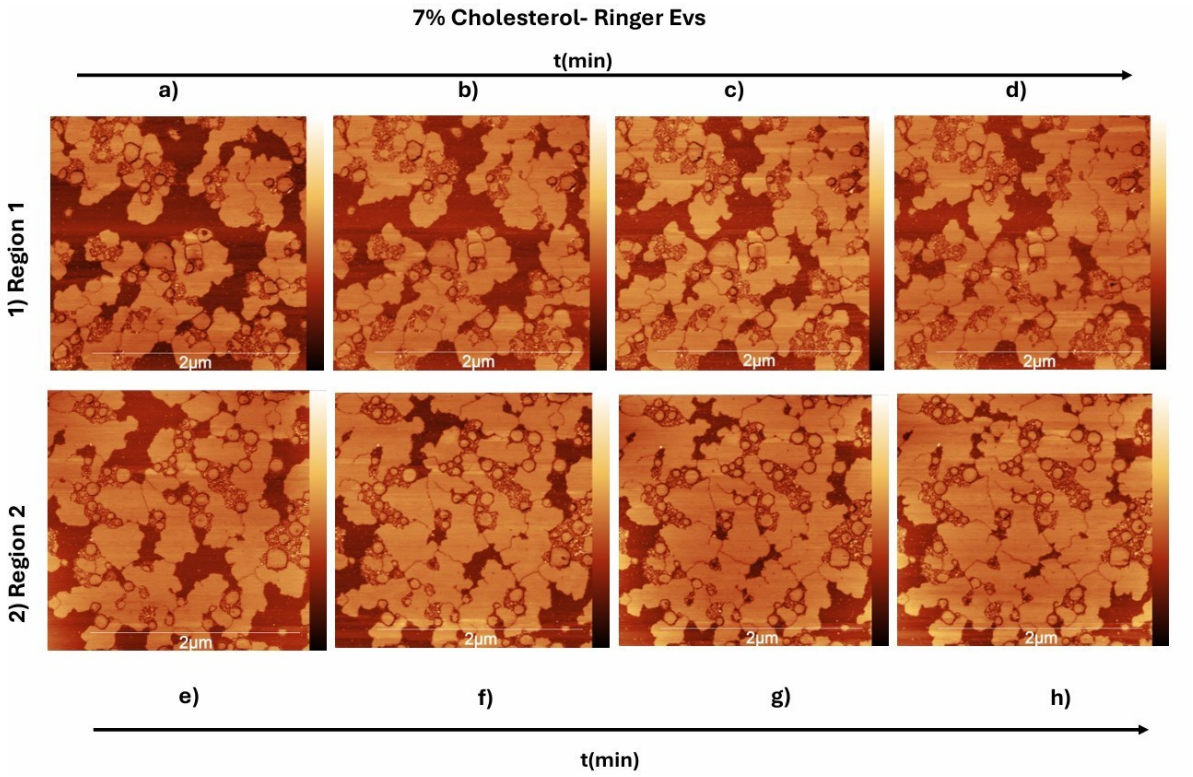

Figure 5.5 AFM Topography Images of SLBs composed of 7 mol% Cholesterol Interacting with EVs in Ringer buffer, highlighting two distinct regions (Region 1 and Region 2). The images capture the evolution of the SLB surface morphology during a 1-hour interaction with EVs. a) and e) t_1 = 5 min: Initial stage of interaction, showing early surface modifications in both regions, marking the onset of lipid reorganization or EV-SLB binding. b) and f) t_2 = 10 min: Further surface development, indicating the progression of interactions with potential differences in the response between the two regions. c) and g) t_3 = 15 min: More pronounced

topographical shifts, reflecting deeper interactions and ongoing binding or fusion processes. d) and h) t_4 = 25 min: Significant structural changes, with clear alterations in surface morphology, suggesting strong EV-SLB interactions.

In figure 5.5, the AFM topography images that illustrate the dynamic interactions between EVs suspended in Ringer buffer and SLBs composed of 7 mol% cholesterol over time are reported. When we compare with the serum-free condition, we can immediately observe a pronounced effect of the buffer on membrane morphology, especially in the case of 7% cholesterol content, where the LRs tend to coalesce. This morphological change can be attributed to the buffer, as these two vesicle preparations differ only in the medium in which they are resuspended. The buffer seems to influence the membrane structure significantly, potentially affecting membrane stability, lipid packing, and the distribution of lipid phases. This observation suggests that the medium composition is a critical factor in modulating membrane properties. This increased fluidity allows the lipid bilayer to more readily accommodate incoming EVs, facilitating their approach and interaction with the membrane. When compared to EVs suspended in serum-free conditions, the differences in interaction types can be attributed to the distinct environments in which the vesicles are stored. The interactions observed with Ringer vesicles can more easily promote membrane fusion, allowing for the incorporation of EV membrane components into the SLB. In this case, it can be observed that vesicles suspended in Ringer buffer preferentially interact with the ordered phase and fuse with lipid rafts, leading to a modification of their morphology. A comparison between the interactions of SLB-EVs in serum free and those in Ringer buffer reveals significant differences and distinct mechanisms of interaction. Once again even in this case during the investigated time range, we did not appreciate significant changes in the LRs height as well as the height of the vesicles. Specifically, for the serum-free condition, we observe a time-dependent increase in the surface area occupied by the disordered phase. In contrast, for vesicles in Ringer buffer, the trend is reversed: there is a progressive decrease in the disordered phase. This behaviour aligns with the fact that, in the presence of Ringer solution, vesicles interact with lipid rafts and gradually fuse with them. Consequently, both the vesicles and the ordered phase show an increase in surface area over time. The overall interaction mechanism between Ringer-EVs and SLBs at low cholesterol levels is influenced by a combination of factors, including electrostatic interactions, enhanced hydration, and dynamic lipid mixing. These elements collectively contribute to the efficient fusion and uptake of EVs, shedding light on their biological significance in cellular communication and signalling pathways.

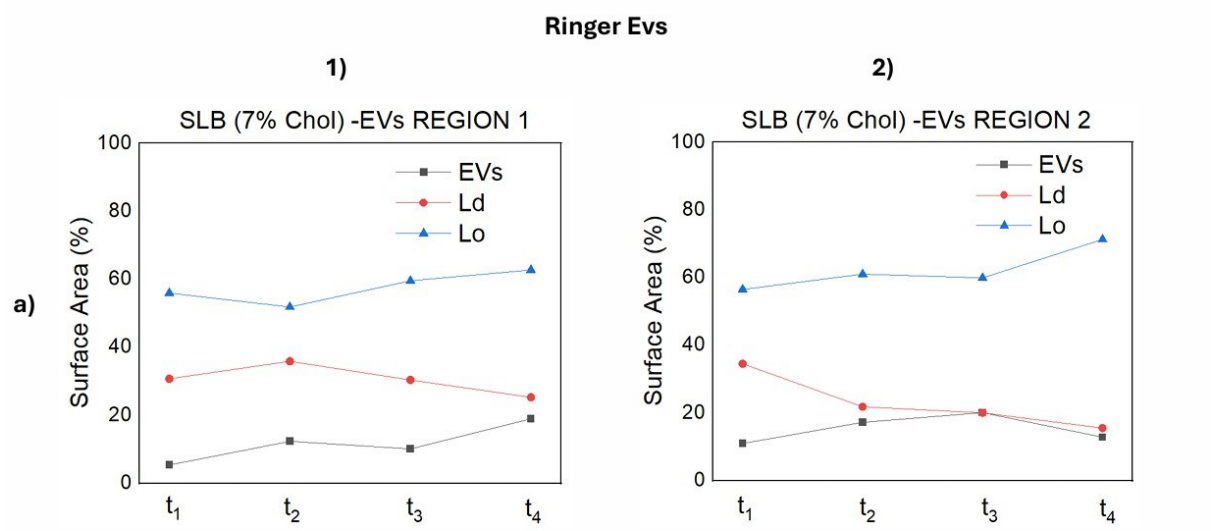

b)

Time (min)	Surface Area (%) EVs	Surface Area (%) Ld	Surface Area (%) Lo
t1	5	39	56
t2	12	36	52
t3	10.1	30.4	59.5
t4	16.3	23.5	60.2

Time (min)	Surface Area (%) EVs	Surface Area (%) Ld	Surface Area (%) Lo
t1	11	34	55
t2	17	22	61
t3	20	20	60
t4	13	15.5	71.5

Figure 5.6 The figure presents two panels: a) a graph depicting changes in surface area (%) over time for the EVs, the liquid-disordered phase (Ld), and the liquid-ordered phase (Lo) of supported lipid bilayers (SLBs) containing 7% cholesterol, and b) a table providing the corresponding numerical surface area data for each component at different time points.

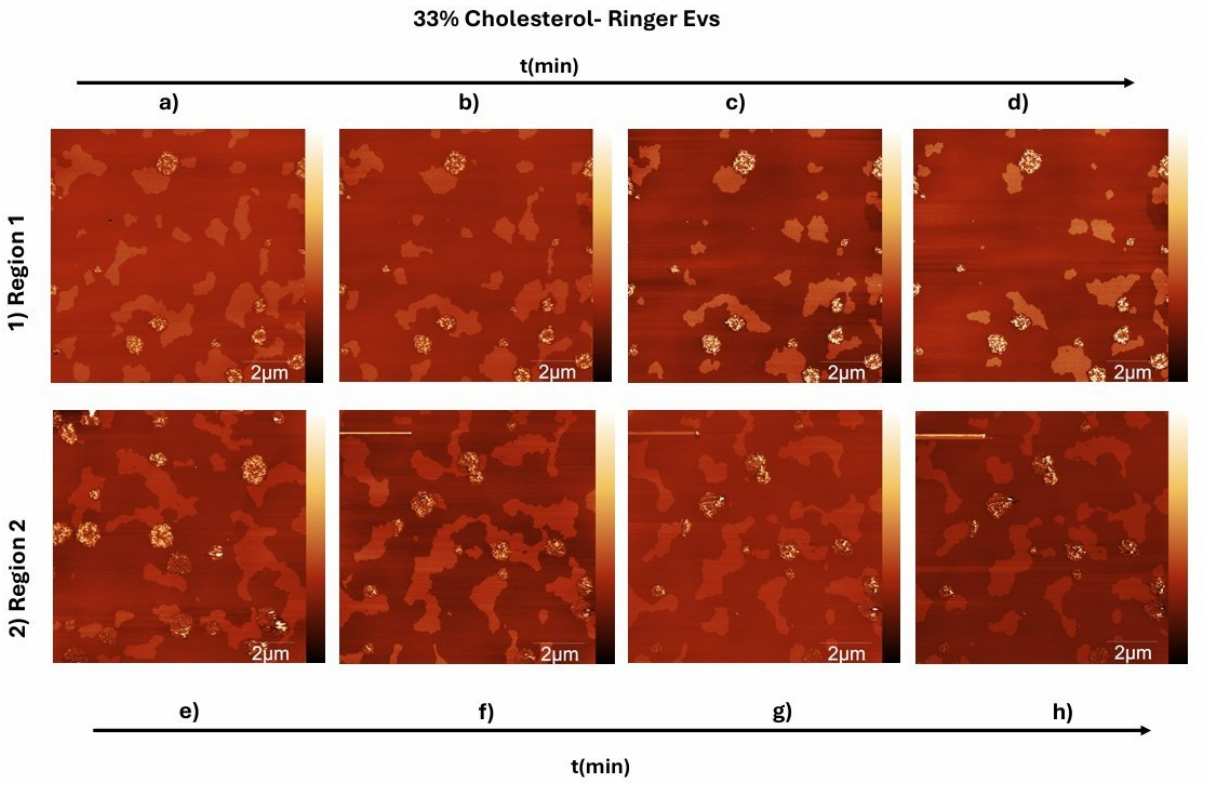

Figure 5.7 AFM Topography Images of SLBs Composed of 33% Cholesterol Interacting with EVs ringer buffer s across two distinct regions (Region 1 and Region 2). These images capture the evolution of SLB surface

morphology during a 1-hour interaction with EVs. a) and e) t_1 = 5 min: Initial interaction stage, showing early surface modifications and the onset of lipid reorganization or EV-SLB binding. b) and f) t_2 = 10 min: Continued surface development indicates progression in the interaction, with potential differences in responses between the two regions. c) and g) t_3 = 15 min: More pronounced topographical changes reflect deeper interactions and ongoing binding or fusion processes. d) and h) t_4 = 23 min: Significant structural alterations indicate deeper integration of EVs into the SLB, with variations in modifications observed between the regions.

The interaction between SLB-Ringer-EVs was then investigated at a concentration of 33 mol % cholesterol SLBs. In this scenario, we observed a preferential interaction of the Ringer-EVs with the edges of the lipid rafts. In contrast, when examining the interaction between serum- free EVs and SLBs containing 33 mol% cholesterol, the vesicles showed a distinct preference for the liquid-disordered phase, consistently positioning themselves near the Lo-Ld phase boundary. These results underscore the significant influence of the isolation medium on the modulation of membrane interactions. Understanding this behaviour is crucial, as the suspension medium can be tailored to promote specific interactions with either the Lo or Ld phase, potentially facilitating targeted applications in membrane biology and drug delivery systems. Moreover, when comparing the interaction trends of serum-free EVs, we noted a time- dependent increase in the surface area occupied by the Ld phase, accompanied by a reduction in the area covered by the Lo phase. Additionally, there was a progressive increase in the area occupied by the Ringer-EVs. These observations suggest an active fusion mechanism that becomes more pronounced over time, indicating a dynamic process where vesicle interactions evolve as a function of their environment. In addition, the interaction between the lipid raft edges and the ringer-EVs is notably more pronounced in presence of the ringer buffer compared to serum-free EVs. This heightened interaction can reasonably be attributed to the presence of the Ringer buffer, which may facilitate or stabilize closer associations at the lipid raft boundaries. The ionic composition of the Ringer buffer could contribute to modulating the membrane properties, potentially enhancing the affinity or structural compatibility between lipid raft edges and the Ringer-buffered EVs.

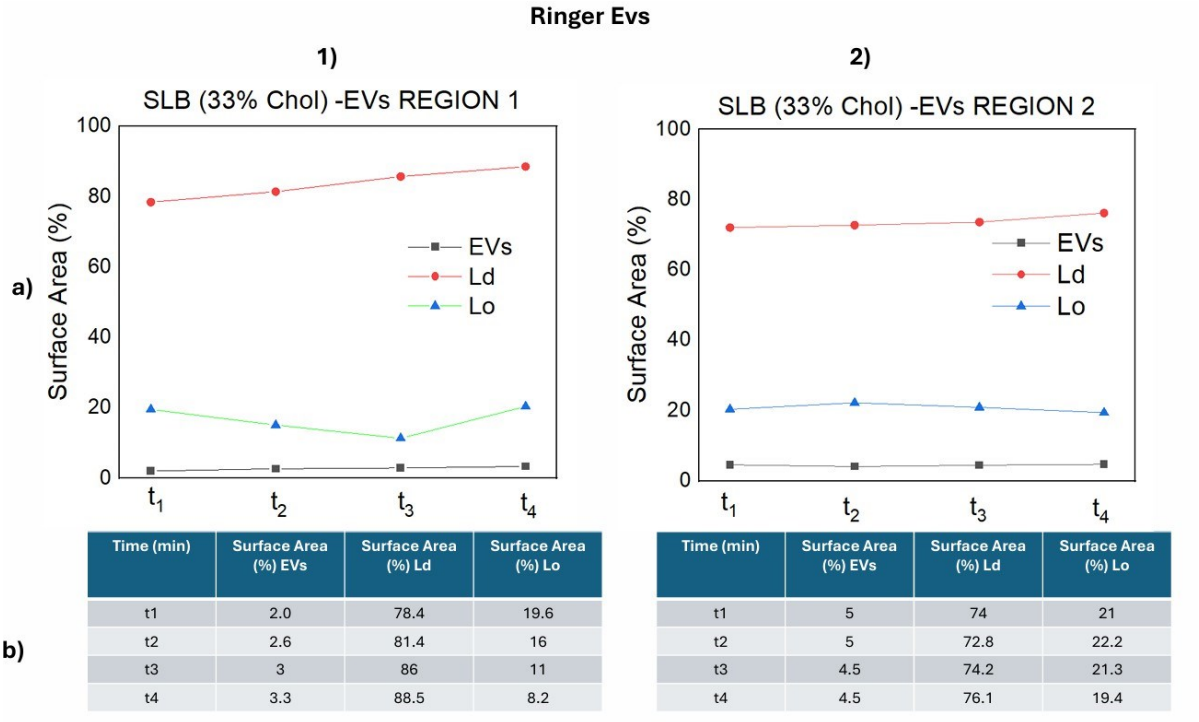

Time (min)	Surface Area (%) EVs	Surface Area (%) Ld	Surface Area (%) Lo
t1	2.0	78.4	19.6
t2	2.6	81.4	16
t3	3	86	11
t4	3.3	88.5	8.2

Time (min)	Surface Area (%) EVs	Surface Area (%) Ld	Surface Area (%) Lo
t1	5	74	21
t2	5	72.8	22.2
t3	4.5	74.2	21.3
t4	4.5	76.1	19.4

Figure 5.8 presents two panels: a) a graph depicting changes in surface area (%) over time for Ringer- EVs, the liquid-disordered phase (Ld), and the liquid-ordered phase (Lo) of SLBs containing 33mol% cholesterol, and b) a table providing the corresponding numerical surface area data for each component at different time points.

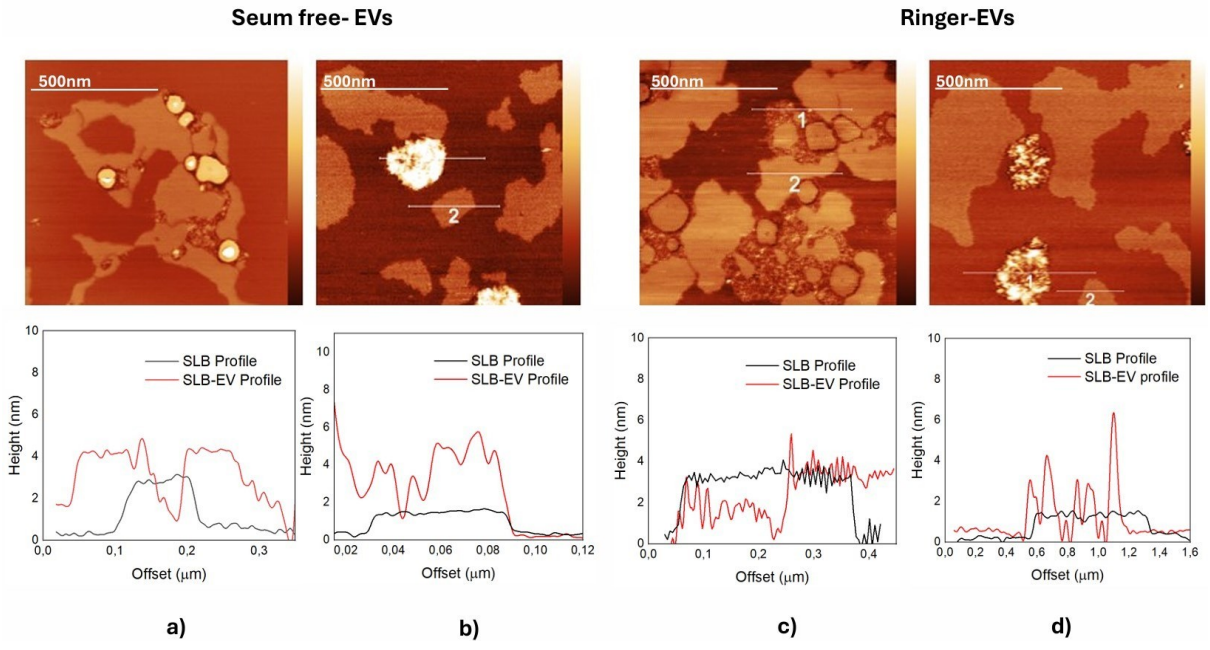

Figure 5.9 AFM topographic images illustrate the interactions between EVs and SLBs composed of DOPC, DSPC, and SM at two different cholesterol concentrations: a) and c) with 7 mol % cholesterol and b) and d) with 33 mol % cholesterol. Panels a) and b) display the topography images of the SLB with 7 mol % and 33 mol % cholesterol, respectively, interacting with serum-free EVs, along with the corresponding height profiles shown below. Panels c) and d) present the topography images of the SLB at the same cholesterol concentrations (7 mol % and 33 mol %) interacting with Ringer EVs, also accompanied by the respective height profiles below.

The interaction of EVs with the SLBs resulted in the formation of small protrusions above the SLB surface, as illustrated in Fig.5.9. Both types of EVs—serum-free and Ringer—induced local destabilizations in the SLB structure, particularly at the edges of their interaction sites for the 33 mol % cholesterol concentration, while interactions at the 7 mol % cholesterol concentration were more pronounced within the raft domains. Given that the average height of the EVs measured on mica was approximately 12 ± 6 nm the observed protrusions can be associated with the EVs fusion process in which there is the formation of the clusters of EVs that have adsorbed onto the SLB via partial fusion. Has been reported a representative image of Serum-free-EVs adsorbed on mica in figure 5.10.

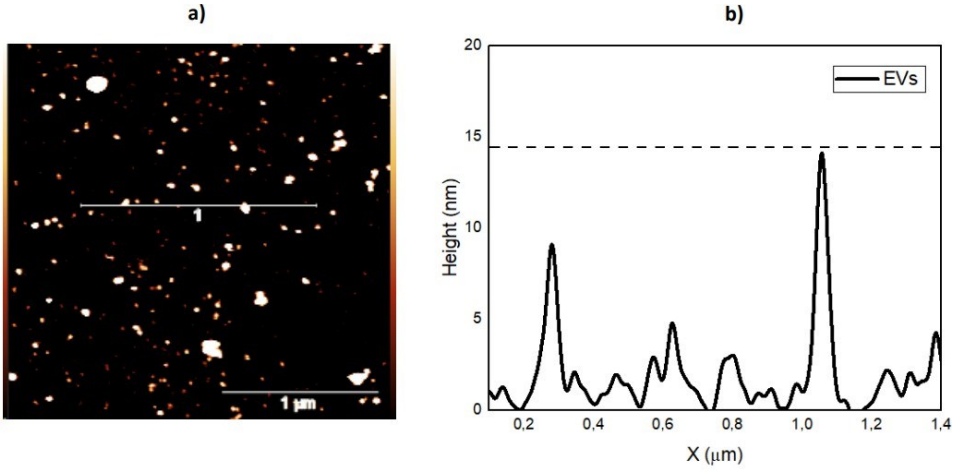

Figure 5.10 AFM topographic image of EVs adsorbed on mica substrate with the height profiles. Vesicles have a size ranging from 13 nm to 20 nm.

The interactions between the EVs and the SLB are influenced by the cholesterol content within the membrane. Notably, at the lower cholesterol concentration (7 mol %), there is a preferential interaction of both serum-free and Ringer EVs with the raft domains, suggesting a potential selectivity based on the lipid composition of the rafts. Conversely, as the cholesterol level increases to 33 mol%, both types of EVs exhibit interactions at the edges of the membrane, indicating a shift in the nature of the interaction. This suggests that higher cholesterol concentrations may alter the fluidity and stability of the SLB, thereby affecting the binding dynamics of the EVs.

Conclusions

In this work, we provided a detailed exploration of supported lipid bilayers as a model for studying lipid raft dynamics and extracellular vesicles interactions. The focus was on how varying cholesterol concentration modulates membrane properties, raft formation, and their subsequent interactions with EVs, highlighting the quantitative data that supports these observations.

Cholesterol's Role in Membrane Properties:

Four-component SLBs with 7 mol% and 33 mol% cholesterol were prepared to mimic the natural heterogeneity of eukaryotic membranes. Atomic force microscopy (AFM) revealed that as cholesterol concentration increased, the differential height of lipid rafts (LRs) with respect to the liquid disordered (Ld) phase decreased from the value of 1.8 ± 0.3 nm at 7% to 1.0 ± 0.2 nm at 33% (Figure 4.3). This indicates that cholesterol compresses LRs, decreasing membrane order and rigidity. At the same time, at 33% cholesterol, the LRs area expanded to 35 ± 6% (Figure 4.3), in contrast with the value of 22 ± 4% measured at 7% cholesterol.

This is in agreement with the concept of releasing the order/increasing the fluidity within the raft domains, obtained at higher cholesterol concentration. In the computation of the relative height of the LR domains, however, we should not discard the opposite contribution adduced by the residual percentage of cholesterol which flows into the Ld domains, which enhances the ordering, therefore the thickening, of the Ld phase. Since with the AFM we measure a relative height, at this stage both contributions should be acknowledged. As cholesterol content increased from 7% to 33%, UV-Vis measurements of the interaction of gold nanoparticles (16 nm diameter) with liposomes with the same composition of the SLBs described above, showed a red shift from 521 nm to 596 nm, indicating greater aggregation of nanoparticles. This is explained with an increased softness of the membranes (Figure 4.18). This suggests that higher cholesterol levels lead to increased membrane fluidity, especially in the liquid ordered (Lo) phase, where lipid molecules are less tightly packed.

Nanoindentation and Mechanical Properties:

Direct, nanoindentation force curves on the different domains of the SLB showed a significant decrease in breakthrough force at higher cholesterol levels. At 7% cholesterol, the Lo phase exhibited a higher resistance (breakthrough force), then at 33%, suggesting increased fluidity (Figure 4.19). Quantitatively, median breakthrough forces decreased by ~40%, confirming that cholesterol softens the Lo phase while slightly stiffening the Ld phase.

While AFM measurements highlighted the changes in differential height of lipid raft domains as cholesterol increased, nanoindentation further clarified these findings by revealing the direct impact of cholesterol on the mechanical properties of the membrane, providing insights into how cholesterol

modulates membrane stiffness; these conclusions are further supported by FRAP experiments, which confirm that the Lo phase becomes significantly more fluid at higher cholesterol levels.

Diffusion Dynamics (FRAP):

Fluorescence Recovery After Photobleaching (FRAP) experiments quantified diffusion coefficients of lipids in both Lo and Ld phases. In the Lo phase, the diffusion coefficient increased from 0.215 $\mu m^2/s$ at 7% cholesterol to 1.19 $\mu m^2/s$ at 33%, with a corresponding decrease in diffusion time from 4.68 s to 1.08 s (Figure 4.21). This substantial increase in diffusion rate further confirms that cholesterol enhances fluidity within the phase. In contrast, the Ld phase showed no significant change in diffusion coefficient, at the two cholesterol concentrations, supporting the notion that cholesterol preferentially modulates the more ordered regions of the membrane. This work demonstrates the pivotal role of cholesterol in modulating membrane structure and dynamics, particularly in the formation and stabilization of lipid rafts. The ability of cholesterol to alter the mechanical and fluid properties of SLBs has profound implications for understanding membrane behaviour, from vesicle fusion to signal transduction. By combining quantitative AFM data, UV-Vis spectroscopy, and FRAP analysis, this study establishes clear relationships between cholesterol concentration, membrane fluidity, and raft domain behaviour. The novel finding that cholesterol increases the fluidity of the Lo phase, while minimally affecting the Ld phase, offers new insights into how membranes organize functional domains. Moreover we showed that cholesterol, changing the fluidity of the membrane, has an important role in the interaction of extracellular vesicles with our model membranes.

Cholesterol's Impact on EV Interactions

At lower membrane fluidity conditions, i.e. at 7% cholesterol, topography images revealed that EVs from GMP production of Umbilical Cord-Mesenchymal Stem Cells (UC-MSC) preferentially disrupted lipid rafts, and membrane fusion events were evident (Fig 5.1). Also under Ringer's solution, which closely mimics physiological ionic conditions, EVs displayed a preferred affinity for lipid rafts edges. In this case, however, rafts disruption is less evident. At higher membrane fluidity conditions, i.e. 33 mol% SLBs, interactions in both Ringer's and serum-free conditions predominantly occurred within the Ld phase and at the edges of lipid rafts, though Ringer's solution enhanced EV recruitment to the raft edges. In both case the mixing of the vesicles with the membrane was favoured. This effect highlights the crucial role of both ionic strength of the solution and membrane fluidity, in modulating EV-lipid raft interactions: the increased recruitment at the raft boundaries in Ringer's conditions, suggest an enhanced stabilization or preferential electrostatic attraction at the raft interfaces.

Implications and Future Directions

This study demonstrates the pivotal role of cholesterol in modulating membrane structure, dynamics, and interactions with EVs. By combining AFM, UV-Vis spectroscopy, and FRAP, we established clear links between cholesterol concentration, membrane fluidity, and lipid raft behaviour. Key findings include:

• Cholesterol increases the fluidity of the Lo phase while minimally affecting the Ld phase.

• Cholesterol significantly influences EV-membrane interactions by altering raft stability and fluidity.

This research provides robust results for further investigations into membrane-associated phenomena such as drug delivery, nanoparticle interactions, and protein reconstitution.

Appendix A

A1: Phase separation in Giant Unilamellar Vesicles (GUVs)

The reconstitution of mimetic models of cell membranes, containing transmembrane proteins, is still challenging in synthetic biology. Much of the current research focuses on developing biomimetic models of eukaryotic cell membranes, where each one aims to replicate key membrane characteristics, such as curvature and/or phase separation, to better understand the role of each membrane fundamental property. The development of Giant Unilamellar Vesicles plays a crucial role in this endeavour. GUVs provide simplified, controllable platforms for investigating membrane dynamics, offering a way to isolate specific phenomena like phase separation. Their large size and unilamellar structure make them ideal for high-resolution imaging and manipulation via microscopy, enabling detailed observation of lipid domain formation and phase transitions in real time. Additionally, one of the most significant characteristics of GUVs is that their radius of curvature closely resembles that of biological cells, making them particularly suitable for studying essential cellular processes. In the framework of the present work, the formation and optimization of GUVs was a crucial step for advancing towards the development of pore-spanning membranes—specialized substrates designed to suspend the lipid bilayers. Pore-spanning membranes are specialized structures designed to bridge and span pores in various substrates, including both biological and synthetic materials. The dimensions of PSMs can vary significantly based on their intended applications. Generally, the thickness of PSMs ranges from a few nm to several μm, while the size of the pores they cover typically ranges from 100 nm to several μm. These biomimetic systems offer a platform that better approximate the native state of biological membranes compared to simpler models, as they allow for the incorporation of functional membrane proteins, for instance relevant in EVs fusion and other types of interactions. For instance, planar pore-spanning membranes containing SNARE proteins were fabricated on highly ordered, functionalized 1.2 μm pore arrays in Si_3N_4. Fusion events were monitored using time- resolved, two-colour confocal laser scanning fluorescence microscopy, allowing for precise distinction between vesicle docking, intermediate stages and the complete fusion [200]. A key objective of this research was to generate GUVs through electroformation—a method that, unlike water-oil emulsion transfer, achieves high GUV yield without the use of mineral oil. Furthermore, we optimized substrates featuring pores of 500 nm and 1 micron in diameter, a geometry that enables the study and incorporation of transmembrane proteins. Notably, this approach facilitates research on HER2, a transmembrane protein of considerable interest in the laboratory where this work was conducted.

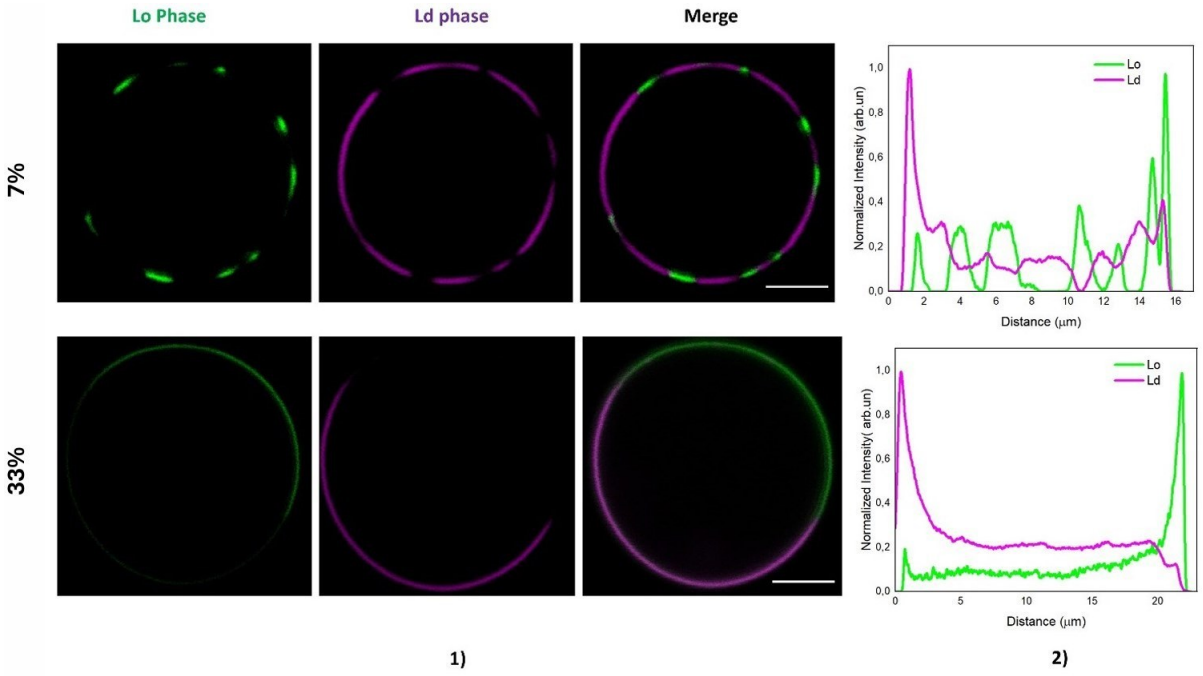

Figure A 1.1 GUVs (2D sections) have been reported, where the entire Lo phase has been fluorescently labeled in green with NBD-DSPE and the Ld phase in magenta with ATTO655-DOPE, for the two investigated cholesterol concentrations (Panel 1). Consistent with AFM results, the area covered by the ordered domains increases with cholesterol concentration, leading to an enlargement of the ordered domains. Panel 2) shows the intensity profiles. The scale bar is 10 μm.

Phase separation was studied using GUVs designed to mimic the lipid composition and curvature of cellular membranes (Figure A 1.1). The GUVs were developed at the equivalent lipid composition of the SLBs optimized and studied in the core of this work (Table 1.1). The results clearly demonstrate phase separation, with the proportion of the membrane occupied by the Lo phase increasing significantly as cholesterol concentration rises. These findings are consistent with the Atomic Force Microscopy and Confocal Laser Scanning Microscopy data obtained from SLBs, further confirming the impact of cholesterol on membrane domain formation. The phases of the membrane shown in Figure A1 have been fluorescently labelled with the green-emitting NBD-DSPE (Lo phase) and the magenta-emitting ATTO655-DOPE (Ld phase), respectively. These phases represent distinct lipid packing states within the membrane. In the case of 7 mol % cholesterol, the Lo phase appears as distinct patches, indicating localized regions where the membrane is tightly packed. In contrast, the Ld phase forms a more continuous distribution, covering a larger portion of the vesicle, suggesting a more fluid, loosely packed membrane structure. The merged image clearly reveals the phase separation, and in the case of 33 mol % cholesterol, both the Lo and Ld phases exhibit a more uniform distribution around the vesicle, with the Lo phase becoming increasingly continuous. The merged image shows much less phase separation compared to the low cholesterol condition, suggesting that the membrane becomes more homogenous as cholesterol concentration increases. The intensity graphs plot the normalized fluorescence intensity as a function of distance (μm) across the membrane for both the Lo and Ld phases. For 7 mol% cholesterol, the intensity profile for the Lo phase (green)

exhibits sharp peaks at specific distances, indicating discrete, concentrated regions of ordered lipid domains. The Ld phase (magenta) displays a more gradual, continuous intensity, reflecting its larger surface coverage and less ordered structure. The distinct peaks and valleys in the profiles correspond to the clear phase separation observed in the fluorescence images. In contrast, for 33 mol % cholesterol, the Lo phase intensity becomes more uniform, with fewer sharp peaks, suggesting a more even distribution of ordered lipid domains across the membrane. The Ld phase intensity also exhibits a smoother, more continuous profile, supporting the visual observation of reduced phase separation. The decrease in sharp intensity variations indicates that, at higher cholesterol levels, the membrane becomes more homogenous, with less distinct domain formation.

A2: Preliminary results on the Optimization of Pore-Spanning Membranes

In this thesis, we present preliminary data on the reconstitution of pore-spanning membranes, a critical step in creating biomimetic systems. This process has proven to be highly challenging, primarily due to the inherent difficulties in forming a homogeneous membrane that adequately spans the pores. Achieving uniform membrane coverage over the pores is crucial but current trials have highlighted the complexity of this task. Membrane rupture, uneven spreading, and inconsistent pore coverage have been common hurdles, which underscore the need for precise experimental conditions and optimization techniques. Additionally, the integration of membrane receptors as, for instance, HER2 protein into these membranes is still in progress and presents its own set of challenges. HER2, part of the ErbB receptor family, plays a vital role in cell growth, differentiation, and survival; its overexpression often correlates with aggressive cancer progression [201]. Integrating HER2 into GUVs provides a realistic model to investigate its dimerization, activation, and signalling pathways within a lipid bilayer that closely mimics natural cell environments. This setup not only allows for the study of HER2's functional structure—particularly its extracellular ligand-binding, hydrophobic transmembrane, and intracellular kinase regions—but also facilitates examination of how HER2 interacts with lipid rafts and caveolae. HER2's tendency to cluster within these lipid rafts, often anchored by gangliosides like GM1 and GM3, enhances its dimerization and activation, increasing oncogenic signalling potential. Disruption of these lipid rafts, however, can reduce HER2 clustering, thereby diminishing its signalling efficacy. By reconstituting HER2 within suspended pore-spanning membranes, this research aims to explore HER2's localization within the membrane and its interactions with lipid rafts, providing insights into potential therapeutic strategies to disrupt HER2-mediated tumor progression. Unlike simple lipid bilayer formation, incorporating a transmembrane protein like HER2 demands specific protocols that include detergent-mediated solubilization and controlled insertion into the lipid bilayer. This detergent-assisted integration must be carefully optimized to ensure that HER2 is correctly inserted in its functional conformation without disrupting the overall membrane structure.

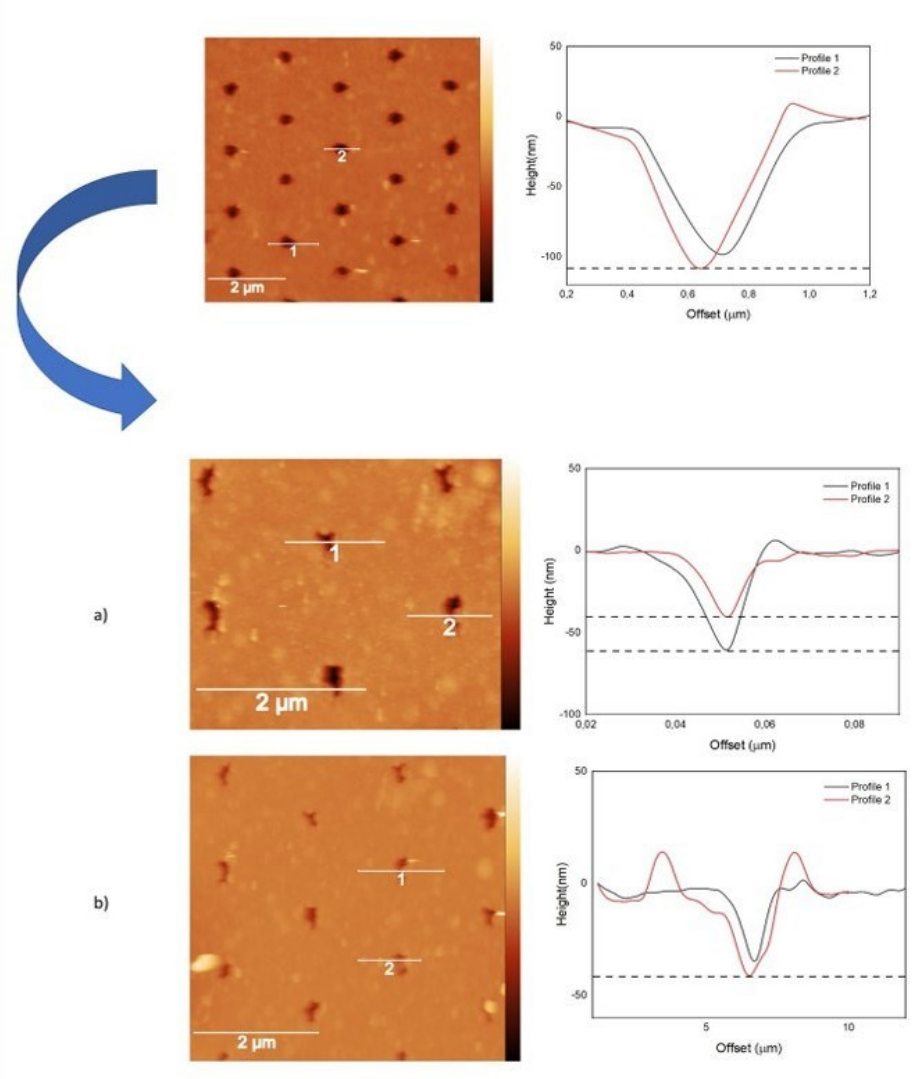

Figure A.2.1 AFM topography images and corresponding height profiles of pore-spanning membranes functionalized with a Self-Assembled Monolayer (SAM) of 6-mercaptohexanol (6MH). After functionalization, Sample 1 (top) was washed, and GUVs were incubated at 55°C for 2 hours. Top image: The AFM topography shows the surface morphology after SAM functionalization. Profiles 1 and 2 depict the cross-sectional height measurements over the designated areas, confirming uniform pore coverage with some depth variability, indicated by the differences in height in the plotted profiles. Middle (a) and bottom (b) images: These images represent the system after incubation. Profiles 1 and 2 measure the depth of the structures, revealing significant changes after incubation, potentially indicating partial pore coverage or vesicle deformation. The height profiles highlight the structural evolution post-incubation, with noticeable differences in depth and membrane coverage compared to the initial state. a) 3.5x3.5 µm b) 4x4 µm of the PSM after the spread of the GUVs. (pore diameter = 500nm).

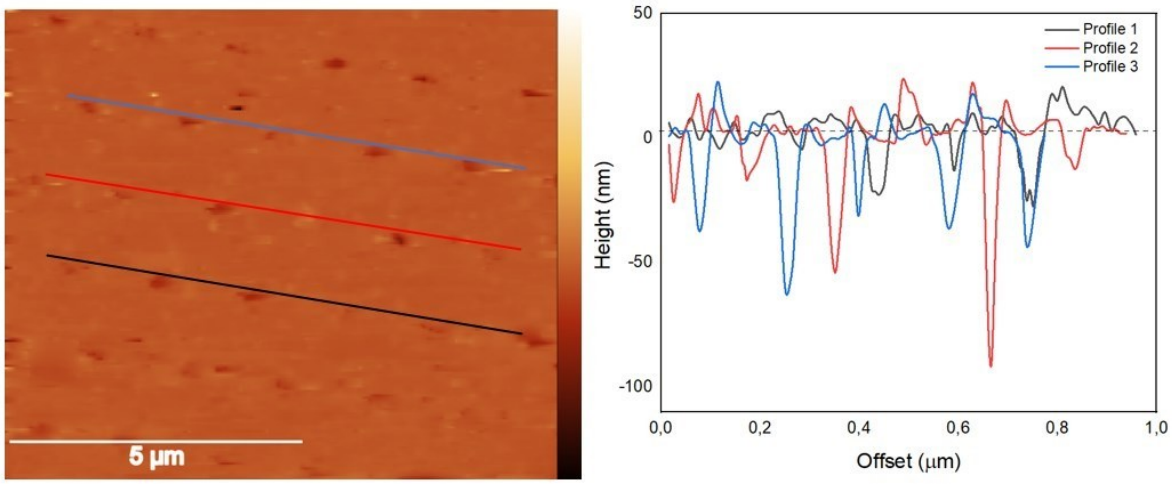

Figure A.2.2 AFM topography image of pore-spanning membranes after functionalization with a self-assembled monolayer (SAM) of 6MH. The pore diameter is 500 nm, and the image size is 8x8 µm, with a 2-hour incubation time of the GUVs. The height profiles corresponding to the blue, red, and black lines are plotted on the right, illustrating variations in surface topography.

In the formation of pore-spanning membranes, we employed the method outlined in the Materials and Methods section. The GUVs used for this process have the same composition as the SLBs, containing 33 mol% cholesterol. This particular lipid ratio closely mimics the composition of natural membranes, enhancing the relevance of our model. Figures A.2.1 and A.2.2 illustrate a partial coverage of the pores, as indicated by the depth profiles obtained from data processing. As mentioned earlier, optimizing the deposition of GUVs onto these substrates presents significant challenges. At the current status of the work, we have not yet achieved a stable coverage of the membranes. We are actively working on refining the optimization process, with the ultimate goal of achieving a uniform and stable coating of the substrates with our membrane. This stability is crucial for accurately studying the functional characteristics of the membrane and its interactions with proteins of interest. Once optimized, this system will allow for detailed studies of HER2 behaviour within a native-like environment, shedding light on its interactions with lipid rafts and other membrane components. These findings could open new avenues for targeted cancer therapies by revealing previously unknown aspects of HER2 signalling and activity in membrane microdomains.

Bibliography

[1] Bayda S, Adeel M, Tuccinardi T, Cordani M, Rizzolio F. The History of Nanoscience and Nanotechnology: From Chemical-Physical Applications to Nanomedicine. Molecules. 2019 Dec 27;25(1):112.

[2] Nanomaterials definition matters. Nat Nanotechnol. 2019 Mar;14(3):193.

[3] B. Mekuye, B. Abera, Nano Select. 2023, 4, 486.

[4] Feynman, R. P. (1959). There's plenty of room at the bottom (accessed December 10, 2021).

[5] Salman Khan, Shazia Mansoor, Zeeshan Rafi, Bhawna Kumari, Ambreen Shoaib, Mohd Saeed, Sultan Alshehri, Mohammed M. Ghoneim, Mohamed Rahamathulla, Umme Hani, Faiyaz Shakeel,A review on nanotechnology: Properties, applications, and mechanistic insights of cellular uptake mechanisms, Journal of Molecular Liquids,Volume 348,2022,118008.

[6] T., Nathwani, J., Nazar, L., Sips, A., Sone, J., van den Berg, A., Weiss, P. S., & Mitra, S. Nanotechnology for a sustainable future: Addressing global challenges with the international network for sustainable nanotechnology.

[7] Mazayen, Z. M., Ghoneim, A. M., Elbatanony, R. S., Basalious, E. B., & Bendas, E. R. (2022). Pharmaceutical nanotechnology: From the bench to the market. Future Journal of Pharmaceutical Sciences, 8(1), 12.

[8] Kagan, C. R., Fernandez, L. E., Gogotsi, Y., Hammond, P. T., Hersam, M. C., Nel, A. E., Penner, R. M., Willson, C. G., & Weiss, P. S. (2016). Nano Day: Celebrating the next decade of nanoscience and nanotechnology. ACS Nano, 10(10), 9093-9103.

[9] Akgönüllü, S., Çimen, D., Göktürk, İ., Yılmaz, G. E., Yılmaz, F., & Denizli, A. (Eds.). (n.d.). Nanodevices and nanomachines at the nanoscale biophysics.

[10] Schaffer, L. V., & Ideker, T. Mapping the multiscale structure of biological systems.

[11] Membranes and evolution. PRIMER| VOLUME 28, ISSUE 8, PR381-R385, APRIL 23, 2018

[12] European Journal for Philosophy of Science. (n.d.). What is a complex system?

[13] Leonard TA, Loose M, Martens S. The membrane surface as a platform that organizes cellular and biochemical processes. Dev Cell. 2023 Aug 7;58(15):1315-1332.

[14] Engelman DM. Membranes are more mosaic than fluid. Nature. 2005 Dec 1;438(7068):578-80.

[15] Singer SJ, Nicolson GL. The fluid mosaic model of the structure of cell membranes. Science. 1972 Feb 18;175(4023):720-31.

[16] Korlach J, Schwille P, Webb WW, Feigenson GW. Characterization of lipid bilayer phases by confocal microscopy and fluorescence correlation spectroscopy. Proc Natl Acad Sci U S A. 1999 Jul 20;96(15):8461-6. 114

[17] Hegde RS, Keenan RJ. The mechanisms of integral membrane protein biogenesis. Nat Rev Mol Cell Biol. 2022 Feb;23(2):107-124.

[18] Kulbacka J, Choromańska A, Rossowska J, Weżgowiec J, Saczko J, Rols MP. Cell Membrane Transport Mechanisms: Ion Channels and Electrical Properties of Cell Membranes. Adv Anat Embryol Cell Biol. 2017;227:39-58.

[19] Picci G, Marchesan S, Caltagirone C. Ion Channels and Transporters as Therapeutic Agents: From Biomolecules to Supramolecular Medicinal Chemistry. Biomedicines. 2022 Apr 12;10(4):885.

[20] J, Choromańska A, Rossowska J, Wężgowiec J, Saczko J, Rols MP. Cell Membrane Transport Mechanisms: Ion Channels and Electrical Properties of Cell Membranes. Adv Anat Embryol Cell Biol. 2017;227:39-58.

[21] Benz RW, Castro-Román F, Tobias DJ, White SH. Experimental validation of molecular dynamics simulations of lipid bilayers: a new approach. Biophys J. 2005 Feb;88(2):805-17.

[22] Tieleman, D. P. (2006). Understanding membrane protein dynamics and organization in cellular membranes through computational simulations. BBA - Biomembranes, 1758(6), 728 739.

[23] Pustovit, E. D. (2023). Recent advances in biomimetic lipid membranes: Exploring membrane dynamics and functionality. Current Opinion in Colloid & Interface Science, 61, 101579.

[24] Bucher, L. D., & Hasegawa, M. K. R. (2022). Engineering biomimetic membranes for cell free studies of membrane proteins and lipids. Nature Reviews Molecular Cell Biology, 23(7), 449-460.

[25] Liu, T., & Zhang, X. (2022). Biomimetic lipid membranes for drug delivery and cellular mechanistic studies. Biomaterials Science, 10(5), 1405-1418.

[26] Paba C, Dorigo V, Senigagliesi B, Tormena N, Parisse P, Voitchovsky K, Casalis L. Lipid bilayer fluidity and degree of order regulates small EVs adsorption on model cell membrane. J Colloid Interface Sci. 2023 Dec 15;652(Pt B):1937-1943.

[27] Chabanon M, Stachowiak JC, Rangamani P. Systems biology of cellular membranes: a convergence with biophysics. Wiley Interdiscip Rev Syst Biol Med. 2017 Sep;9(5):10.1002/wsbm.1386.

[28] Lamparter L, Galic M. Cellular Membranes, a Versatile Adaptive Composite Material. Front Cell Dev Biol. 2020 Aug 5;8:684.

[29] Cavalli M, et al. Dynamic plasma membrane organization: a complex symphony. Trends Cell Biol. 2020;30(4):287-299.

[30] Ralston, J. et al. Structure of the plasma membrane. In: The Cell. National Center for Biotechnology Information

(NCBI)https://www.ncbi.nlm.nih.gov/books/NBK11330/.

[31] van Meer, G., Voelker, D. R., Feigenson, G. W. Membrane lipids: where they are and how they behave. Nat Rev Mol Cell Biol. 2008;9(2):112-124.

[32] Simons K, Gerl MJ. A polarizing view on the lipid raft concept. Nat Rev Mol Cell Biol. 2010;11(6):440-451.

[33]. McIntosh T. Membrane heterogeneity beyond the plasma membrane. PMC. 2015;6(2):100-108.

[34] Alberts B, et al. The lipid bilayer. In: Molecular Biology of the Cell. NCBI Bookshelf. Available from: https://www.ncbi.nlm.nih.gov/books/NBK26863/.

[35] Levental I, et al. Lipid organization of the plasma membrane. J Am Chem Soc. 2020;142(5):2370-2380.

[36] Singer SJ, Nicolson GL. The fluid mosaic model of the structure of cell membranes. Science. 1972;175(4022):720-731.

[37] Mikhailov AS, et al. An outlook on the organization of lipids in membranes: searching for a realistic connection with the organization of biological membranes. PubMed. 2021;62(3):321-336.

[38] D'Auria S, et al. The mystery of membrane organization: composition, regulation and roles of lipid rafts. Nat Rev Mol Cell Biol. 2021;22(5):289-303.

[39] Hsu CL, et al. Plasma membrane integrity: implications for health and disease. BMC Biol. 2018;16(1):9.

[40] Van der Veen JN, Kennelly JP, Wan S, Vance JE, Vance DE, Jacobs RL. The critical role of phosphatidylcholine and phosphatidylethanolamine metabolism in health and disease. Biochim Biophys Acta Biomembr. 2017 Sep;1859(9 Pt B):1558-1572.

[41] Cockcroft S. Mammalian lipids: structure, synthesis and function. Essays Biochem. 2021 Nov 2;65(5):813-845. doi: 10.1042/EBC20200067.

[42] Yoon H, Shaw JL, Haigis MC, Greka A. Lipid metabolism in sickness and in health: Emerging regulators of lipotoxicity. Mol Cell. 2021 Sep 16;81(18):3708-3730.

[43] Saini RK, Prasad P, Shang X, Keum YS. Advances in Lipid Extraction Methods-A Review. Int J Mol Sci. 2021 Dec 20;22(24):13643.

[44] Alberts B, Johnson A, Lewis J, et al. New York: Garland Science; 2002.

[45] Kuo, A., Hla, T. Regulation of cellular and systemic sphingolipid homeostasis. Nat Rev Mol Cell Biol 25, 802–821 (2024).

[46] Jennifer L. Johnson, Lance A. Johnson,Homeostasis of Lipid Metabolism in Disorders of the Brain, Editor(s): Sergio Della Sala,Encyclopedia of Behavioral Neuroscience, 2nd edition (Second Edition),Elsevier,2022,Pages 372-382.

[47] Lee TH, Charchar P, Separovic F, Reid GE, Yarovsky I, Aguilar MI. The intricate link between membrane lipid structure and composition and membrane structural properties in bacterial membranes. Chem Sci. 2024 Jan 31;15(10):3408-3427.

[48] van Meer, G., Voelker, D. R., Feigenson, G. W. Membrane lipids: where they are and how they behave. Nat Rev Mol Cell Biol. 2008;9(2):112-124.

[49] Ballweg, S., Sezgin, E., Doktorova, M. et al. Regulation of lipid saturation without sensing membrane fluidity. Nat Commun 11, 756 (2020).

[50] Lorent JH, Levental KR, Ganesan L, Rivera-Longsworth G, Sezgin E, Doktorova M, Lyman E, Levental I. Plasma membranes are asymmetric in lipid unsaturation, packing and protein shape. Nat Chem Biol. 2020 Jun;16(6):644-652.

[51] Harayama T, Riezman H. Understanding the diversity of membrane lipid composition. Nat Rev Mol Cell Biol. 2018 May;19(5):281-296. doi: 10.1038/nrm.2017.138. Epub 2018 Feb 7.

[52] Holthuis JC, Levine TP. Lipid traffic: floppy drives and a superhighway. Nat Rev Mol Cell Biol. 2005 Mar;6(3):209-20.

[53] Li C, Quintana Perez Y, Lamaze C, Blouin CM. Lipid nanodomains and receptor signaling: From actin-based organization to membrane mechanics. Curr Opin Cell Biol. 2024 Feb;86:102308.

[54] F.-Xabier Contreras, Lissete Sánchez-Magraner, Alicia Alonso, Félix M. Goñi,Transbilayer (flip-flop) lipid motion and lipid scrambling in membranes,FEBS Letters,Volume 584, Issue 9,2010,Pages 1779-1786, ISSN 0014-5793

[55] Mike F. Renne, Robert Ernst,Membrane homeostasis beyond fluidity: control of membrane compressibility,

Trends in Biochemical Sciences,Volume 48, Issue 11,2023,Pages 963-977

[56] Alberts B, Johnson A, Lewis J, et al.New York: Garland Science; 2002.

[57] Cooper GM. The Cell: A Molecular Approach. 2nd edition. Sunderland (MA): Sinauer Associates; 2000. Signaling Molecules and Their Receptors.

[58] Alberts B, Johnson A, Lewis J, et al. Molecular Biology of the Cell. 4th edition. New York: Garland Science; 2002. Membrane Proteins.

[59] Boes DM, Godoy-Hernandez A, McMillan DGG. Peripheral Membrane Proteins: Promising Therapeutic Targets across Domains of Life. Membranes (Basel). 2021 May 8;11(5):346.

[60] Paul Burn, Bruno H. Dalle Carbonare,Chapter 3 Lipid-protein interactions in biological membranes, Editor(s): E. Edward Bittar, Neville Bittar,Principles of Medical Biology,Elsevier,Volume 7,1997,Pages 39-66.

[61] Qian S, Sharma VK, Clifton LA. Understanding the Structure and Dynamics of Complex Biomembrane Interactions by Neutron Scattering Techniques. Langmuir. 2020 Dec 22;36(50):15189-15211.

[62] Cell Membrane: Structure and Physical Properties. (2008). In: Integrated Molecular and Cellular Biophysics. Springer, Dordrecht. https://doi.org/10.1007/978-1-4020-8268-9_3

[63] Grouleff J, Irudayam SJ, Skeby KK, Schiøtt B. The influence of cholesterol on membrane protein structure, function, and dynamics studied by molecular dynamics simulations. Biochim Biophys Acta. 2015 Sep;1848(9):1783-95.

[64] Marquardt D, Kučerka N, Wassall SR, Harroun TA, Katsaras J. Cholesterol's location in lipid bilayers. Chem Phys Lipids. 2016 Sep;199:17-25.

[65] Grouleff J, Irudayam SJ, Skeby KK, Schiøtt B. The influence of cholesterol on membrane protein structure, function, and dynamics studied by molecular dynamics simulations. Biochim Biophys Acta. 2015 Sep;1848(9):1783-95.

[66] Bhattarai A, Likos EM, Weyman CM, Shukla GC. Regulation of cholesterol biosynthesis and lipid metabolism: A microRNA management perspective. Steroids. 2021 Sep;173:108878.

[67] Sviridov D, Mukhamedova N, Miller YI. Lipid rafts as a therapeutic target. J Lipid Res. 2020 May;61(5):687-695.

[68] Levental I, Lyman E. Regulation of membrane protein structure and function by their lipid nano-environment. Nat Rev Mol Cell Biol. 2023 Feb;24(2):107-122.

[69] Mollinedo F, Gajate C. Lipid rafts as signalling hubs in cancer cell survival/death and invasion: implications in tumor progression and therapy: Thematic Review Series: Biology of Lipid Rafts. J Lipid Res. 2020 May;61(5):611-635.

[70] Swain SM, Shastry M, Hamilton E. Targeting HER2-positive breast cancer: advances and future directions. Nat Rev Drug Discov. 2023 Feb;22(2):101-126.

[71] Nelson ER, Chang CY, McDonnell DP. Cholesterol and breast cancer pathophysiology. Trends Endocrinol Metab. 2014 Dec;25(12):649-55.

[72] Ouweneel AB, Thomas MJ, Sorci-Thomas MG. The ins and outs of lipid rafts: functions in intracellular cholesterol homeostasis, microparticles, and cell membranes: Thematic Review Series: Biology of Lipid Rafts. J Lipid Res. 2020 May;61(5):676-686.

[73] Pöhnl M, Trollmann MFW, Böckmann RA. Nonuniversal impact of cholesterol on membranes mobility, curvature sensing and elasticity. Nat Commun. 2023 Dec 11;14(1):8038

[74] Róg T, Pasenkiewicz-Gierula M, Vattulainen I, Karttunen M. Ordering effects of cholesterol and its analogues. Biochim Biophys Acta. 2009 Jan;1788(1):97-121.

[75] Subczynski WK, Pasenkiewicz-Gierula M, Widomska J, Mainali L, Raguz M. High Cholesterol/Low Cholesterol: Effects in Biological Membranes: A Review. Cell Biochem Biophys. 2017 Dec;75(3-4):369-385.

[76] Harayama T, Riezman H. Understanding the diversity of membrane lipid composition. Nat Rev Mol Cell Biol. 2018 May;19(5):281-296. doi: 10.1038/nrm.2017.138. Epub 2018 Feb 7. Erratum in: Nat Rev Mol Cell Biol. 2019 Nov;20(11):715.

[77] Kalani J. Seu, Lee R. Cambrea, R. Michael Everly, Jennifer S. Hovis,Influence of Lipid Chemistry on Membrane Fluidity: Tail and Headgroup Interactions, Biophysical Journal, Volume 91, Issue 10,2006,Pages 3727-3735,ISSN 0006-3495.

[78] Ma Y, Ghosh SK, DiLena DA, Bera S, Lurio LB, Parikh AN, Sinha SK. Cholesterol Partition and Condensing Effect in Phase-Separated Ternary Mixture Lipid Multilayers. Biophys J. 2016 Mar 29;110(6):1355-66.

[79] Krause MR, Regen SL. The structural role of cholesterol in cell membranes: from condensed bilayers to lipid rafts. Acc Chem Res. 2014 Dec 16;47(12):3512-21.

[80] Chen W, Duša F, Witos J, Ruokonen SK, Wiedmer SK. Determination of the Main Phase Transition Temperature of Phospholipids by Nanoplasmonic Sensing. Sci Rep. 2018 Oct 4;8(1):14815.

[81] Barba-Bon A, Nilam M, Hennig A. Supramolecular Chemistry in the Biomembrane. Chembiochem. 2020 Apr 1;21(7):886-910.

[82] Pöhnl M, Trollmann MFW, Böckmann RA. Nonuniversal impact of cholesterol on membranes mobility, curvature sensing and elasticity. Nat Commun. 2023 Dec 11;14(1):8038.

[83] Simons K, Toomre D. Lipid rafts and signal transduction. Nat Rev Mol Cell Biol. 2000 Oct;1(1):31-9.

[84] Ripa I, Andreu S, López-Guerrero JA, Bello-Morales R. Membrane Rafts: Portals for Viral Entry. Front Microbiol. 2021 Feb 4;12:631274.

[85] Bieberich E. Sphingolipids and lipid rafts: Novel concepts and methods of analysis. Chem Phys Lipids. 2018 Nov;216:114-131.

[86] Sezgin E, Levental I, Mayor S, Eggeling C. The mystery of membrane organization: composition, regulation and roles of lipid rafts. Nat Rev Mol Cell Biol. 2017 Jun;18(6):361-374.

[87] Su WC, Ho JCS, Gettel DL, Rowland AT, Keating CD, Parikh AN. Kinetic control of shape deformations and membrane phase separation inside giant vesicles. Nat Chem. 2024 Jan;16(1):54-62.

[88] Yue-xiao Shen, Patrick O. Saboe, Ian T. Sines, Mustafa Erbakan, Manish Kumar,Biomimetic membranes: A review,Journal of Membrane Science,Volume 454,2014,Pages 359-381, ISSN 0376-7388.

[89] Pantelopulos GA, Straub JE. Regimes of Complex Lipid Bilayer Phases Induced by Cholesterol Concentration in MD Simulation. Biophys J. 2018 Dec 4;115(11):2167-2178.

[90] Nsairat H, Khater D, Sayed U, Odeh F, Al Bawab A, Alshaer W. Liposomes: structure, composition, types, and clinical applications. Heliyon. 2022 May 13;8(5):e09394.

[91] Lombardo D, Kiselev MA. Methods of Liposomes Preparation: Formation and Control Factors of Versatile Nanocarriers for Biomedical and Nanomedicine Application. Pharmaceutics. 2022 Feb 28;14(3):543. 119

[92] Luchini A, Vitiello G. Mimicking the Mammalian Plasma Membrane: An Overview of Lipid Membrane Models for Biophysical Studies. Biomimetics (Basel). 2020 Dec 31;6(1):3.

[93] Hardy GJ, Nayak R, Zauscher S. Model cell membranes: Techniques to form complex biomimetic supported lipid bilayers via vesicle fusion. Curr Opin Colloid Interface Sci. 2013 Oct 1;18(5):448-458.

[94] Gao W, Hu CM, Fang RH, Zhang L. Liposome-like Nanostructures for Drug Delivery. J Mater Chem B. 2013 Dec 28;1(48):10.1039/C3TB21238F.

[95] Chiantia S, Schwille P, Klymchenko AS, London E. Asymmetric GUVs prepared by MβCD mediated lipid exchange: an FCS study. Biophys J. 2011 Jan 5;100(1):L1-3.

[96] Van de Cauter L, van Buren L, Koenderink GH, Ganzinger KA. Exploring Giant Unilamellar Vesicle Production for Artificial Cells - Current Challenges and Future Directions. Small Methods. 2023 Dec;7(12):e2300416.

[97] Zhang Y, Obuchi H, Toyota T. A Practical Guide to Preparation and Applications of Giant Unilamellar Vesicles Formed via Centrifugation of Water-in-Oil Emulsion Droplets. Membranes (Basel). 2023 Apr 18;13(4):440.

[98] Nishu Kanwa, Svetozar Gavrilovic, Gereon A. Brüggenthies, Yusuf Qutbuddin, Petra Schwille. Inducing Lipid Domains in Membranes by Self-Assembly of DNA Origami. First published: 18 April 2023

[99] Miglena I. Angelova and Dimiter S. Dimitrov, Faraday Discuss. Chem. Soc., 1986,81, 303311. Liposome electroformation.

[100] Sibold J, Tewaag VE, Vagedes T, Mey I, Steinem C. Phase separation in pore-spanning membranes induced by differences in surface adhesion. Phys Chem Chem Phys. 2020 May 6;22(17)

[101] Schütte OM, Mey I, Enderlein J, Savić F, Geil B, Janshoff A, Steinem C. Size and mobility of lipid domains tuned by geometrical constraints. Proc Natl Acad Sci U S A. 2017 Jul 25;114(30):E6064-E6071

[102] Kramer K, Sari M, Schulze K, Flegel H, Stehr M, Mey I, Janshoff A, Steinem C. From LUVs to GUVs—How to Cover Micrometer-Sized Pores with Membranes. J Phys Chem B. 2022 Oct 20;126(41):8233-8244.

[103] Doyle LM, Wang MZ. Overview of Extracellular Vesicles, Their Origin, Composition, Purpose, and Methods for Exosome Isolation and Analysis. Cells. 2019 Jul 15;8(7):727.

[104] Di Bella MA. Overview and Update on Extracellular Vesicles: Considerations on Exosomes and Their Application in Modern Medicine. Biology (Basel). 2022 May 24;11(6):804.

[105] Van der Pol E, Böing AN, Harrison P, Sturk A, Nieuwland R. Classification, functions, and clinical relevance of extracellular vesicles. Pharmacol Rev. 2012 Jul;64(3):676-705 120

[106] Wiklander OPB, Brennan MÁ, Lötvall J, Breakefield XO, El Andaloussi S. Advances in therapeutic applications of extracellular vesicles. Sci Transl Med. 2019 May 15;11(492):eaav8521.

[107] Jordi Rovira, Fritz Diekmann, Josep Campistol, maría josé ramírez-bajo. Therapeutic application of extracellular vesicles in acute and chronic renal injury. May 2017 Nefrología (English Edition) 37(2).

[108] Di Bella MA. Overview and Update on Extracellular Vesicles: Considerations on Exosomes and Their Application in Modern Medicine. Biology (Basel). 2022 May 24;11(6):804.

[109] Kowal J, Arras G, Colombo M, Jouve M, Morath JP, Primdal-Bengtson B, Dingli F, Loew D, Tkach M, Théry C. Proteomic comparison defines novel markers to characterize heterogeneous populations of extracellular vesicle subtypes. Proc Natl Acad Sci U S A. 2016 Feb 23;113(8):E968-77.

[110] Colombo M, Moita C, van Niel G, Kowal J, Vigneron J, Benaroch P, Manel N, Moita LF, Théry C, Raposo G. Analysis of ESCRT functions in exosome biogenesis, composition and secretion highlights the heterogeneity of extracellular vesicles. J Cell Sci. 2013 Dec 15;126(Pt 24):5553-65.

[111] Lötvall J, Hill AF, Hochberg F, Buzás EI, Di Vizio D, Gardiner C, Gho YS, Kurochkin IV, Mathivanan S, Quesenberry P, Sahoo S, Tahara H, Wauben MH, Witwer KW, Théry C. Minimal experimental requirements for definition of extracellular vesicles and their functions: a

position statement from the International Society for Extracellular Vesicles. J Extracell Vesicles. 2014 Dec 22;3:26913.

[112] Mathivanan S, Ji H, Simpson RJ. Exosomes: extracellular organelles important in intercellular communication. J Proteomics. 2010 Sep 10;73(10):1907-20.

[113] Raposo G, Stahl PD. Extracellular vesicles: a new communication paradigm? Nat Rev Mol Cell Biol. 2019 Sep;20(9):509-510.

[114] Krok E, Franquelim HG, Chattopadhyay M, Orlikowska-Rzeznik H, Schwille P, Piatkowski L. Nanoscale structural response of biomimetic cell membranes to controlled dehydration. Nanoscale. 2023 Dec 21;16(1):72-84.

[115] Abolfazl Akbarzadeh et al. “Liposome: classification, preparation, and applications”. In: Nanoscale research letters 8 (2013), pp. 1–9.

[116] Hamdi Nsairat et al. “Liposomes: Structure, composition, types, and clinical applications”. In: Heliyon (2022).

[117] Oliveira, A.E.F.; Pereira, A.C.; Resende, M.A.C.; Ferreira, L.F. Gold Nanoparticles: A Didactic Step-by-Step of the Synthesis Using the Turkevich Method, Mechanisms, and Characterizations. Analytica 2023, 4, 250–263.

[118] Alsadig A, Vondracek H, Pengo P, Pasquato L, Posocco P, Parisse P, Casalis L. Label-Free, Rapid and Facile Gold-Nanoparticles-Based Assay as a Potential Spectroscopic Tool for Trastuzumab Quantification. Nanomaterials (Basel). 2021 Nov 24;11(12):3181.

[119] Stein H, Spindler S, Bonakdar N, Wang C, Sandoghdar V. Production of Isolated Giant Unilamellar Vesicles under High Salt Concentrations. Front Physiol. 2017 Feb 13;8:63.

[120] G. Binnig, C. F. Quate, and C. Gerber, “Atomic force microscope”, PhysicalReview Letters, vol. 56, no. 9, pp. 930-933, 1986.)

[121] De Pablo PJ. Introduction to atomic force microscopy. Methods Mol Biol. 2011;783:197212.

[122] Se-Hui Jung et al. “Molecular imaging of membrane proteins and microfilaments using atomic force microscopy”. In: Experimental & Molecular Medicine 42.9 (2010), pp. 597–605.

[123] Dagdeviren OE, Schwarz UD. Accuracy of tip-sample interaction measurements using dynamic atomic force microscopy techniques: Dependence on oscillation amplitude, interaction strength, and tip-sample distance. Rev Sci Instrum. 2019 Mar;90(3):033707.

[124] Gavara N. A beginner's guide to atomic force microscopy probing for cell mechanics. Microsc Res Tech. 2017 Jan;80(1):75-84.

[125] Voigtländer, B. (2019). Forces Between Tip and Sample. In: Atomic Force Microscopy. NanoScience and Technology. Springer, Cham.

[126] C Y Maghfiroh et al 2020 J. Phys.: Conf. Ser. 1491 012022

[127] Jeong Y, Jayanth GR, Menq CH. Control of tip-to-sample distance in atomic force microscopy: a dual-actuator tip-motion control scheme. Rev Sci Instrum. 2007 Sep;78(9):093706.

[128] Hans-Jürgen Butt, Brunero Cappella, Michael Kappl,Force measurements with the atomic force microscope: Technique, interpretation and applications, Surface Science Reports, Volume 59, Issues 1–6, 2005, Pages 1-152

[129] Garcia R., Perez R., “Dynamic atomic force microscopy methods”, Surface Science Reports 47 (2002), 197-301

[130] Xia F, Youcef-Toumi K. Review: Advanced Atomic Force Microscopy Modes for Biomedical Research. Biosensors (Basel). 2022 Dec 2;12(12):1116.

[131] Wala, J., Das, S. Mapping of biomechanical properties of cell lines on altered matrix stiffness using atomic force microscopy. Biomech Model Mechanobiol 19, 1523–1536 (2020).

[132] Garcia-Manyes S, Redondo-Morata L, Oncins G, Sanz F. Nanomechanics of lipid bilayers: heads or tails? J Am Chem Soc. 2010 Sep 22;132(37):12874-86.

[133] Pleshakova TO, Bukharina NS, Archakov AI, Ivanov YD. Atomic Force Microscopy for Protein Detection and Their Physicochemical Characterization. Int J Mol Sci. 2018 Apr 10;19(4):1142.

[134] Alessandrini, Andrea and Facci, Paolo, Phase transitions in supported lipid bilayers studied by AFM,Soft Matter, 2014, volume 10, issue 37, Pages 7145-7164, The Royal Society of Chemistry.

[135] Gumí-Audenis B, Costa L, Carlá F, Comin F, Sanz F, Giannotti MI. Structure and Nanomechanics of Model Membranes by Atomic Force Microscopy and Spectroscopy: Insights into the Role of Cholesterol and Sphingolipids. Membranes (Basel). 2016 Dec 19;6(4):58.

[136] Redondo-Morata L, Giannotti MI, Sanz F. AFM-based force-clamp monitors lipid bilayer failure kinetics. Langmuir. 2012 Apr 17;28(15):6403-10.

[137] Fischer-Cripps, A.C. The Hertzian contact surface. Journal of Materials Science 34, 129–137 (1999). [138] M. Minsky, Memoir on inventing the confocal scanning microscope. Scanning 10, 128138 (1988).

[139] S. W. Paddock, Principles and practices of laser scanning confocal microscopy. Molecular biotechnology 16, 127-149 (2000).

[140] Elliott AD. Confocal Microscopy: Principles and Modern Practices. Curr Protoc Cytom. 2020 Mar;92(1):e68.

[141] Brown CM. Fluorescence microscopy--avoiding the pitfalls. J Cell Sci. 2007 May 15;120(Pt 10):1703-5. doi: 10.1242/jcs.03433.

[142] Jonkman, J., Brown, C.M., Wright, G.D. et al. Tutorial: guidance for quantitative confocal microscopy. Nat Protoc 15, 1585–1611 (2020).

[143] Axelrod D, Koppel DE, Schlessinger J, Elson E, Webb WW. Mobility measurement by analysis of fluorescence photobleaching recovery kinetics. Biophys J. 1976 Sep;16(9):1055-69.

[144] Wihelm, S., et al. Confocal Laser Scanning Microscopy Principles. Zeiss.

[145] Axelrod D, Elson EL, Schlessinger J, Koppel DE. Reminiscences on the "Classic" 1976 FRAP Article in Biophysical Journal. Biophys J. 2018 Oct 2;115(7):1156-1159.

[146] Ishikawa-Ankerhold, H., Ankerhold, R. and Drummen, G. (2014). Fluorescence Recovery After Photobleaching (FRAP). In eLS, John Wiley & Sons, Ltd (Ed.).

[147] Day CA, Kraft LJ, Kang M, Kenworthy AK. Analysis of protein and lipid dynamics using confocal fluorescence recovery after photobleaching (FRAP). Curr Protoc Cytom. 2012 Oct;Chapter 2:Unit2.19.

[148] Rayan G, Guet JE, Taulier N, Pincet F, Urbach W. Recent applications of fluorescence recovery after photobleaching (FRAP) to membrane bio-macromolecules. Sensors (Basel). 2010;10(6):5927-48.

[149] Pincet F, Adrien V, Yang R, Delacotte J, Rothman JE, Urbach W, Tareste D. FRAP to Characterize Molecular Diffusion and Interaction in Various Membrane Environments. PLoS One. 2016 Jul 7;11(7):e0158457.

[150] Soumpasis, D. M. (1983) Theoretical Analysis of Fluorescence Photobleaching Recovery Experiments, Biophysical Journal 41, 95-97.

[151] P. Gill, T. T. Moghadam, and B. Ranjbar, ‘Differential scanning calorimetry techniques: applications in biology and nanoscience’, J Biomol Tech, vol. 21, no. 4, p. 167, 2010.

[152] S. M. Ohline, M. L. Campbell, M. T. Turnbull, and S. J. Kohler, ‘Differential scanning calorimetric study of bilayer membrane phase transitions. A biophysical chemistry

experiment’, J Chem Educ, vol. 78, no. 9, p. 1251, 2001.

[153] Chiu MH, Prenner EJ. Differential scanning calorimetry: An invaluable tool for a detailed thermodynamic characterization of macromolecules and their interactions. J Pharm Bioallied Sci. 2011 Jan;3(1):39-59.

[154] A Raudino, MG Sarpietro, and M Pannuzzo. “Differential scanning calorimetry (DSC): theoretical fundamentals”. In: Drug-Biomembrane Interaction Studies. Elsevier, 2013, pp. 127–168.

[155] R.N.A.H. Lewis, D. A. Mannock, and R. N. McElhaney, 'Differential scanning calorimetry in the study of lipid phase transitions in model and biological membranes: practical considerations', Methods in Membrane Lipids, pp. 171–195, 2007.

[156] Ali O, Szabó A. Review of Eukaryote Cellular Membrane Lipid Composition, with Special Attention to the Fatty Acids. Int J Mol Sci. 2023 Oct 28;24(21):15693.

[157] F. Perissinotto et al., 'GM1 Ganglioside role in the interaction of Alpha-synuclein with lipid membranes: Morphology and structure', Biophys Chem, vol. 255, p. 106272, 2019.

[158] C. Paba et al., 'Lipid bilayer fluidity and degree of order regulates small EVs adsorption on model cell membrane', J Colloid Interface Sci, vol. 652, pp. 1937 1943, 2023.

[159] Perissinotto, Fabio and Rondelli, Valeria and Senigagliesi, Beatrice and Brocca, Paola and Almásy, László and Bottyán, László and Merkel, Dániel Géza and Amenitsch, Heinz and Sartori, Barbara and Pachler, Karin and Mayr, Magdalena and Gimona, Mario and Rohde, Eva and Casalis, Loredana and Parisse, Pietro", Structural insights into fusion mechanisms of small extracellular vesicles with model plasma membranes,Nanoscale,2021, volume 13,issue 10, pages 5224-5233.

[160] Krasnobaev, V.D.; Bershatsky, Y.V.; Bocharova, O.V.; Bocharov, E.V.; Batishchev, O.V. Amyloid Precursor Protein Changes Arrangement in a Membrane and Its Structure Depending on the Cholesterol Content. Membranes 2023, 13, 706.

[161] Pöhnl, M., Trollmann, M.F.W. & Böckmann, R.A. Nonuniversal impact of cholesterol on membranes mobility, curvature sensing and elasticity. Nat Commun 14, 8038 (2023).

[162] Risselada HJ. Cholesterol: The Plasma Membrane's Constituent that Chooses Sides. Biophys J. 2019 Jun 18;116(12):2235-2236.

[163] Pinkwart K, Schneider F, Lukoseviciute M, Sauka-Spengler T, Lyman E, Eggeling C, Sezgin E. Nanoscale dynamics of cholesterol in the cell membrane. J Biol Chem. 2019 Aug 23;294(34):12599-12609.

[164] Connell SD, Smith DA. The atomic force microscope as a tool for studying phase separation in lipid membranes. Mol Membr Biol. 2006 Jan-Feb;23(1):17-28.

[165] van Meer G, Voelker DR, Feigenson GW. Membrane lipids: where they are and how they behave. Nat Rev Mol Cell Biol. 2008 Feb;9(2):112-24.

[166] Ikonen E, Zhou X. Cholesterol transport between cellular membranes: A balancing act between interconnected lipid fluxes. Dev Cell. 2021 May 17;56(10):1430-1436.

[167] (Phase Transition Temperatures for Glycerophospholipids | Avanti Research

[168] Socrier L, Ahadi S, Bosse M, Montag C, Werz DB, Steinem C. Optical Manipulation of Gb3 Enriched Lipid Domains: Impact of Isomerization on Gb3 -Shiga Toxin B Interaction. Chemistry. 2023 Jan 18;29(4):e202202766.

[169] Binder WH, Barragan V, Menger FM. Domains and rafts in lipid membranes. Angew Chem Int Ed Engl. 2003;42(47):5802-27.

[170] Craig D Blanchette et al. "Using nucleation rates to determine the interfacial line tension of symmetric and asymmetric lipid bilayer domains". In: Langmuir 23.11 (2007), pp. 5875 5877.

[171] Blanchette CD, Lin WC, Orme CA, Ratto TV, Longo ML. Using nucleation rates to determine the interfacial line tension of symmetric and asymmetric lipid bilayer domains. Langmuir. 2007 May 22;23(11):5875-7.

[172] Crane JM, Tamm LK. Fluorescence microscopy to study domains in supported lipid bilayers. Methods Mol Biol. 2007;400:481-8.

[173] Wan C, Kiessling V, Tamm LK. Coupling of cholesterol-rich lipid phases in asymmetric bilayers. Biochemistry. 2008 Feb 19;47(7):2190-8.

[174] Filipe, H.A.L.; Moreno, M.J.; Loura, L.M.S. The Secret Lives of Fluorescent Membrane Probes as Revealed by Molecular Dynamics Simulations. Molecules 2020, 25, 3424.

[175] Lenne, Pierre-François and Nicolas, Alice, Physics puzzles on membrane domains posed by cell biology, Soft Matter, 2009", volume 5 issue 15, pages 2841-2848. The Royal Society of Chemistry

[176] Tsai WC, Feigenson GW. Lowering line tension with high cholesterol content induces a transition from macroscopic to nanoscopic phase domains in model biomembranes. Biochim Biophys Acta Biomembr. 2019 Feb 1;1861(2):478-485.

[177] Alessandrini, Andrea and Facci, Paolo,Phase transitions in supported lipid bilayers studied by AFM, Soft Matter, 2014, volume 10, issue 37, pages 7145-7164

[178] Shahane, G., Ding, W., Palaiokostas, M. et al. Physical properties of model biological lipid bilayers: insights from all-atom molecular dynamics simulations. J Mol Model 25, 76 (2019).

[179] Pöhnl, M., Trollmann, M.F.W. & Böckmann, R.A. Nonuniversal impact of cholesterol on membranes mobility, curvature sensing and elasticity. Nat Commun 14, 8038 (2023).

[180] Mielke S, Sorkin R, Klein J. Effect of cholesterol on the mechanical stability of gel-phase phospholipid bilayers studied by AFM force spectroscopy. Eur Phys J E Soft Matter. 2023 Sep 6;46(9):77.

[181] Andrews JT, Baker KE, Handloser JT, Bridges N, Krone AA, Kett PJN. Formation of Supported Lipid Bilayers (SLBs) from Buffers Containing Low Concentrations of Group I Chloride Salts. Langmuir. 2021 Nov 9;37(44):12819-12833.

[182] Chattopadhyay M, Krok E, Orlikowska-Rzeznik H, Piatkowski L. Cooperativity between sodium ions and water molecules facilitates lipid mobility in model cell membranes. Chem Sci. 2023 Mar 22;14(15):4002-4011.

[183] Rainer A. Böckmann, Agnieszka Hac, Thomas Heimburg, Helmut Grubmüller, Effect of Sodium Chloride on a Lipid Bilayer, Biophysical Journal, Volume 85, Issue 3, 2003, Pages 1647-1655.

[184] Weber RE. Use of ionic and zwitterionic (Tris/BisTris and HEPES) buffers in studies on hemoglobin function. J Appl Physiol (1985). 1992 Apr;72(4):1611-5.

[185] Kato N, Ishijima A, Inaba T, Nomura F, Takeda S, Takiguchi K. Effects of lipid composition and solution conditions on the mechanical properties of membrane vesicles. Membranes (Basel). 2015 Jan 20;5(1):22-47.

[186] Caselli L, Ridolfi A, Cardellini J, Sharpnack L, Paolini L, Brucale M, Valle F, Montis C, Bergese P, Berti D. A plasmon-based nanoruler to probe the mechanical properties of synthetic and biogenic nanosized lipid vesicles. Nanoscale Horiz. 2021 Jun 28;6(7):543-550.

[187] Kim S, Lee Y, Lee M, An S, Cho SJ. Quantitative Visualization of the Nanomechanical Young's Modulus of Soft Materials by Atomic Force Microscopy. Nanomaterials (Basel). 2021 Jun 17;11(6):1593.

[188] Liang X, Mao G, Ng KY. Mechanical properties and stability measurement of cholesterol containing liposome on mica by atomic force microscopy. J Colloid Interface Sci. 2004 Oct 1;278(1):53-62.

[189] Ruby May A. Sullan, James K. Li, Changchun Hao, Gilbert C. Walker, Shan Zou,Cholesterol-Dependent Nanomechanical Stability of Phase-Segregated Multicomponent Lipid Bilayers,Biophysical Journal,Volume 99, Issue 2,2010,Pages 507-516

[190] Samar Kaddah, Nathalie Khreich, Fouad Kaddah, Catherine Charcosset, Hélène Greige Gerges, Cholesterol modulates the liposome membrane fluidity and permeability for a hydrophilic molecule,Food and Chemical Toxicology,Volume 113,2018,Pages 40-48.

[191] Subczynski WK, Pasenkiewicz-Gierula M, Widomska J, Mainali L, Raguz M. High Cholesterol/Low Cholesterol: Effects in Biological Membranes: A Review. Cell Biochem Biophys. 2017 Dec;75(3-4):369-385. [190] Khadka NK, Timsina R, Rowe E, O'Dell M, Mainali L. Mechanical properties of the high cholesterol-containing membrane: An AFM study. Biochim Biophys Acta Biomembr. 2021 Aug 1;1863(8):183625.

[192] Schachter I, Paananen RO, Fábián B, Jurkiewicz P, Javanainen M. The Two Faces of the Liquid Ordered Phase. J Phys Chem Lett. 2022 Feb 10;13(5):1307-1313.

[193] Ying Zhang, Qingchuan Li, Mingdong Dong, Xiaojun Han, Effect of cholesterol on the fluidity of supported lipid bilayers,Colloids and Surfaces B: Biointerfaces,Volume 196,2020, 111353.

[194] Yáñez-Mó M, Siljander PR, Andreu Z, Zavec AB, Borràs FE, Buzas EI, Buzas K, Casal E, Cappello F, Carvalho J, Colás E, Cordeiro-da Silva A, Fais S, Falcon-Perez JM, Ghobrial IM, Giebel B, Gimona M, Graner M, Gursel I, Gursel M, Heegaard NH, Hendrix A, Kierulf P, Kokubun K, Kosanovic M, Kralj-Iglic V, Krämer-Albers EM, Laitinen S, Lässer C, Lener T, Ligeti E, Linē A, Lipps G, Llorente A, Lötvall J, Manček-Keber M, Marcilla A, Mittelbrunn M, Nazarenko I, Nolte-'t Hoen EN, Nyman TA, O'Driscoll L, Olivan M, Oliveira C, Pállinger É, Del Portillo HA, Reventós J, Rigau M, Rohde E, Sammar M, Sánchez-Madrid F, Santarém N, Schallmoser K, Ostenfeld MS, Stoorvogel W, Stukelj R, Van der Grein SG, Vasconcelos MH, Wauben MH, De Wever O. Biological properties of extracellular vesicles and their physiological functions. J Extracell Vesicles. 2015 May 14;4:27066.

[195] Kwok, Z.H.; Wang, C.; Jin, Y. Extracellular Vesicle Transportation and Uptake by Recipient Cells: A Critical Process to Regulate Human Diseases. Processes 2021, 9, 273.

[196] Costanza Montis, Annalisa Salvatore, Francesco Valle, Lucia Paolini, Francesco Carlà, Paolo Bergese, Debora Berti,Biogenic supported lipid bilayers as a tool to investigate nano-bio interfaces, Journal of Colloid and Interface Science,Volume 570, 2020, Pages 340-349, ISSN 0021-9797.

[197] Lai CP, Mardini O, Ericsson M, Prabhakar S, Maguire C, Chen JW, Tannous BA, Breakefield XO. Dynamic biodistribution of extracellular vesicles in vivo using a multimodal imaging reporter. ACS Nano. 2014 Jan 28;8(1):483-494.

[198] Liu YJ, Wang C. A review of the regulatory mechanisms of extracellular vesicles-mediated intercellular communication. Cell Commun Signal. 2023 Apr 13;21(1):77.

[199] Mohammadipoor A, Hershfield MR, Linsenbardt HR, Smith J, Mack J, Natesan S, Averitt DL, Stark TR, Sosanya NM. Biological function of Extracellular Vesicles (EVs): a review of the field. Mol Biol Rep. 2023 Oct;50(10):8639-8651

[200] Schwenen LL, Hubrich R, Milovanovic D, Geil B, Yang J, Kros A, Jahn R, Steinem C. Resolving single membrane fusion events on planar pore-spanning membranes. Sci Rep. 2015 Jul 13;5:12006. doi: 10.1038/srep12006.

[201] Cheng X. A Comprehensive Review of HER2 in Cancer Biology and Therapeutics. Genes (Basel). 2024 Jul 11;15(7):903. doi: 10.3390/genes15070903.

Acknowledgements

First and foremost, I would like to express my deepest gratitude to my supervisor, Dr. Loredana Casalis, and my co-supervisor, Dr. Pietro Parisse, for their invaluable guidance, unwavering support, and insightful advice throughout my PhD journey. Their mentorship has not only guided me through the challenges and intricacies of my research but has also been instrumental in shaping my growth as a researcher and individual. I am profoundly grateful for their patience and encouragement. Being part of their group has been a transformative experience, one that has greatly enriched both my academic and personal life.

I am also deeply appreciative of Prof. Petra Schwille, who welcomed me to spend a research period within her group at the Max Planck Institute of Biochemistry. This opportunity expanded my knowledge and perspective in immeasurable ways. I extend a special thanks to Dr. Kanwa Nishu, whose mentorship and friendship have been a lasting source of inspiration and support, extending well beyond our time working together.

My heartfelt thanks go to my colleagues and friends at the NanoInnovation Lab, in particular Marcelina, Ana, Caterina, and Carolina—for their support and friendship. A special thanks goes to Luca, whose invaluable assistance made key parts of this work possible. Working alongside each of you has created an environment of laughter, collaboration, and encouragement that has been invaluable to me.

I would also like to acknowledge the financial support provided by the Ministry of Universities and Research (MUR) and Elettra Sincrotrone Trieste, without which this research would not have been possible.

To my family, who have been my unwavering source of strength and motivation, thank you. Your love, sacrifices, and steadfast belief in me have been the foundation upon which this journey was built. Riky, Ale e Mamy siete il mio posto felice nel mondo. To Jan, la persona che mi sta vicino in ogni momento nonostante tutto, la mia roccia e tutto ciò a cui penso quando penso alla parola “casa”. Non importa dove, ma insieme. I owe a special thank you for filling this journey with endless support, patience, and encouragement, especially during the most challenging moments. Your presence and belief in me have been a true gift.

Finally, I am grateful to everyone who, in one way or another, has supported me on this path. Your contributions, no matter how big or small, have made this achievement possible.

Thank you.